Theses and Dissertations   Graduate School

2024

Exploration of Dopaminergic and Serotonergic Pathways Utilizing Pleiotropic Agents

Charles B. Jones III
Virginia Commonwealth University

Exploration of Dopaminergic and Serotonergic Pathways Utilizing Pleiotropic Agents

A dissertation submitted in partial fulfillment of the requirements for the degree of Doctor of Philosophy at Virginia Commonwealth University.

by

Charles Bernard Jones III

Bachelor of Science in Chemistry, University of Central Florida 2014

Master of Science in Medicinal Chemistry, Virginia Commonwealth University 2021

Director: MAŁGORZATA DUKAT

Professor, Department of Medicinal Chemistry

Virginia Commonwealth University

Richmond, Virginia

August, 2024

i

Acknowledgement

Thank you to Dr. Dukat who has been a tremendous mentor and advisor to me, who continuously strives for perfection and pushes me to continually challenge myself and become a better scientist. You are a role model for what a professor should be. Your integrity and discipline in your profession cannot be matched. You have instilled in me critical thinking skills, where I feel as if any problem can be solved, as well as the determination to troubleshoot any issue. Thank you to Dr. Glennon who has filled my mind with neuronal pollution to the extent that I will awaken in the night and ponder structure activity relationships and new molecules. I cherish every Friday group meeting, where your insights continually have me contemplate new ideas and critically consider all possibilities. Thank you to Dr. Eltit who has ignited my interest in the biological side of my work and helped me to be successful in my studies. Without your guidance the molecules I make would just be molecules. I would like to also thank the rest of my graduate committee members, Drs. Kellogg and Selley. Both of you have been supportive of my journey and have always been accommodating to my hectic schedule. Thank you to all current and former members of the lab, each one of you has supported me and taught me invaluable lessons. I cherish our friendship as no one else in the world will have experienced what we have. Thank you to my wife, Sara, I could not do any of this without your boundless love. You are my rock. You always support me and make me a better person. You give me the drive and the encouragement to achieve anything. You make me feel like anything is possible and let me chase my dreams to make them a reality. Thank you to my parents. To my mom, you have instilled in me the importance of integrity. To Frank, you have been a great father and have kept me in the realm of practicality. To

my dad, you make me realize just how precious life is and you have taught me how to persevere through anything. Thank you to the rest of my family. All of you have been immensely supportive of my journey and I truly cherish any time we get to spend together. Thank you to all of my friends, you are the family I get to choose, and I could not have made a better choice. The sacrifices we endure to make time for each other in life show me how invaluable our bond is. I would not be the person I am today without each and every one of you.

Table of Contents

List of Tables

List of Figures

List of Schemes

List of Abbreviations

25I-NBOMe	2-(4-Iodo-2,5-dimethoxyphenyl)-*N*-(2-methoxybenzyl)ethan-1-amine
5-MeO-DMT	5-Methoxy-*N*,*N*-dimethyltryptamine
α-ET	α-Ethyltryptamine
5-HT	Serotonin
5-HT$_{2A}$	Serotonin 2A receptor
ADHD	Attention deficit hyperactivity disorder
APP$^+$	4-(4-(Dimethylamino)phenyl)-1-methylpyridinium
BOP	(Benzotriazol-1-yloxy)tris(dimethylamino)phosphonium
BP	2-(Benzoyl)piperidines
DA	Dopamine
DAG	Diacylglycerol
DAT	Dopamine transporter
DCBP	(3,4-Dichlorophenyl)(piperidin-2-yl)methanone
dDAT	*Drosophila* dopamine transporter
DMBP	(3,4-Dimethylphenyl)(piperidin-2-yl)methanone
DMT	*N*,*N*-Dimethyltryptamine
DOI	2,5-Dimethoxy-4-iodoamphetamine

DOM	2,5-Dimethoxy-4-methylamphetamine
DOPE	Discrete optimized protein energy
DSM	Diagnostic and statistical manual of mental disorders
EBP	Extended binding pocket
ee	Enantiomeric excess
EL2	Extracellular loop 2
EMCDDA	European monitoring centre for drug and drug addiction
Fmoc	Fluorenylmethoxycarbonyl
GAD	Generalized anxiety disorder
GDP	Guanosine diphosphate
GPCR	G-protein coupled receptor
GTP	Guanosine-5'-triphosphate
hDAT	Human dopamine transporter
HEK	Human embryonic kidney
HINT	Hydropathic interactions
hSERT	Human serotonin transporter
IP_3	Inositol triphosphate
IS	Imaging solution

LeuT	Leucine transporter
LGIC	Ligand-gated ion channel
LSD	Lysergic acid diethylamide
MAOI	Monoamine oxidase inhibitor
MAT	Monoamine transporter
MDD	Major depressive disorder
MDMA	3,4-methylenedioxymethamphetamine
MPH	Methylphenidate
NA	Nucleus accumbens
NE	Norepinephrine
NET	Norepinephrine transporter
NP	Naphthalen-2-yl(piperidin-2-yl)methanone
NRI	Norepinephrine reuptake inhibitor
OCD	Obsessive compulsive disorder
PIP_2	Phosphatidylinositol-4,5-bisphosphate
PKC	Protein kinase C
PLC	Phospholipase C
PRC-063	Extended-release methylphenidate formulation

PTSD	Post traumatic stress disorder
ROI	Region of interest
SAR	Structure activity relationship
SERT	Serotonin transporter
SNRI	Serotonin and norepinephrine reuptake inhibitor
spl	Sybyl's programing language
SSRI	Selective serotonin reuptake inhibitor
SUD	Substance use disorder
TAAR1	Trace amine-associated receptor 1
TCA	Tricyclic antidepressant
TLC	Thin layer chromatography
TMS	Tetramethylsilane
TQD	Tandem quadrupole
TRD	Treatment resistant depression
UN	United nations
VMAT2	Vesicular monoamine transporter 2
VTA	Ventral tegmental area
WT	Wild type

Abstract

Exploration of Dopaminergic and Serotonergic Pathways Utilizing Pleiotropic Agents

By Charles Bernard Jones III

A dissertation submitted in partial fulfillment of the requirements for the degree of Doctor of Philosophy at Virginia Commonwealth University.

Virginia Commonwealth University, 2024

Major Director: Małgorzata Dukat, Professor

Department of Medicinal Chemistry

2-(Benzoyl)piperidines (BPs) are at a crossroads of therapy and abuse. These compounds are a hybrid between the ADHD medication methylphenidate and abused stimulant cathinones. Here we use computational molecular modeling, synthesis, mutagenesis, and epifluorescence microscopy to further improve the understanding of and potential treatments for several neuropsychiatric disorders. Utilizing the BP scaffold and controlling chirality and aryl substitution, these agents were examined at DAT and SERT. From these investigations it has now been established that R isomer BPs are favored for DAT while S isomer BPs are favored for SERT. Aryl-substitution can greatly affect the selectivity of these agents with a m-chloro-substituent having the ability to

partake in halogen bonding interactions with SER149 in DAT, thus increasing its DAT activity whereas the benz-fused substituent was able to vastly increase activity at SERT. The nature of BPs interaction with SERT has also been elucidated, demonstrating reuptake inhibition. Due to the predictability and spectrum in selectivity, this series of agents is well suited to be further investigated for therapeutic potential and the study of neuropsychiatric disorders.

Recently, it has been reported that agonists of the 5-HT$_{2A}$ receptor elicit fast-acting and long-lasting efficacy towards treatment resistant depression. A bygone antidepressant agent, alpha-ethyltryptamine (α-ET), was chosen to be reevaluated with the aid of current medicinal chemistry techniques. Stereoisomers and substituted analogs of α-ET (4- and 5-bromo and methoxy) were examined using 3D molecular modeling and docking studies to predict their relative binding modes to each other and elucidate protein-ligand interactions that might contribute to binding affinity and agonist activity at 5-HT$_{2A}$ receptors. To validate the computational studies and previously published activity data, α-ET and analogs were synthesized and assayed at cloned human 5-HT$_{2A}$ receptors for binding affinity and agonist activity. For the first time, binding affinity data have been provided for this class of compounds. Our results indicated that all analogs examined bind at 5-HT$_{2A}$ receptors, and all compounds exhibit partial agonist activity except for racemic and (R) α-ET. These two agents bind at 5-HT$_{2A}$ receptors but failed to show any activity in a calcium mobilization assay. Future examination of these compounds will be required to determine whether they might be non-hallucinogenic agents that elicit rapid and long-lasting antidepressant effects via a 5-HT$_{2A}$ receptor mediated pathway.

I. Introduction

There is great interest in developing agents with selective drug target profiles. ADHD pharmacotherapies, stimulant drugs of abuse, and SSRI antidepressants primarily work through interaction with the monoamine transporters NET, DAT, and SERT with ADHD therapeutics and stimulants possessing selectivity towards DAT and SSRI antidepressants with selectivity towards SERT. The issue with current ADHD pharmacotherapies is that although they are effective in the treatment of symptoms, they also display high potential for abuse. SSRIs are plagued with side effects such as weight gain and drowsiness. The ability to shift selectivity between transporters is a worthwhile pursuit to further understand the intricacies of these molecular targets that contribute to therapy or abuse. With continuous construction of comprehension on these neuropsychiatric disorders down to a molecular level it might be possible to develop new therapeutics such as low abuse liability ADHD treatments, stimulant use disorder treatments, and more effective antidepressants with less side effects. Our lab has developed a novel class of compounds, BPs, that show advantageous activity at the monoamine transporters. Making use of aryl-substitution and chirality, BPs can be used as molecular tools to probe selectivity profiles and examine structure activity relationships for the monoamine transporters. The development of tailored selective compounds can have a dramatic impact on therapeutic agents that might present fewer side effects than currently available ones (e.g., SSRIs). Additionally, in the interest of preserving the therapeutic effects of these drugs (e.g., ADHD treatment), while dispelling their liability for abuse proposedly produced by DAT selective agents, features for modulating the selectivity between transporters can be elucidated and these features can be exploited in

the structures of drugs developed in the future, thus enhancing their pharmacological profile.

5-HT$_{2A}$ receptor agonists commonly referred to as serotonergic psychedelics have recently been a popular subject of interest in the medical field for their ability to elicit fast acting and long-lasting efficacy towards treatment resistant depression. Despite the untoward hallucinogenic effects brought on by these agents, the allure of infrequent and efficacious treatments for depression is quite enticing compared to current FDA approved pharmacotherapies that are plagued with chronic dosing, negative side effects, delayed onset of symptom relief, and ineffectiveness for significant populations. α-ET, a previously approved but withdrawn antidepressant agent is a prime candidate to be revaluated as a rapid acting antidepressant. Published studies on the activities of α-ET stereoisomers and analogs has provided a basis from which binding affinity and modes are to be further assessed. α-ET seems to be a 5-HT$_{2A}$ agonist, but there is scarce data on the possibility of it producing hallucinogenic effects in man. Being previously FDA approved as an antidepressant, α-ET has an advantage over other 5-HT$_{2A}$ agents being developed as antidepressants because it can already be assumed that α-ET has a relatively high safety profile and has already demonstrated antidepressant effects. It is of interest then to examine α-ETs further as little data is currently available concerning α-ET stereoisomers and analogs. These studies will involve molecular modeling, synthesis and pharmacological evaluation of these enigmatic compounds. At the conclusion of this study, the binding modes, binding affinity, and functional activity of α-ET will be further established.

II. Background

A. Selected neuropsychiatric disorders involving the neurotransmitters dopamine and serotonin.

There is a myriad of neuropsychiatric disorders that occupy the Diagnostic and Statistical Manual of Mental Disorders (DSM-5)[1] published by the American Psychiatric Association that are heavily influenced by the innerworkings of the neurotransmitters dopamine (DA), serotonin (5-HT), and their signaling systems (**Table 1**). Many of these disorders have some overlap or even coexist. While pharmacotherapies have been developed for most of these conditions, some are still without treatment, have severe side effects, or only a small population of patients responds to the treatment. By no means does **Table 1** envelop all current pharmacotherapies but goes to highlight a selection of some different drug classes as well as show that there is overlap of these classes to treat several disorders. The major classes of drugs that are on the market for these ailments broadly are neurotransmitter releasers/reuptake inhibitors, receptor antagonists/agonists, enzyme inhibitors, or allosteric modulators.

Table 1. Selected neuropsychiatric disorders and assorted pharmacotherapies.

DSM-5 Disorder[1]	Pharmacotherapy	Mechanism of Action
Schizophrenia	Aripiprazole, Clozapine, Risperidone	receptor antagonists
Obsessive compulsive disorder (**OCD**)	Sertraline, Fluoxetine, Clomipramine	neurotransmitter reuptake inhibitors
Generalized anxiety disorder (**GAD**)	Citalopram, Duloxetine, Imipramine, Lorazempam	neurotransmitter reuptake inhibitors, allosteric modulators
Post traumatic stress disorder (**PTSD**)	Alprazolam, Paroxetine, Reboxetine	neurotransmitter reuptake inhibitors, allosteric modulators
Depression	Fluoxetine, Bupropion, Isocarboxazid, Ketamine	neurotransmitter reuptake inhibitors, enzyme inhibitors, receptor antagonists
Substance use disorder (**SUD**)*	Naloxone, Naltrexone, Methadone, Buprenorphine	receptor agonists/antagonists
Attention deficit hyperactivity disorder (**ADHD**)	Amphetamine, Methylphenidate	neurotransmitter reuptake inhibitors/releasers

*Treatments only for opioid use disorder.

With such a substantial array of neuropsychiatric disorders and a plethora of current pharmacotherapies, this dissertation will solely focus on three disease states and three related drug targets. The three disease states are depression, specifically treatment resistant depression (TRD), substance use disorder (SUD), specifically stimulant use disorder, and attention deficit hyperactivity disorder (ADHD). Primarily due to recent studies showing the efficacy of classical serotonergic psychedelics in the rapid treatment of TRD, the serotonin 2A receptor (5-HT$_{2A}$), known to play a crucial role in the hallucinogenic activity of classical serotonergic psychedelics, will be examined here. The second and third targets are the dopamine transporter (DAT) and serotonin transporter (SERT), which can involve both stimulant use disorder, the subcategory of SUD and ADHD. These two disorders overlap because there are currently no pharmacotherapies indicated for stimulant use disorder and the majority of current ADHD medications are highly abused stimulants. Also, there is overlap with depression due to the fact that the majority of current treatments are reuptake inhibitors of the monoamine transporters (MATs). All three of these disorders and what is currently known of their innerworkings will be discussed further in the next three sections.

B. Attention Deficit Hyperactivity Disorder (ADHD)

ADHD is a neurodevelopmental condition originating in childhood, characterized by persistent symptoms of inattention, impulsivity, restlessness, and hyperactivity.[2] It is the most common neurobehavioral disorder of childhood.[3] While initially recognized primarily in the pediatric population, focus has shifted towards acknowledging and treating ADHD in adults.[4] The prevalence of ADHD among adults is estimated to be around 2-3%

globally.[5,6] Moreover, ADHD is closely associated with various psychiatric disorders such as mood disorders, oppositional and antisocial personality disorders, self-harm, and SUD, leading to significant social and familial burdens.[7]

Despite its impact, ADHD in adults has received comparatively less attention in epidemiological studies, largely due to the absence of established diagnostic criteria.[7] The DSM-5 serves as a widely utilized framework for diagnosing adult ADHD, stipulating childhood onset as a requirement.[1,7]

ADHD symptoms arise from a combination of factors encompassing genetics, neurodevelopmental anomalies, aberrant neuronal development, brain trauma, environmental exposures, and consanguinity. The role of environmental risk factors in contributing to ADHD symptoms across prenatal, perinatal, and postnatal stages have been examined.[7] Prenatal and perinatal factors including prematurity, low birth weight, maternal smoking, stress, trauma, and maternal obesity demonstrate significant associations with ADHD. Similarly, postnatal risk factors such as trauma, parenting practices, artificial additives, pollutants, and pesticides can exacerbate ADHD symptoms.[2]

1. Symptoms and treatments

In adults, ADHD manifests through distinct behavioral criteria including inattentiveness, impulsivity, hyperactivity, and restlessness.[8] The DSM-5 classifies ADHD into three subtypes: predominantly hyperactive/impulsive, predominantly inattentive, and

combined.[1] Inattentiveness has been implicated as the most prevalent symptom domain, affecting approximately 90% of individuals with ADHD.[9]

Adolescents often present with the combined subtype, with around 66% displaying this pattern, which is associated with a higher incidence of comorbid conditions such as neuroticism and SUD.[10–13] In adulthood, individuals with ADHD commonly experience difficulties in organization, planning, and decision-making, leading to unstable employment and relationships.[14] Academic and professional performance is often hindered by reading disabilities, resulting in grade repetition and attendance at special educational facilities, limiting higher educational opportunities.[15] Furthermore, recurrent job changes and poor job performance contribute to professional instability, while challenges in forming and maintaining close friendships and negative perceptions of marriage can lead to relationship difficulties, separation, and divorce.[16,17]

ADHD in adults is also associated with increased risks of driving accidents and incarceration.[18,19] More recently, attention has turned to symptoms of emotional dysregulation, including irritability, emotional fluctuations, low frustration tolerance, and excessive daydreaming, which may lead to misdiagnosis of mood disorders and hinder appropriate intervention.[19–21] Adults with ADHD often struggle to interpret social cues and may exhibit a lack of social propriety, contributing to feelings of being different from others.

Despite these challenges, there are positive aspects to ADHD. Many individuals with ADHD demonstrate creativity, thriving in artistic fields. They often find tasks rewarding when aligned with their interests and develop coping strategies such as maintaining to-do lists and setting alarms.[22] Diagnosis plays a crucial role in helping individuals come to terms with their limitations.

Comorbidity is common among adults with ADHD, with two-thirds presenting with at least one additional psychiatric disorder.[23] Studies indicate that ADHD is present in 15% of psychiatric patients, with comorbidities often masking ADHD symptoms and reducing the frequency of accurate diagnoses.[24,25] Common comorbidities include bipolar disorder, personality disorders, depression, anxiety disorders, and SUD.[4]

While medication-based interventions have demonstrated short-term effectiveness and affordability, their long-term impact on clinical, occupational, and social outcomes remains uncertain. [26] It is evident that there is a pressing need for improved long-term therapeutic approaches for ADHD.

Psychostimulant medications have long been established as the cornerstone of ADHD therapy. Extensive evidence supports their ability to increase the levels of dopamine and norepinephrine in the frontal lobes (Figure 1), thereby improving information processing efficiency, particularly within the pyramidal cells, and consequently alleviating ADHD symptoms.[27] Stimulants are widely recognized as the primary pharmacological intervention for ADHD.
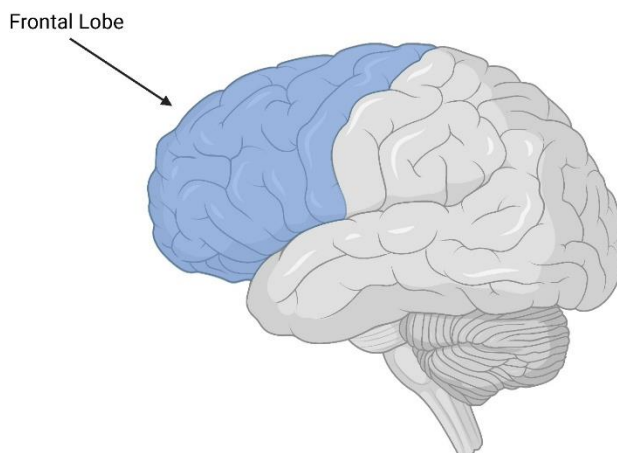
Figure 1. Frontal lobe region of the brain (created with BioRender.com).

Commonly prescribed psychostimulant medications for ADHD include methylphenidate (MPH, **1**, Figure 2) and various forms of amphetamine, such as dextroamphetamine, lisdexamfetamine, and mixed amphetamine salts (see amphetaminergic agents for further discussion).[28,29] Lisdexamfetamine has the amino acid *L*-lysine attached to dextroamphetamine and is an inactive prodrug for dextroamphetamine. There are estimates of a success rate of up to 70% for amphetamines in treating adults with onset ADHD.[30] These treatments effectively address the core manifestations of ADHD, including inattentiveness, hyperactivity, impulsiveness, and poor concentration. Furthermore, stimulants enhance alertness, comprehension, response inhibition, and immediate memory function.[31] Amphetamines exert their therapeutic effects through three primary mechanisms of action.[30]

Firstly, they inhibit the reuptake of neurotransmitters (Figure 3) by binding to monoamine transporters, specifically those for norepinephrine (NE) and DA.[29] Secondly, they facilitate the phosphorylation of the dopamine transporter via trace amine-associated receptor 1 (TAAR1), leading to endocytosis of DAT and reduced dopamine transport.[32–34] Thirdly, amphetamines may induce the release of neurotransmitters into the synaptic cleft by entering presynaptic vesicles through the vesicular monoamine transporter 2 (VMAT2).[30]

(±) MPH (**1**)
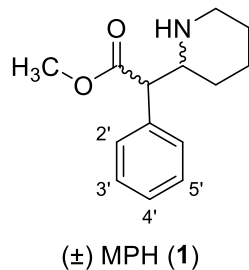
Figure 2. Structure of methylphenidate or (±) methyl 2-phenyl-2-(piperidin-2-yl)acetate (**1**).
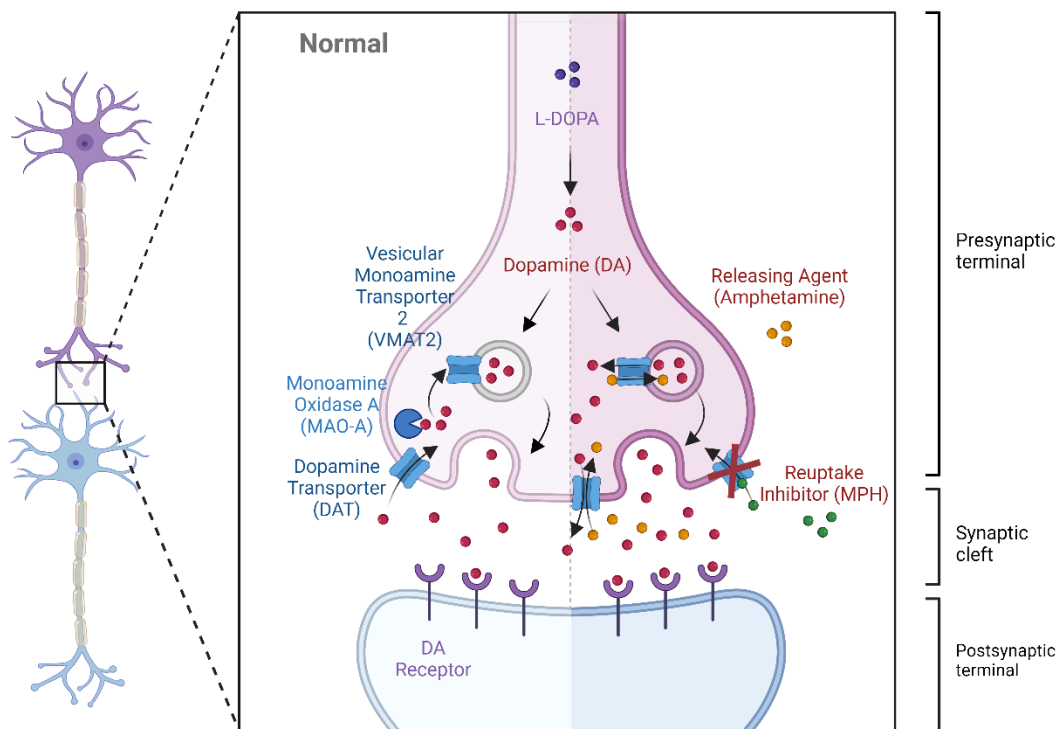
Figure 3. Action of releasing agents and reuptake inhibitors on the dopaminergic pathway (created with BioRender.com).

An investigation of the efficacy of three forms of amphetamine—dexamphetamine, lisdexamfetamine, and mixed amphetamine salts demonstrated that all three forms

effectively reduced ADHD-related symptoms, with no significant variation in effectiveness observed across different doses or formulations, including immediate- and sustained-release formulations.[35] When amphetamines are utilized for ADHD treatment, anorexia and weight loss are common anticipated side effects. Other adverse effects associated with amphetamine use include vomiting, nausea, abdominal discomfort, hypertension, and tachycardia.[36] If agitation or rebound symptoms occur later in the day, administering an additional dose at noon may be beneficial.[37] Initial insomnia is a frequent side effect of stimulants, and it is essential to differentiate whether it precedes treatment or is induced by the medication.[31] To mitigate insomnia, it is recommended to limit doses in the latter part of the day and maintain healthy sleep habits.[31]

2. Methylphenidate

MPH (**1**) is the most commonly used ADHD medication worldwide.[38] In 2016 there was a recorded 16.46 metric tons of MPH prescription use in the United States.[39] It was first synthesized in 1944 and originally patented by CIBA pharmaceuticals in 1950, and was used as an analeptic for barbiturate-induced coma.[40–42] Later MPH was patented for method of use in 1954 as a treatment of psychiatric disorders but is now predominantly used for ADHD treatment.[43] Its mechanism of action involves amplifying neuronal DA and NE efflux and inhibiting DA and NE reuptake, achieved by binding to DAT and the norepinephrine transporter (NET) on presynaptic cells, thereby increasing extracellular DA and NE levels in the synaptic gap.[31,43,44] MPH has a slight binding selectivity for DAT over NET with a number of analogs tested maintaining this trend (Table 2).[45]

11

Table 2. DAT and NET affinities (IC_{50}, nM) of MPH and selected analogs.[46]

MPH (**1**; R = H)
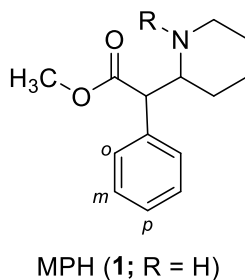
Compound	R	DAT IC_{50} (nM)	NET IC_{50} (nM)
-H (MPH) (**1**)	-H	84	514
o-Br (**2**)	-H	880	20000
m-Br (**3**)	-H	4	20
p-Br (**4**)	-H	21	31
p-OH (**5**)	-H	125	270
p-OMe (**6**)	-H	42	410
p-NO$_2$ (**7**)	-H	180	360
p-I (**8**)	-H	26	32
m-I, *p*-OH (**9**)	-H	42	370
-H (**10**)	-CH$_3$	1400	2800

MPH exists in four stereoisomeric forms (Figure 4): dextro-/levo-threo and dextro-/levo-erythro. Single crystal structures have been elucidated to confirm conformations.[46–48] Most methylphenidate preparations contain a racemic mixture of *d*-MPH and *l*-MPH, with *d*-MPH being approximately 10-fold more potent than the *l*-isomer.[49] The structure activity

relationships (SAR) of MPH have been extensively studied with over 80 analogs having been examined at DAT and several at NET and SERT.[45,50,51]

d-threo-methylphenidate (dtMPH, **1a**)   l-threo-methylphenidate (ltMPH, **1b**)

d-erythro-methylphenidate (deMPH, **1c**)   l-erythro-methylphenidate (leMPH, **1d**)
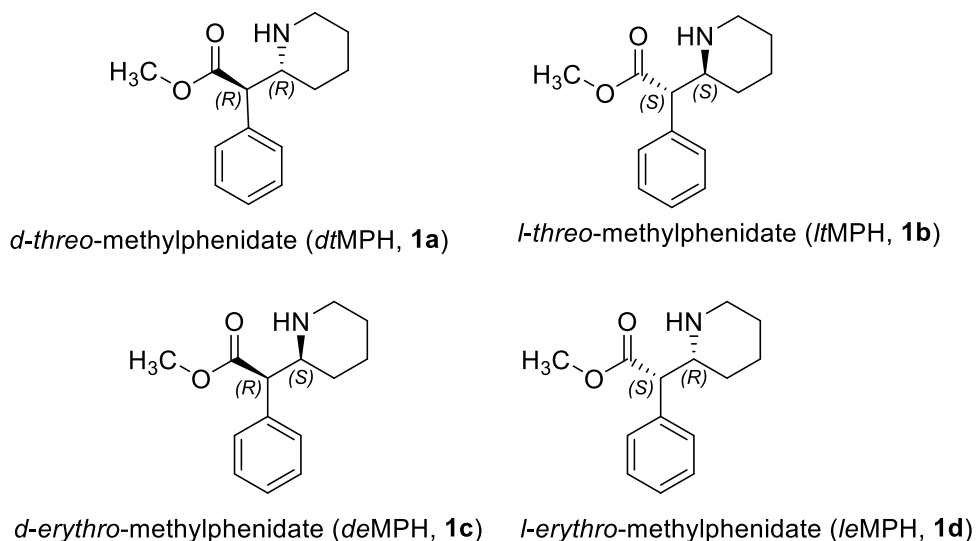
Figure 4. Four stereoisomers of methylphenidate.

The data suggest that the 2' position of the phenyl ring cannot accommodate much steric bulk, while the addition of electron-withdrawing groups to the 3' or 4' positions enhances DAT binding affinity.[51] Optimal substituents are those primarily situated within the plane of the phenyl ring, whereas substituents with significant bulk above or below the ring's plane reduce binding affinity.[51] Misra et al. proposed modifications for designing new MPH compounds that include placing electron-withdrawing groups at the 3' and 4' positions of the phenyl ring, such as halogen substituents or a 3',4'-benzo analog.[51] In fact, the 3',4'-dichloro halogen substituted dtMPH analog (Figure 5) was the most potent compound tested in the entire series with an IC_{50} of 1.7 nM compared to dtMPH IC_{50} of 83 nM.[51] The 3',4'-benzo dtMPH analog (Figure 5) also had potent activity with an IC_{50} of 11 nM and

remarkably also had affinity for SERT with a K_i of 94.8 nM.[50,51] *dt*MPH itself and the 3',4'-dichloro analog do not seem to have any appreciable affinity for SERT, highlighting that the addition of a 3',4'-benzo substituent, typically considered a bioisotere of 3',4'-dichloro, is a novel strategy to enhance SERT selectivity.[50]

d-threo-methylphenidate (dtMPH, **1a**)
DAT IC_{50} = 83 nM
SERT K_i = >10,000 nM

d-threo-3',4'-dichloromethylphenidate (**11**)
DAT IC_{50} = 1.7 nM
SERT K_i = >10,000 nM

d-threo-3',4'-benzomethylphenidate (**12**)
DAT IC_{50} = 11 nM
SERT K_i = 94.8 nM
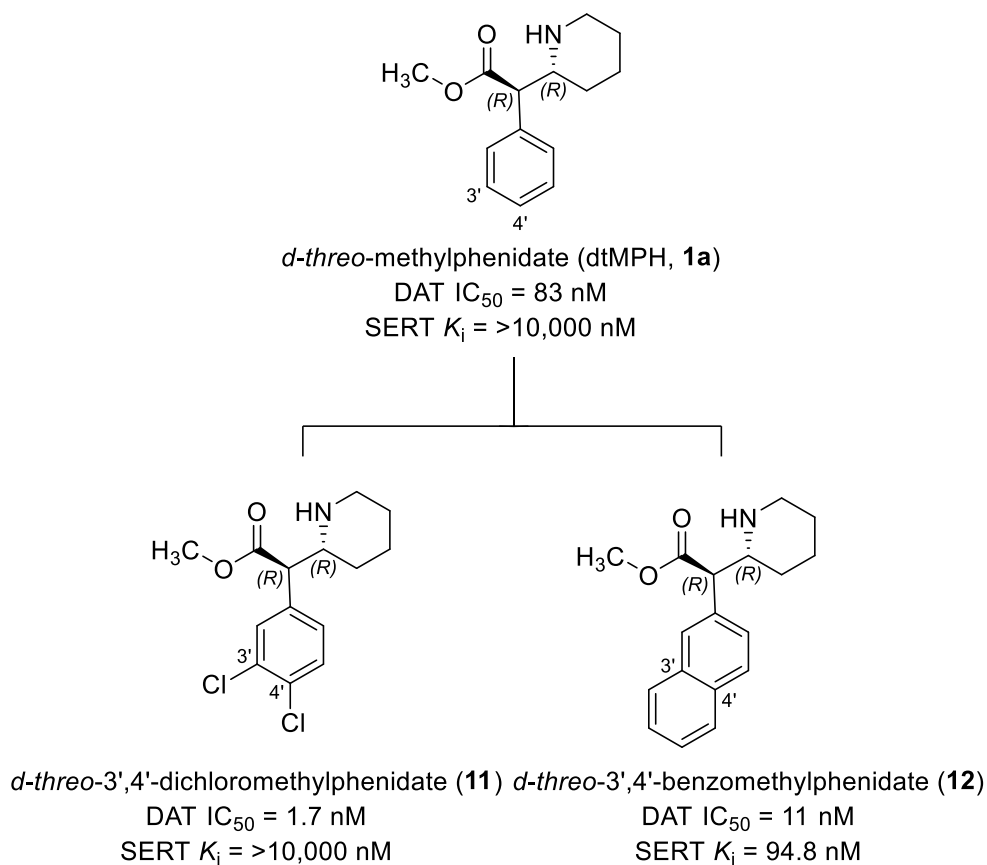
Figure 5. Structures, DAT activity, and SERT affinity for *dt*MPH, 3',4'-dichloro, and 3',4'-benzo analogs.[50,51]

MPH hydrochloride's alkaline nature enables high gastrointestinal solubility, facilitating oral administration.[14] Minimal drug degradation occurs in the acidic stomach environment, with immediate-release formulations being rapidly and completely absorbed, reaching

peak plasma concentrations within one to three hours, albeit with individual variability.[52] Immediate-release MPH has shown efficacy in treating the core symptoms of ADHD— hyperactivity, impulsiveness, and inattention—compared to placebo. However, its effectiveness in addressing accompanying anxiety or depression remains inconclusive due to inconsistent findings.[53]

Multilayer-release MPH formulations have also been developed that are designed to provide extended symptom relief from morning to evening.[54] A study has demonstrated the safety and efficacy of an extended-release formulation with a randomized controlled trial evaluating the 16-hour multilayer-release methylphenidate (PRC-063) in community-based adults with ADHD.[53,54] The findings demonstrated significant symptom improvement compared to placebo. Headache, decreased sleep, and appetite loss are the most common adverse effects.[54,55]

MPH is associated with a higher risk of mild side effects such as sleep disturbances and decreased appetite, although major adverse effects are rare.[31] Other potential side effects include elevated heart rate, increased blood pressure, anxiety, and insomnia. Rarely, MPH use may be linked to arrhythmias, rash, and urticaria. Intravenous administration of MPH may induce a sense of euphoria and can be symptomatic of stimulant use disorder (vide infra).[52]

C. Treatment-Resistant Depression (TRD)

Depression has been a part of the human condition for millennia. It even has been considered a root of the well-known seven deadly sins. In the western world, writing of

15

sorrow or depression originates from early Christian theologians, particularly Evagrius Ponticus, a 4th-century monk and ascetic.[56] Evagrius drew inspiration from the works of the Roman poet Horace, who listed nine logismoi, or evil thoughts, as obstacles to spiritual growth.[56] Evagrius distilled these nine thoughts into eight, one of which was sorrow or sadness as a fundamental spiritual affliction.[56] In Evagrius's schema, sorrow, or tristitia, occupied a significant place among the eight logismoi. He believed that sorrow, when unchecked, could lead to despondency and spiritual apathy, making it a precursor to other sins. This emphasis on sorrow reflected Evagrius's understanding of the human condition, where sadness could arise from a sense of alienation from God and the world. The eight logismoi, including sorrow, were further developed later by Pope Gregory I, who categorized them as the seven deadly sins: pride, greed, lust, envy, gluttony, wrath, and sloth.[56] While sorrow or depression did not make the final list for the traditional deadly sins, its underlying presence was acknowledged as a contributing factor to spiritual malaise. Today, the concept of sorrow or sadness has evolved beyond its theological origins and is often understood in psychological terms. While not inherently sinful, prolonged or intense feelings of sadness also known as depression is a serious mental health condition.

The relationship between sorrow and depression underscores the enduring relevance of the seven deadly sins in understanding human behavior and moral psychology. Just as Evagrius recognized the destructive potential of unchecked sorrow in the spiritual realm, modern interpretations highlight the importance of addressing and managing sadness to promote psychological well-being and moral growth.

1. Symptoms and Incidence of Depression

Depression, according to data from the World Health Organization, is categorized as one of the enduring mental disorders impacting over 350 million individuals globally.[57] This condition disproportionately affects women and is more prevalent among both the young and elderly populations.[58] Numerous indicators may hint at its presence, with common psychological symptoms including persistent sadness, diminished interest in once enjoyable activities, reduced attention span, pessimistic outlook on the future, and a pervasive sense of guilt or worthlessness.[58] Additionally, many sufferers experience physical manifestations such as chronic pain, fatigue, disrupted sleep patterns, decreased appetite leading to weight loss, and diminished libido.[59] Depending on symptom severity, patients can be categorized as experiencing mild, moderate, or severe depression and may be recommended specific treatments upon diagnosis.[59] The primary therapeutic approaches encompass psychological interventions and pharmacotherapy. Due to the heightened risk of recurrence with each episode, patients often undergo prolonged treatment. However, there are no definitive guidelines dictating the duration of treatment following the initial episode of depression.[60]

Despite the substantial evidence backing the effectiveness of traditional antidepressants, manual-based psychotherapies, and certain neurostimulation techniques, many individuals diagnosed with Major Depressive Disorder (MDD) show inadequate responses to initial treatment approaches.[61–64] Furthermore, a significant portion of these individuals do not respond to multiple attempts with antidepressant medications, leading to what is termed treatment resistant depression (TRD).[63–66] While non-response frequently occurs when treating with multiple traditional antidepressants, there is currently

no agreed-upon consensus definition of TRD that provides predictive utility.[67] Instead, various definitions have been put forward, varying in conceptual framework, operational criteria, and underlying assumptions.[67,68] This diversity in definitions has led to a broad spectrum of estimates regarding the prevalence of TRD. The incidence of TRD tends to be higher when employing multidimensional definitions, particularly those incorporating patient-reported outcomes.[67–69]

2. Clinically Used Antidepressants

The pharmacotherapy of depression is a complex and underexplored subject due to the numerous factors involved in the disorder's pathomechanism. Medications commonly prescribed for depression augment neurotransmission of 5-HT and fall into six main categories: serotonin reuptake inhibitors (SSRIs), norepinephrine reuptake inhibitors (NRIs), serotonin and norepinephrine reuptake inhibitors (SNRIs), tricyclic antidepressants (TCAs), monoamine oxidase inhibitors (MAOIs), and atypical antidepressants. While the NRI category may appear to only modulate norepinephrine, the mechanism behind the antidepressant effect of NRIs involves the facilitation of serotonin release, which is mediated by α1-adrenoceptors on serotonergic cell bodies.[70] This stimulation increases the firing rate of serotonergic neurons.[70] The agents currently used for the treatment of depression have been thoroughly reviewed.[71]

Before 1954, apart from electroconvulsive therapy, there were no effective treatments for depression.[71] The discovery of the two major classes of antidepressants, MAOIs and monoamine transport inhibitors (Figure 6), occurred by chance in the 1950s.[71]

18
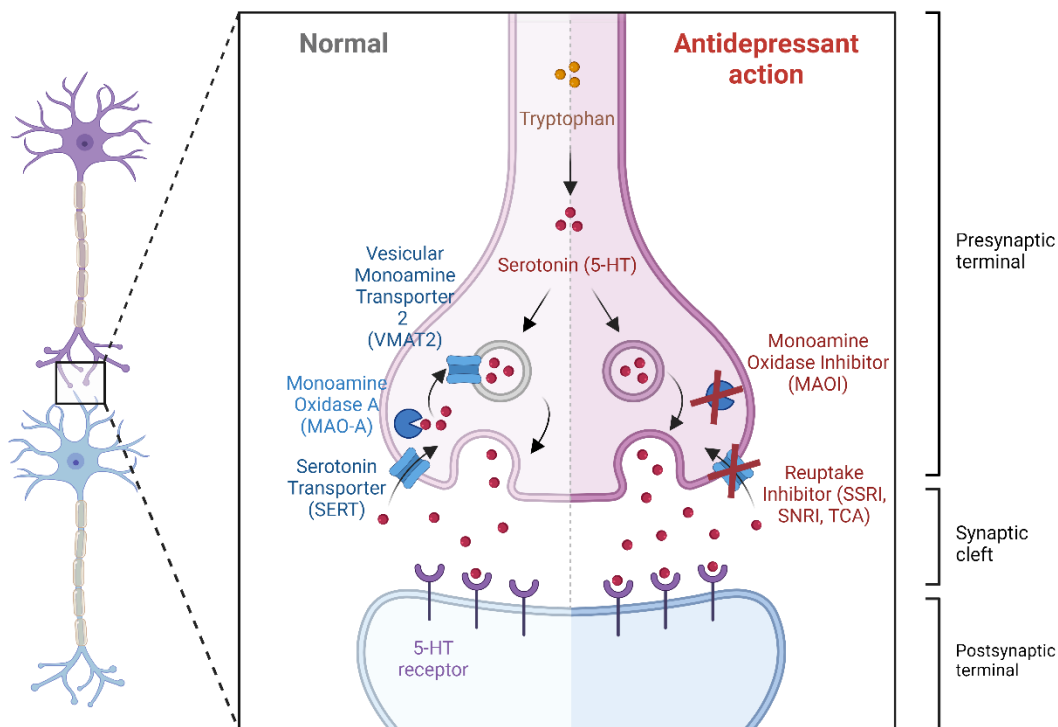
Figure 6. Action of reuptake inhibitors and MAOI antidepressants (created with BioRender.com).

Iproniazid (**13**, Figure 7), a drug used to treat tuberculosis, was found to possess mood-elevating properties.[71,72] Clinical studies conducted by George Crane and Nathan Kline in the United States demonstrated its effectiveness in treating major depression.[71,73,74] These effects were attributed to its ability to inhibit the monoamine-degrading enzyme MAO (Figure 7).[71,75] Although MAOIs and subsequent developments were highly effective in treating depression, concerns over their potential risks led to their replacement by safer monoamine transport inhibitors (e.g., TCAs, Figure 7).[71] The earliest widely used examples of these drugs were imipramine (**14**) in Europe and amitriptyline (**15**) in the

United States (Figure 7). Originally synthesized by the Swiss company Geigy as a chlorpromazine-like compound with antipsychotic potential, **14** was later found by Swiss psychiatrist Roland Kuhn to be an effective antidepressant.[71,76,77] Merck initially produced **15** as a chlorpromazine-like molecule, which was subsequently demonstrated to have antidepressant properties by Frank Ayd.[66,71]

Iproniazid (**13**) Imipramine (**14**) Amitriptyline (**15**) Fluoxetine (**16**)
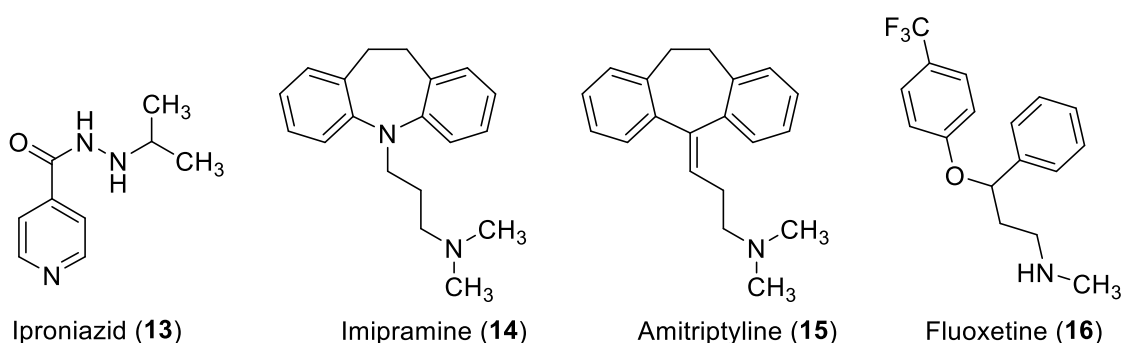
Figure 7. Structures of first clinically used antidepressants.

TCAs non-selectively inhibit the reuptake of 5-HT, NE, and DA into presynaptic storage vesicles in the brain. Although they are effective in treating depression, their effects on other receptor systems, including histaminic, cholinergic, adrenergic, and postsynaptic serotonin receptors unrelated to depression, led to the development of significant, often intolerable adverse effects that limited their use in clinical practice.[78,79] Although TCAs are effective, they have a narrow therapeutic range. At high doses, they can trigger seizures and even fatalities by slowing intraventricular conduction, resulting in complete heart block or ventricular reentry arrhythmias.[79] As a result, there was a shift in research towards developing drugs that maintain efficacy while enhancing safety and tolerability.

Though not the first SSRI, but the first commercially successful SSRI, fluoxetine (**16**), was introduced in the United States at the very end of 1987.[71,80] Its adverse effect profile marked a significant improvement over other available antidepressants due to its selectivity for serotonin transporters. Subsequently, other SSRIs were introduced in the United States and globally. While the efficacy of SSRIs is comparable to that of TCAs, SSRIs exhibit significantly fewer side effects.[81] This was evidenced by fewer patients discontinuing SSRI therapy due to adverse effects compared to those taking TCAs.[82] Unlike TCAs, SSRIs do not induce cardiac conduction abnormalities in overdose and have a low risk of causing seizures.[79] Hence, the development of SSRIs represented a significant milestone in the treatment of depression. SSRIs were initially perceived as nearly devoid of side effects compared to TCAs. Unlike TCAs, they could be safely administered to various patient groups, including the elderly and children, who are particularly susceptible to TCA-related adverse effects. SSRIs could also be prescribed for patients with multiple comorbidities. Due to their efficacy, safety, and tolerability profile, SSRIs have become the frontline pharmacotherapy prescribed by primary care physicians. As a result, more patients are now effectively treated for depression than ever before. Concerns regarding the safety and tolerability of SSRIs have arisen with their chronic prolonged use. For instance, while the original placebo-controlled clinical trials of fluoxetine in depressed patients reported sexual dysfunction in 1.9% of participants receiving fluoxetine, post-marketing clinical trials have indicated rates as high as 75%.[83] Additionally, severe SSRI-induced hyponatremia, not initially reported in clinical trials, is now recognized to occur in approximately 1 in 200 elderly patients annually receiving

fluoxetine.[84] This condition, often associated with the syndrome of inappropriate antidiuretic hormone, is less prevalent in patients treated with other SSRIs.[84]

3. Trends in Treatment of Depression (i.e., 5-HT$_{2A}$ receptor agonists)

A variety of novel antidepressants are currently in clinical trials, and some of them involve agonism or antagonism of 5-HT receptors. 5-HT receptors are divided into seven major families, 5-HT$_1$-5-HT$_7$, and most consist of subfamilies.[65] All are G-protein coupled (GPCR) except for 5-HT$_3$ receptors that are ligand-gated ion channels (LGIC).[65] The 5-HT$_2$ receptor family is the only group that couples to excitatory G$_q$/G$_{11}$ in which agonist activation leads to intracellular Ca^{2+} release and neuronal excitation (Figure 8).[85] The process is initiated once an agonist binds to the receptor's orthosteric binding pocket and the receptor undergoes a conformational change that recruits the G-protein heterotrimer (Gαq, β, and γ proteins). This is followed by the exchange of guanosine diphosphate (GDP) for guanosine-5'-triphosphate (GTP) and subsequent dissociation of the G-protein heterotrimer into a Gαq monomer and βγ heterodimer. The Gαq monomer activates phospholipase C (PLC), leading to the hydrolysis of phosphatidylinositol-4,5-bisphosphate (PIP$_2$), yielding inositol triphosphate (IP$_3$) and diacylglycerol (DAG). IP$_3$ triggers intracellular Ca^{2+} release, while DAG and Ca^{2+} activate protein kinase C (PKC), resulting in increasing neuronal excitability. In order to adapt to over stimulation or persistent activation, the 5-HT$_2$ receptors also interact with β-arrestins for desensitization.[86] The recruitment of β-arrestins causes endocytosis through the process of scaffolding the protein into intracellular compartments. [87]
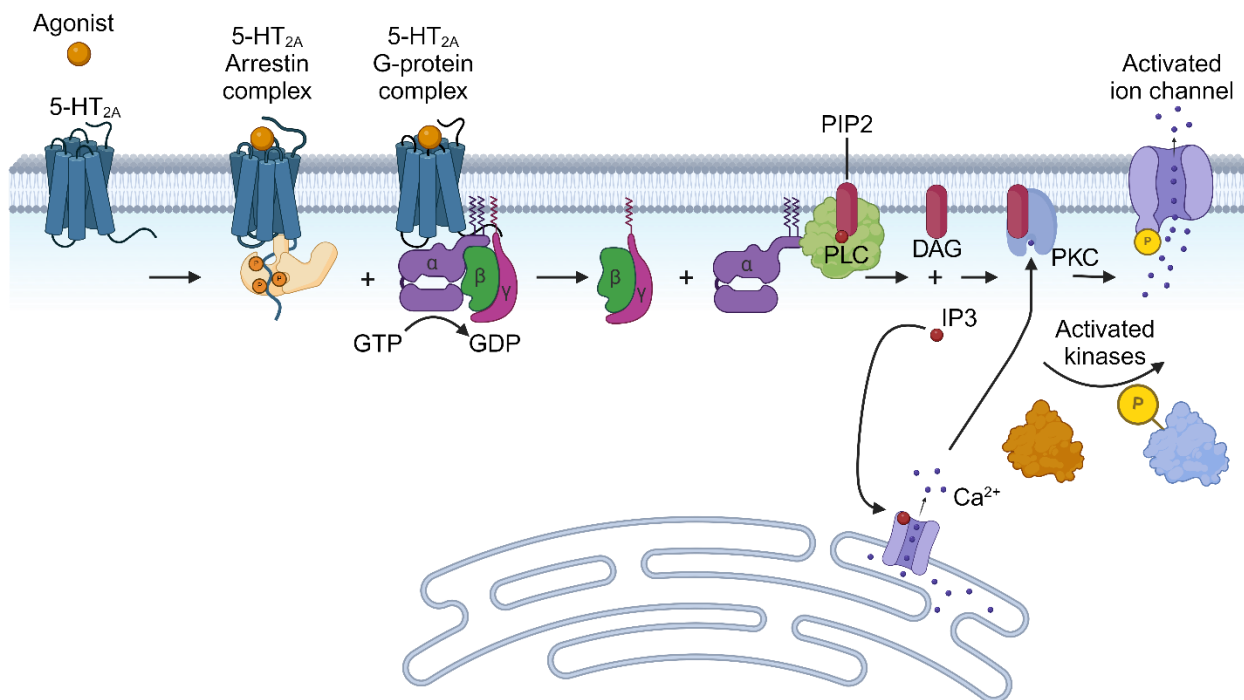
Figure 8. 5-HT$_{2A}$ receptor signaling pathway (created with BioRender.com).

The 5-HT$_2$ receptor subfamily consists of 5-HT$_{2A}$, 5-HT$_{2B}$, and 5-HT$_{2C}$, and of particular interest here are the 5-HT$_{2A}$ receptors. These receptors are predominantly found on layer V cortical pyramidal neurons and localized on apical dendrites.[88] Traditionally, in neuropsychopharmacology, the activation of 5-HT$_{2A}$ receptors has been viewed as potentially detrimental or at least non-conducive to mental health. This perspective is supported by two main arguments. First, 5-HT$_{2A}$ receptor agonists such as LSD (**17**) and psilocybin (**18**) are considered to mimic certain symptoms of psychosis and second, many antidepressants and antipsychotics possess 5-HT$_{2A}$ receptor antagonist properties.[89–92] However, recent research has begun to challenge the notion that 5-HT$_{2A}$ receptor agonism is inherently undesirable for psychotropic medications and specifically antidepressant treatment.[93] Classical hallucinogens, currently referred to as serotonergic

psychedelics, can be divided into two broad structural families: indolealkylamines such as LSD (**17**), psilocybin (**18**), and phenylalkylamines such as DOM (**19**), DOI (**20**), mescaline (**21**), and 25I-NBOMe (**22**) (Figure 9). These hallucinogenic agents act as 5-HT$_{2A}$ receptor agonists.[94–96]
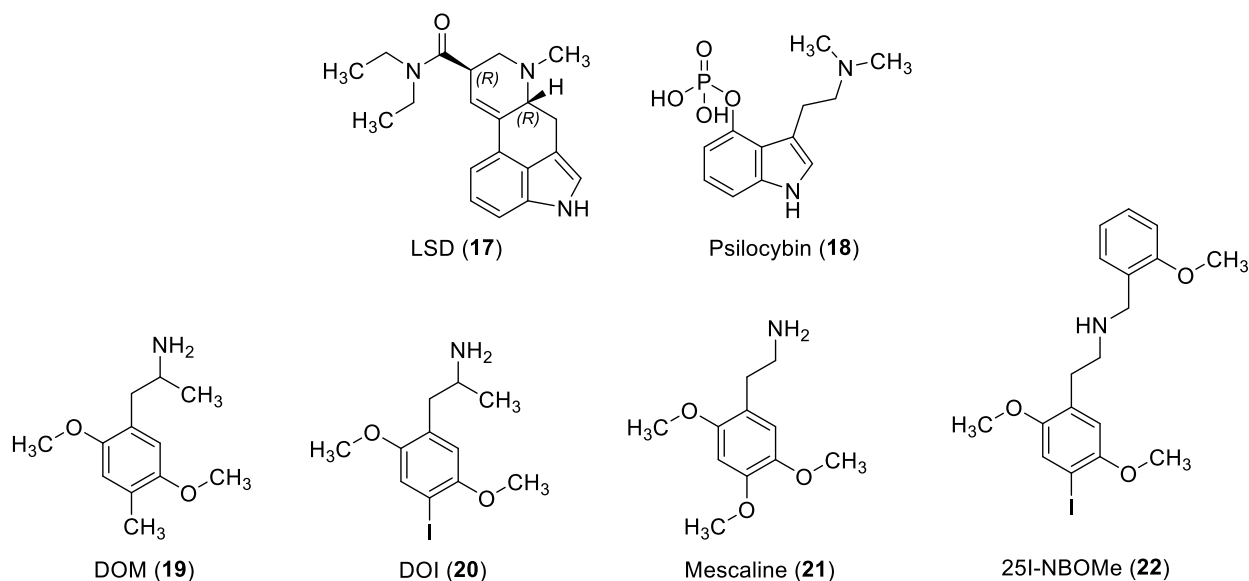
Figure 9. Selected serotonergic psychedelic agents.

In terms of harm, comparative rating scales suggest that 5-HT$_{2A}$ agonist psychedelics such as psilocybin (**18**) rank among the least harmful drugs with potential for misuse.[97] Furthermore, an increasing body of evidence reports lasting positive mental health outcomes and enhanced psychological well-being associated with the administration and use of 5-HT$_{2A}$ receptor agonist psychedelics.[98,99] Additionally, several studies have identified associations between 5-HT$_{2A}$ receptor polymorphisms and SSRI response, although it remains unclear whether alleles predicting better response are linked to

increased or decreased 5-HT$_{2A}$ receptor functioning.[100] Supporting the notion that targeting the 5-HT$_{2A}$ receptor can serve as a viable approach for antidepressant therapy, a growing body of research has demonstrated the antidepressant potential of 5-HT$_{2A}$ receptor agonist psychedelics. For instance, several studies have reported rapid and sustained improvements in depressive symptoms following psilocybin treatment sessions in patients with TRD.[101–103] These findings align with other studies reporting reductions in depressive symptoms in depressed individuals treated with ayahuasca, as well as in patients with end-of-life anxiety treated with psilocybin.[104–106] Ayahuasca is a plant-derived concoction that consists of several *β*-carbolines such as harmine (**23**) and the indolealkylamines DMT (**24**) and 5-MeO-DMT (**25**) (Figure 10).[107] Additionally, a population-based study revealed lower rates of psychological distress and suicidality associated with psychedelic drug use.[98] Collectively, these results challenge the conventional view that psychedelics pose harm to mental health and prompt a reevaluation of the role of 5-HT$_{2A}$ receptor signaling in depression pharmacology.
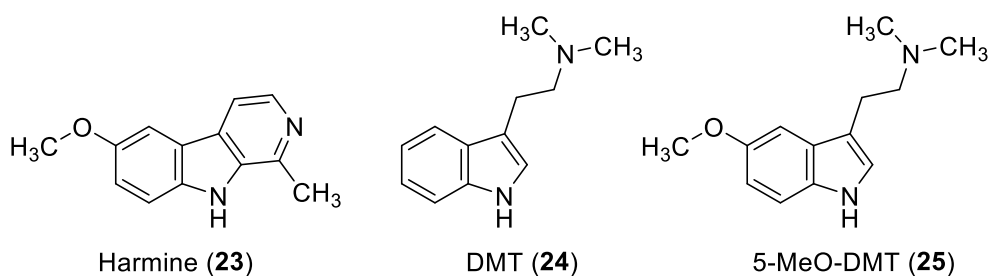
Figure 10. Selected constituents of ayahuasca.

Additional evidence supporting a positive link between 5-HT$_{2A}$ receptor signaling and psychological well-being comes from human PET imaging studies, that have revealed a positive association between 5-HT$_{2A}$ receptor binding and traits such as neuroticism, pessimism, and personality disorders.[108–110] Cortical expression of 5-HT$_{2A}$ receptors is influenced by basal 5-HT levels, with 5-HT$_{2A}$ receptors becoming more abundant and/or available in response to decreased synaptic 5-HT, and less available in response to increased synaptic 5-HT. Heightened 5-HT$_{2A}$ receptor binding and associated pessimistic tendencies might stem from deficient 5-HT$_{2A}$ receptor signaling.[109] Furthermore, the enduring enhancements in optimism observed with LSD (**17**) use could be interpreted as evidence of profound 5-HT$_{2A}$ signaling exerting a lasting influence on positive thinking.[111]

Postmortem investigations revealing elevated 5-HT$_{2A}$ receptor availability in untreated depressed individuals and individuals who died by suicide could support the notion of an adaptive upregulation of 5-HT$_{2A}$ receptors in response to deficient signaling in depression.[112,113] However, conflicting findings (such as reduced 5-HT$_{2A}$ receptor availability in depression and suicide cases) challenging this hypothesis might be attributed to the confounding influence of antidepressant and other psychiatric medications.[114,115] These medications can reverse this relationship by downregulating 5-HT$_{2A}$ receptor availability.[115]

The paradoxical nature of 5-HT$_{2A}$ receptor agonist psychedelics, which can induce acute psychotomimetic effects while also yielding long-term benefits for well-being and mental health, has been previously explored.[111] It has been suggested that the acute state induced by these psychedelics does not directly influence mood valence, meaning it does not inherently promote either positive or negative mood.[111] However, this argument may

be contested based on evidence showing positive mood effects following acute administration of psychedelics, as well as the positive mood effects of substances such as MDMA (**26**, Figure 11), LSD, psilocybin, and ayahuasca, which are all diminished by pretreatment with a 5-HT$_{2A}$ receptor antagonist. Similarly, the prosocial effects of MDMA are also attenuated by 5-HT$_{2A}$ receptor antagonism.[116] On the other hand, anxiety and psychosis-like symptoms are frequently observed acutely with psychedelics, and these effects can also be mitigated by 5-HT$_{2A}$ receptor antagonists.[117]

MDMA (**26**)
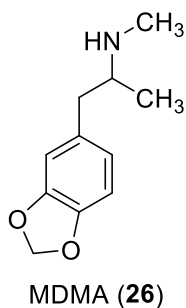
Figure 11. Structure of MDMA or 3,4-methylenedioxymethamphetamine (**26**).

Furthermore, studies reporting enhanced mood with psychedelics often provided psychological preparation and support, which could influence the experience positively. Similarly, volunteers might have harbored positive expectations about their experience, biasing their perception of the acute effects.[116] Regardless, research into effective treatments for TRD through the use of 5-HT$_{2A}$ receptor agonists is currently going through a belle époque.

4. Alpha-ethyltryptamine (α-ET)

Alpha-ethyltryptamine (α-ET, **27**) is quite the enigmatic substance as being a controlled U.S. schedule I drug that during a short period in the 1960s was an FDA approved antidepressant or "psychic energizer".[118] Its removal from the market was due to idiosyncratic agranulocytosis with at least four deaths being attributed to use.[119] Inexplicably, in the original patent from Upjohn, α-ET was specifically stated to not cause agranulocytosis and in addition could be used as a treatment for arthritis.[120] Between removal from the market in 1962 and DEA scheduling in 1993, α-ET was sold as a fine chemical by Aldrich Chemical Company.[121] Scheduling occurred directly resulting from the court case of United States v. Forbes, 806 F. Supp. 232 (D. Colo. 1992). In this case α-ET was legally purchased by the defendant but then sold for human consumption. The prosecution argued that α-ET was substantially similar in structure to the already illegal DMT (**24**). Several expert chemists and neuropharmacologists on the defense and prosecution could not agree on the similarity of α-ET and **24** in both structure and effects. Overall, the case was dropped due to the unconstitutional vagueness of the Controlled Substances Analogue Enforcement Act of 1986. As far as effects, originally α-ET was considered to primarily work through MAO inhibition as a reversible MAOI similar to other antidepressants of the 1950s.[122,123] Decades later it was shown to cause reuptake inhibition of 5-HT and release of 5-HT back through SERT as well as showing stereospecific activity as a 5-HT$_{2A}$ receptor partial agonist.[118,123–126] There is one chiral center which translates to two possible stereoisomers (Figure 12).
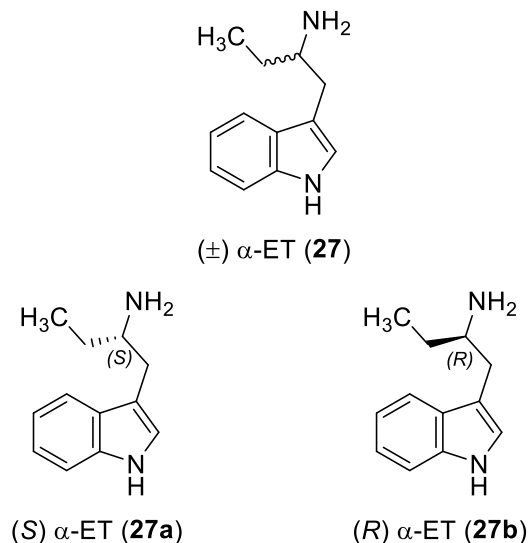
Figure 12. Structure of α-ET or 1-(1*H*-indol-3-yl)butan-2-amine (**27**) and stereoisomers (**27a** and **27b**).

The *S* isomer (**27a**) was not only active as a weak partial agonist at the 5-HT$_{2A}$ receptor in a Ca^{2+} mobilization assay with an EC$_{50}$ = 1250 nM and an E$_{MAX}$ of 61% it was also shown to generalize to the hallucinogens LSD (**17**) and DOM (**19**) in drug discrimination studies.[118,124] However, (*R*) α-ET (**27b**) was inactive in the in vitro study and did not generalize to either classical hallucinogen in drug discrimination.[118,124] This stereospecificity found in mechanism and effects of α-ET also posits the question: Is it possible that only one stereoisomer is responsible for the idiosyncratic agranulocytosis caused by α-ET?

D. Substance Use Disorders (SUD)

Drug addiction remains a significant public health concern worldwide, with devastating consequences for individuals, families, and societies. Understanding the neurobiological mechanisms underlying addiction, particularly the role of DA, is crucial for developing effective prevention and treatment strategies. In this expanded discussion, we will delve deeper into various aspects of SUD specifically focusing on stimulant use disorder and DA's involvement in addiction, including its role in reward processing, reinforcement learning, and the development of addictive behaviors.

DA is a neurotransmitter that plays a central role in the brain's reward system, which is involved in motivating behavior and reinforcing certain actions.[127] There are four major dopaminergic pathways in the brain (Figure 13) that include the nigrostriatial, mesocortical, tuberoinfundibular, and mesolimbic pathways.[128] The mesolimbic DA pathway, originating from the ventral tegmental area (VTA) and projecting to the nucleus accumbens (NA) and other regions of the brain, is particularly implicated in reward processing and reinforcement learning.[129] When we engage in activities that are pleasurable or rewarding, such as eating food or engaging in social interactions, DA neurons in the VTA are activated, leading to the release of DA in the NA and other target regions.[129]
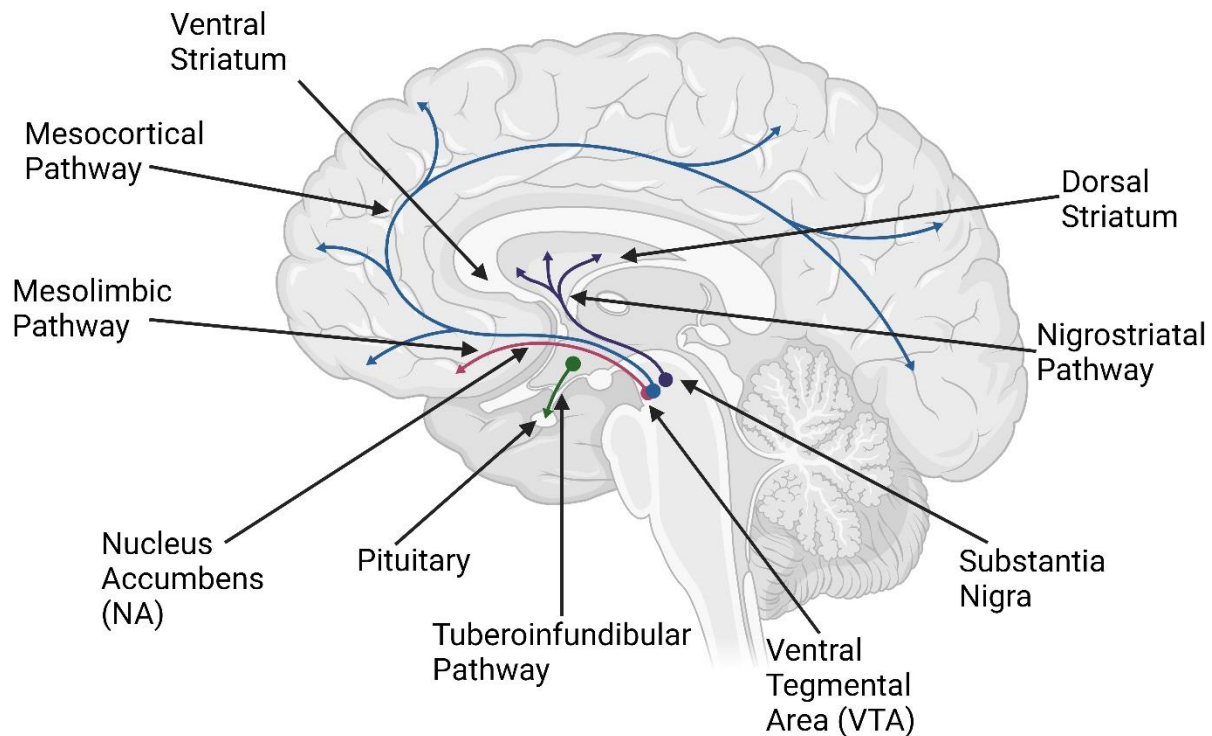
Figure 13. Major dopaminergic pathways of the brain (created with BioRender.com).

In the context of drug addiction, drugs of abuse hijack the brain's reward system, leading to dysregulation of DA signaling. Many addictive substances, including cocaine, amphetamines, opioids, and alcohol, directly or indirectly increase DA levels in the NA, resulting in feelings of euphoria and reinforcing the association between drug use and pleasure.[130] Over time, repeated drug use can lead to neuroadaptations in the brain, including changes in DA receptor expression and function, which contribute to the development of addiction.[131]

One of the key features of addiction is the compulsive seeking and use of drugs despite adverse consequences. DA plays a critical role in mediating the reinforcing effects of drugs and the development of addictive behaviors. Animal studies have shown that DA

signaling in the NA is essential for the acquisition and expression of drug-seeking behaviors.[132] DA release in response to drug-associated cues or contexts can strengthen the association between environmental stimuli and drug rewards, leading to cue-induced craving and relapse.[133]

Moreover, DA is involved in reinforcement learning processes that underlie the formation of habits and automatic behaviors. Through its actions in the striatum and other brain regions, DA helps to reinforce actions and behaviors that lead to reward while suppressing those that do not.[134] In the context of addiction, this can manifest as the compulsive seeking and use of drugs despite negative consequences, as drug-associated cues and contexts acquire strong incentive value through their association with DA-mediated rewards.[135]

The role of DA in addiction extends beyond reward processing and reinforcement learning to include aspects of decision-making, impulsivity, and executive function. Dysfunction in DA signaling has been implicated in various neuropsychiatric disorders characterized by impaired impulse control and decision-making, including addiction, ADHD, and impulse control disorders.[136] Changes in DA receptor expression and function in the prefrontal cortex, a brain region critical for executive function and decision-making, have been observed in individuals with addiction.[137] These alterations may contribute to deficits in self-control and decision-making observed in addicted individuals, leading to continued drug use despite negative consequences.

In addition to its role in the acute reinforcing effects of drugs and the development of addictive behaviors, DA also plays a crucial role in relapse, which is a major challenge in the treatment of addiction. Relapse can occur in response to various triggers, including

drug-associated cues, stress, and negative emotions, and is thought to involve dysregulation of DA signaling in the brain.[138] Animal studies have shown that exposure to drug-associated cues or contexts can trigger DA release in the NA and other regions of the brain, leading to reinstatement of drug-seeking behavior.[139] Moreover, chronic drug exposure can lead to neuroadaptations in the DA system, rendering individuals more vulnerable to relapse even after a period of abstinence.[140]

Understanding the neurobiological mechanisms underlying relapse is essential for developing effective treatments for addiction. Recent advances in neuroscience have shed light on the neural circuits and neurotransmitter systems involved in relapse, including the role of DA, glutamate, and other neurotransmitters.[141] DA signaling in the ventral striatum has been implicated in stress-induced reinstatement of drug seeking.[142] Targeting these neurobiological mechanisms with pharmacological or behavioral interventions holds promise for preventing relapse and promoting long-term recovery in individuals with addiction.

1. Central Stimulants

The abuse of central stimulants is on the rise. There are currently no pharmacotherapies approved for treatment of misuse. When compared individually (e.g., cocaine, methamphetamine, amphetamine) to opioids, the stimulants are far outpaced by opioid related deaths.[143] On the other hand, when all stimulants are combined, they have had the largest increase of associated deaths nationwide from 1999 to 2022.[143] Stimulants can be categorized from two perspectives. One viewpoint is to group them by mechanistic characteristics. That is to say categorization based on whether the agent is a monoamine

releasing substrate or a monoamine reuptake inhibitor. While this perspective gets to the root of understanding drug actions and is invaluable from a drug design or therapeutic aspect, it lacks the simplicity found in the viewpoint of structural backbone classification. The next three subsections will explore the most well-known and popular central stimulants of abuse utilizing this latter frame of reference.

a. Amphetaminergic agents

Amphetamine (**28**, Figure 14), discovered over a century ago, has evolved significantly from a widely available over-the-counter remedy for various ailments to a tightly regulated controlled substance, primarily prescribed for attention deficit hyperactivity disorder (ADHD, vide supra) and narcolepsy.[36,144] Amphetamine's wide range of pharmacological effects contributes to its therapeutic benefits but also leads to adverse effects and potential for recreational misuse. Balancing its benefits and risks is a key challenge in its clinical application. Although racemic α-methylphenethylamine (**28**) was discovered by the Romanian chemist Lazăr Edeleano in 1887 it was not studied for its sympathomimetic effects until 1910 by Barger and Dale.[145,146] The sulfate salt was synthesized in 1927 by chemist G. A. Alles, who was seeking a cheaper and more easily produced alternative to ephedrine.[147] Experiments conducted by Alles and others on animals and humans clearly demonstrated the compound's ability to counteract drug-induced anesthesia and induce arousal and insomnia.[148–150] The pharmaceutical company Smith, Kline, and French registered the trade name "Benzedrine" for racemic **28**.[36] The term "amphetamine"—the generic name for Benzedrine—was adopted much later, as designated by the Council on Pharmacy and Chemistry of the American Medical Association, which is why early

publications refer to Benzedrine rather than amphetamine.[36] Smith, Kline, and French introduced Benzedrine to the market in 1935 as a treatment for narcolepsy (a use that continues today), mild depression, post-encephalitic Parkinsonism, and a variety of other conditions.[36] Two isomers of **28** exists due to the chiral center at the α-carbon atom. Both isomers were synthesized, and it was discovered that the *S* isomer (**28a**) was the more potent of the two and by 1937 Smith, Kline, and French marketed this isomer under the trade name Dexedrine.[36] Today, the *R* isomer is sold over the counter as a nasal decongestant while mixed salt formulations are on the market for ADHD treatment.

The other most well-known amphetaminergic agent is the methylated amine derivative of **28** known as methamphetamine (**29**). Following the discovery of **28** by six years, **29** was first synthesized from ephedrine in 1893 by the Japanese pharmacologist Nagayoshi Nagai, although, it did not see widespread use until World War II.[151]
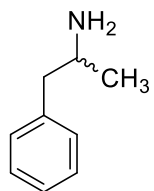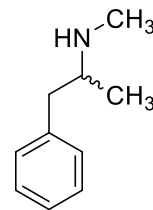
Figure 14. Structures of α-methylphenethylamine or amphetamine (**28**), methamphetamine (**29**), their *R* and *S* isomers (**28a**, **28b**, **29a**, and **29b**, respectively), and lisdexamfetamine (**30**).

During the war, Japan, Germany, and the United States provided the drug to military personnel to increase endurance and performance.[152] In Japan, **29** was also used to improve productivity among civilian factory workers in military support industries.[152,153] Starting in 1941, **29** was sold over the counter in Japan under the names Philopon and

36

Sedrin, marketed as products to "fight sleepiness and enhance vitality."[152,153] However, widespread abuse only became apparent after the war when surplus army stocks of **29** flooded the market, leading to the "First Epidemic" (1945-1957).[153] By 1948, approximately 5% of Japanese individuals aged 16 to 25 had abused **29**.[153] By 1954, it was estimated that there were 550,000 methamphetamine (**29**) abusers in Japan, with about 10% showing symptoms of methamphetamine-induced psychosis.[153] In the United States, **20** was widely prescribed in the 1950s and 1960s as a treatment for depression and obesity, peaking at 31 million prescriptions in the United States in 1967.[152] As with amphetamine, the *R* isomer (**29a**) is the distomer while the *S* isomer (**29b**) is the eutomer. Currently **29** is U.S. Schedule II and one of the most widely abused stimulants.[143,151]

A non-active prodrug amphetaminergic agent, lisdexamfetamine (**30**), is also presently prescribed as an ADHD medication. The body metabolizes off the lysine moiety attached to the amphetamine nitrogen atom producing the most potent amphetamine stereoisomer **28b**. It was designed as a lower abuse potential ADHD therapy, yet abuse and misuse is still prevalent.

b. Cocaine

Cocaine (**31**, Figure 15) is a naturally occurring sympathomimetic alkaloid derived from the *Erythroxylon coca* plant, that has been used as a stimulant in South America for over 5,000 years through chewing of the leaves or brewing teas.[154] It was first isolated from the leaves in the mid-1800s and was initially considered safe, being used in toothache drops, nausea pills, energy tonics, and the original 'Coca-Cola' beverage.[155,156] Today, **31** is typically abused as either the hydrochloride salt or as the free base.[154] The salt is most

often consumed nasally insufflated or injected whereas the free base is consumed via inhalation. Abuse of **31** remains a major public health issue with significant socio-economic impacts worldwide. According to the World Drug Report, 0.4% of the global population aged 15–64 used cocaine in 2019, equating to approximately 20 million people.[157] The latest European Monitoring Centre for Drug and Drug Addiction (EMCDDA) Drug Report indicates that cocaine is the second most abused substance in the European Union.[158]
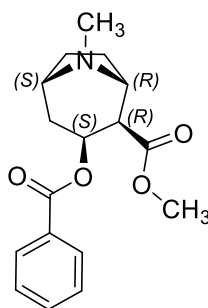
Cocaine (**31**)

Figure 15. Structure of cocaine (**31**).

c. Cathinones

Found to naturally occur in both the plant *Catha edulis* Forsk and the entomopathogenic fungus *Massospora cicadina*, cathinone (**32**, Figure 16), is a monoamine releasing substrate with similar structure and activity to amphetamine (**28**) with a β-ketone moiety being the only difference in structures.[159,160] The plant, also known as khat, has been used both for special occasions and recreationally for centuries in Eastern and Southern Africa, Southwest Arabian Peninsula and in Afghanistan.[161] Fresh leaves and stalk are

chewed; use still persists to today with a high prevalence (e.g., in Yemen, use among men ranges from 80 to 90%) and has even spread to Europe and the United States.[162] Khat leaves are chewed fresh due to older, dried-leave enzymatic processes that reduce the β-ketone to the hydroxyl-group containing cathine (**33**, Figure 16).[163] Originally, **33** was believed to be responsible for the stimulant effects induced by the plant and was first detected in 1887 by Flückiger and Gerock then identified in 1930 by Wolfes.[164,165] It was not until 1975 that the psychostimulatory potency was correctly attributed to **32** isolated from fresh khat leaves.[166]

Cathinone (**32**)   Cathine (**33**)
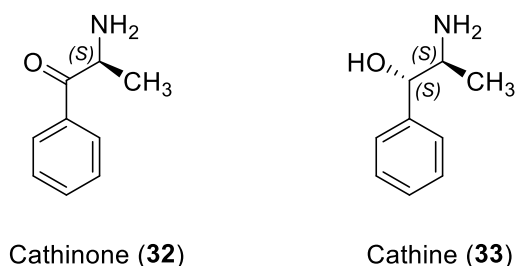
Figure 16. Structures of naturally occurring cathinone (**32**) and cathine (**33**).

Cathinone has two possible isomers but naturally occurring cathinone exists as the *S* isomer.[166] By 1984, the *S* isomer was found to be the eutomer similarly to amphetamine.[167]

More recently, naturally occurring **32** has been discovered in the active host transmitting parasitic fungus, *Massospora*, that infects at least 21 different species of cicadas worldwide.[160] The infected insect loses its abdomen, approximately one third of its body, and it is replaced by an emerging conspicuous conidial "plug".[160] Consequently, spores

are dispersed from the posterior while the infected insect attempts mating and flight that are in no way reduced despite the robust infection.[160] In fact, hypersexual behaviors are observed, and data suggest that **32** produced by *Massospora* is responsible for this frenzied response.[160] The parasite essentially hijacks cicadas and renders the insects into manic mating machines for fungus proliferation.

Synthetic cathinones were first reported in 1928 by Hyde with the preparation of methcathinone (**34**, Figure 17, term coined 1987).[168,169] The following year, 1929, mephedrone (**35**, Figure 17) was described by Saem de Burnaga Sanchez.[170] By 1958, amfepramone (**36**, Figure 17) was the first synthetic cathinone introduced in the market as an appetite suppressant but was subsequently included in the Schedule I of the 1971 United Nations (UN) Convention on Psychotropic Substances along with **32**, **34**, and pyrovalerone (**37**, Figure 17).[171,172] The United States did not schedule **36** until 1973.[173] Currently, the only approved therapeutic cathinone on the market is bupropion (**38**, Figure 17) that was FDA approved in 1985 presently indicated for adult depression, seasonal affective disorder, and smoking cessation. [174]

Methcathinone (**34**)   Mephedrone (**35**)   Amfepramone (**36**)   Pyrovalerone (**37**)   Bupropion (**38**)
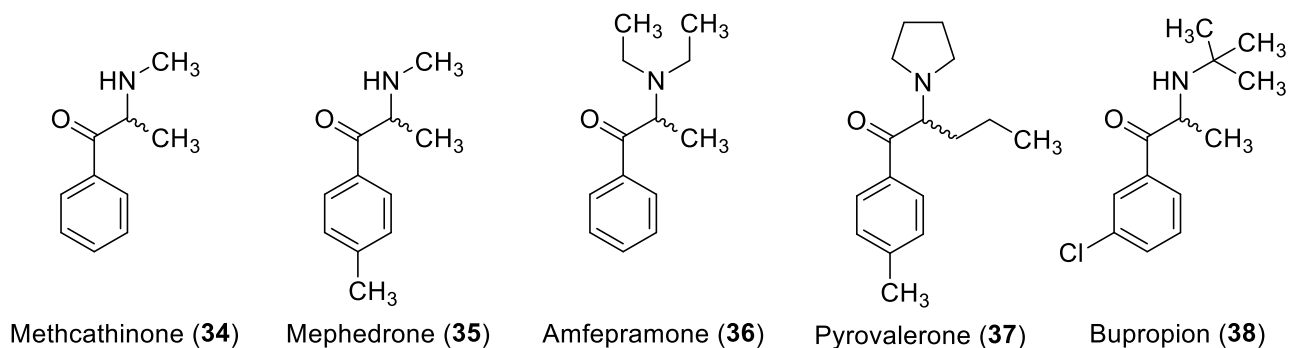
Figure 17. Structures of synthetic cathinones methcathinone (**34**), mephedrone (**35**), amfepramone (**36**), pyrovalerone (**37**) and bupropion (**38**).

Illicit misuse of synthetic cathinones first occurred in the United States with **34** during the 1990s and by the early 2000s there was an explosion of new cathinones on the illicit market with estimates of over 150 different chemical entities.[159,175,176] Some have been scheduled but the number of new synthetic cathinones on the illicit market continues to climb. The most alarming aspect is the lack of known pharmacology on these agents, which presents a significant health concern. Efforts have been made to understand these agents as a class by examining their SAR in comparison to the extensively studied SAR of MPH (**1**) using small molecules as molecular tools.[51,177]

Our lab has developed a hybrid series of compounds utilizing structural motifs from both classes of compounds known as 2-(benzoyl)piperidines or BPs (**39**, Figure 18) in an attempt to determine SAR of unexplored synthetic cathinones for scheduling and harm reduction.[177] That is, MPH is a DAT reuptake inhibitor. Structurally the methyl ester of MPH (Figure 18) contributes to activity at DAT, although its presence is not essential.[51,177–179] Cathinone analogs, depending upon their substituents, can act as reuptake inhibitors or releasing agents. Cathinones with tertiary or bulky amine substituents and/or extended α-alkyl chains act as reuptake inhibitors at DAT but can show mixed action at other monoamine transporters (MATs).[175] For example, pentedrone (**40**) shows reuptake inhibition at DAT and also acts as a substrate releasing agent at SERT.[180] Several cathinones have even demonstrated affinity for 5-HT$_{2A}$ receptors.[181,182]
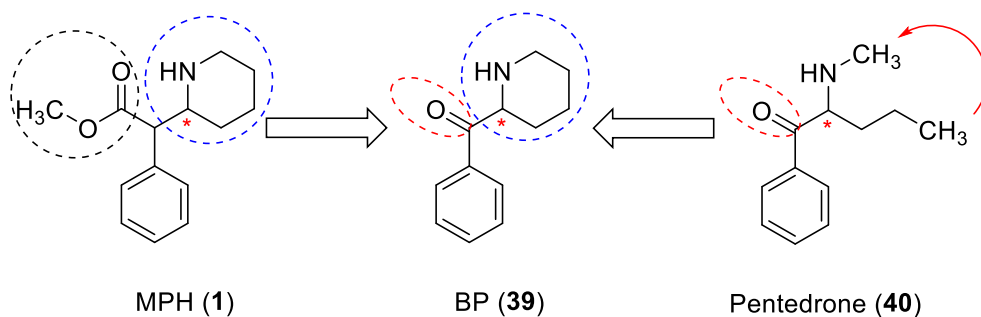
Figure 18. Structure of MPH (**1**), 2-(benzoyl)piperidine or BP (**39**) and pentedrone (**40**).

A robust correlation was found between the sets of BP analogs and MPH (Figure 19).[177] These BP agents might then be considered their own chemical class and could potentially be developed as new, low abuse-liability ADHD pharmacotherapies, antidepressants, or even stimulant use disorder treatments.
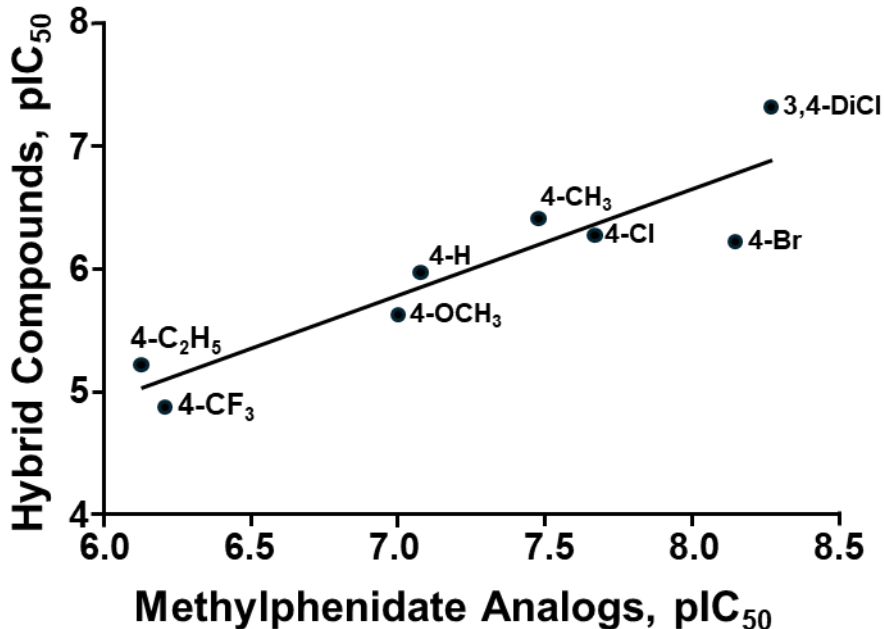
Figure 19. Correlation between DAT binding data for MPH analogs (x-axis) and APP+ uptake assay data (y-axis) for the corresponding BPs.[181]

Three BP agents, DCBP, DMBP and NP (**41**, **42**, and **43**, respectively; Figure 20) will be highlighted and used as molecular tools for this dissertation. These three compounds were previously studied in order to elucidate the cause for the potency of **41**.[183]
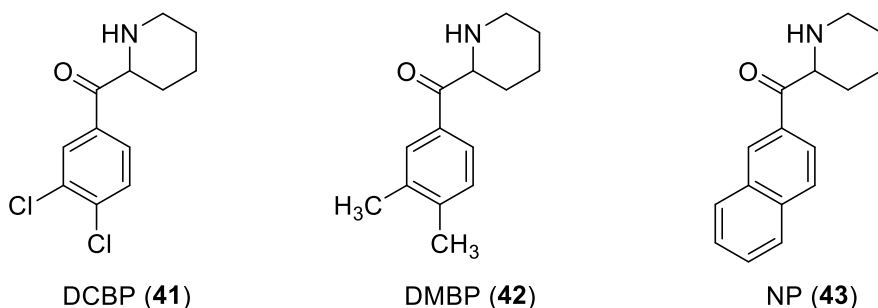
Figure 20. Structures of DCBP (**41**), DMBP (**42**), and NP (**43**).

From the series of BPs with different aryl substituents evaluated at DAT, the most potent compound tested was **41** demonstrating an IC_{50} = 47 nM at DAT.[177] Both **42** and **43** were designed to aid in the assessment of **41** taking advantage of different molecular parameters such as size, electronic character, lipophilicity, and ability to form different types of bonds (Table 3).[183]

Table 3. Lipophilic (π), electronic (σ), steric (Vol), hydrogen bond (HB) acceptor, and halogen bond formation properties of compounds **41-43**.

Parameter	41	42	43
π	1.46[a]	1.03[b]	1.32[a]
σ	0.60[c]	-0.24[c]	0.08[a]
Vol (Å^3)[d]	90.9	88.2	100.0
HB Acceptor	Yes	No	Yes
Halogen Bond	Yes	No	No

[a]Values as reported by Hansch et al.[184] [b]Values as reported by Fujita et al.[185] [c]Values as reported by Jaffé.[186] [d]Volume measured using SybylX 2.1.1.

Initial results indicated that whereas all three compounds were more potent at DAT than BP (**39**) (Table 4), the potency of **41** is not solely related to lipophilicity or size. The question is then posed: Is a halogen bond responsible for the enhanced potency of **41**?

Table 4. DAT uptake inhibition potency (IC_{50}, nM) of germane aryl ring modified BPs.
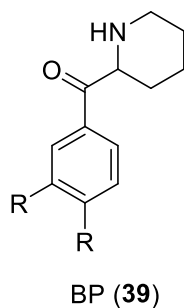
BP (**39**)

Compound		R	IC_{50} (nM)
BP	(**39**)	-H	1080[a]
DCBP	(**41**)	-Cl	47[a]/17[b]
DMBP	(**42**)	-CH$_3$	379[b]
NP	(**43**)	-CHCHCHCH-	50[b]

III. Research Objectives

Serotonergic psychedelic agents act as 5-HT$_{2A}$ receptor agonists, whereas SSRIs act at SERT (Figure 21). MPH (**1**) is a reuptake inhibitor at DAT. The BPs are reuptake inhibitors at DAT but their action at SERT is unknown. α-ET, depending upon the individual optical isomers, acts at 5-HT$_{2A}$ receptors, DAT/NET and/or SERT (Figure 21). Most agents that act at DAT also interact at NET, for example, the potency of MPH analogs at NET was significantly correlated ($r^2 = 0.9$) with their potency at DAT.[45]
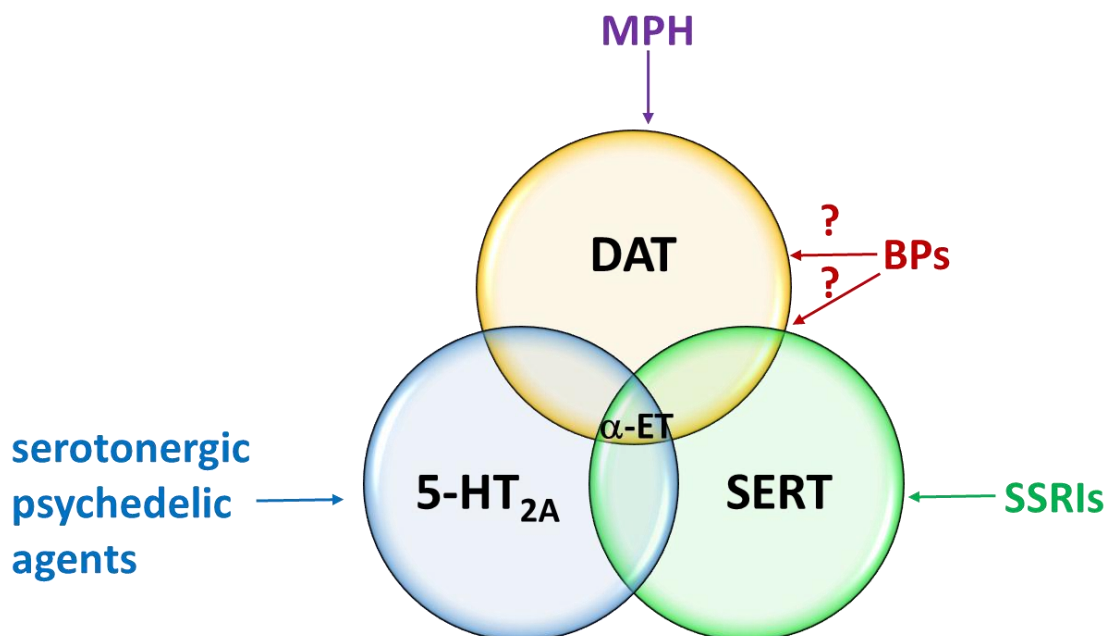
Figure 21. Mechanistic Venn relationship of germane agents.

A. Determine stereoselectivity of benzoylpiperidines at DAT

MPH (**1**) and abused synthetic cathinones seem to share a common SAR as DAT reuptake inhibitors, however, the stereoselectivity of the two scaffolds appears opposite. That is, the MPH eutomer (see Figure 4) at DAT is the *R* stereoisomer at the piperidine 2-position,[49] whereas the abused cathinones eutomer is *S*.[175,187] With BPs being a hybrid between the two molecular scaffolds (Figure 18), it is unknown which isomer is more potent and whether it will mimic MPH or cathinone stereoselectivity (Figure 22). Hence, the optical isomers of **41-43** will be prepared and examined at DAT using computational modeling and in vitro fluorescence assays.

Hypothesis: If BPs behave like MPH, then the *R* isomer should be the eutomer at DAT. If the eutomer is determined to be the *S* isomer, then the benzoylpiperidines can be considered to more closely mimic cathinones.
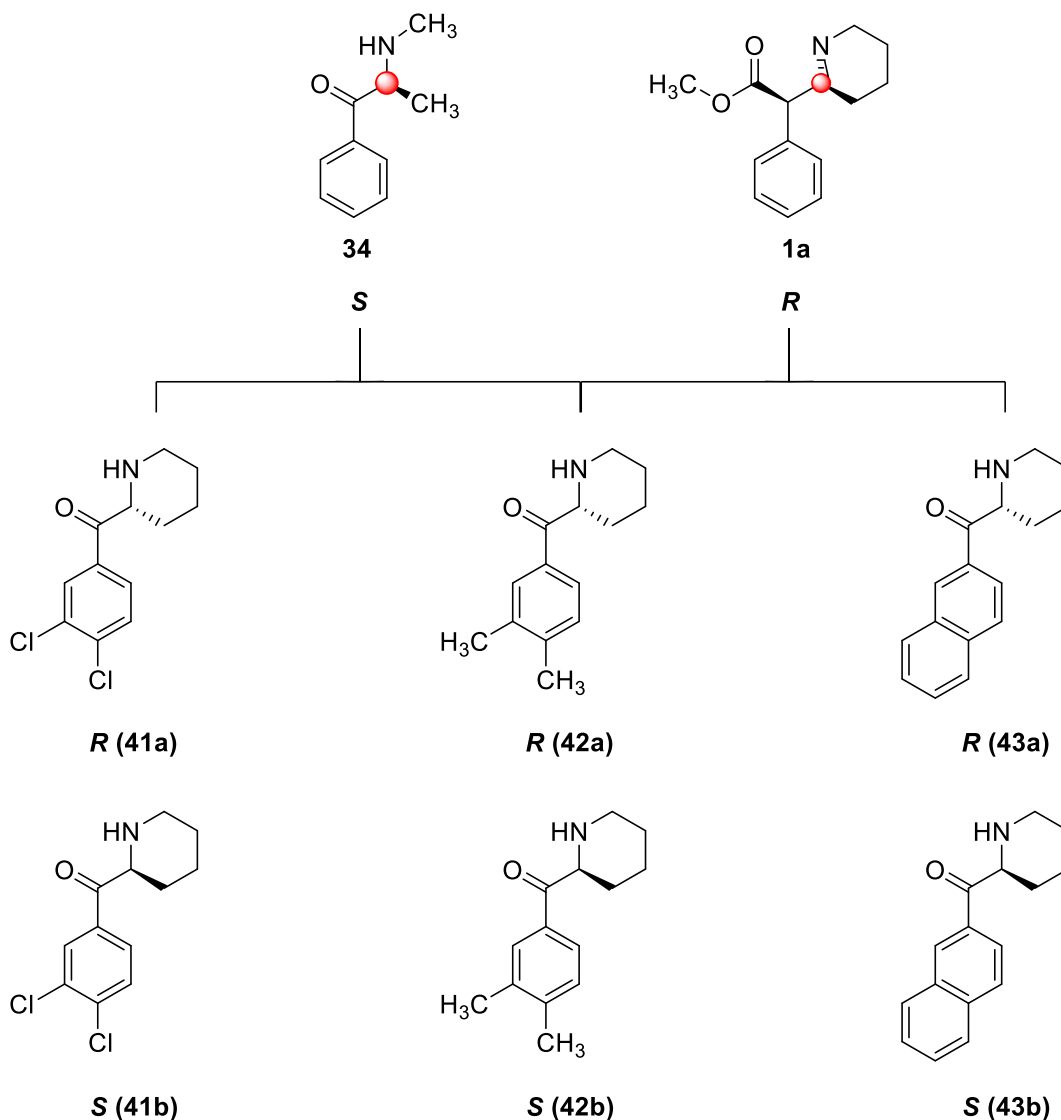
Figure 22. Eutomers of methcathinone (**34**), MPH (**1**), and proposed stereoisomers of DCBP, DMBP, and NP (**41-43**, respectively).

B. Determine activity and stereoselectivity of benzoylpiperidines at SERT

Many cathinone compounds have activity at multiple monoamine transporters (i.e., DAT, SERT, NET). MPH has little to no affinity for SERT and out of only a few MPH analogs that have been examined previously only the 3,4-benz fused analog **12** (Figure 5) showed any appreciable affinity for SERT with the eutomer having the *S* configuration on the piperidine ring. It is unknown if BPs possess any activity and/or stereoselectivity at SERT. Hence, **41-43** and its optical isomers will be examined at SERT using computational modeling, synthesis, and in vitro fluorescence assays performed. If BPs do indeed behave like MPH analogs, then NP should have activity at SERT and the *S* isomer should be the eutomer.

C. Determine function of benzoylpiperidines at SERT

The BPs demonstrate reuptake inhibition at DAT. The substrate/inhibition activity of BPs at SERT is currently not known. Hence, the activity of **41-43** will be examined at SERT using Ca^{2+} channels as sensors. Being a conformationally constrained analog of **40**, BPs might show substrate like activity at SERT.

D. Explore halogen bond formation for DAT S149/DCBP

Computational modeling, as will be seen, suggests that DMBP (**42**) and DCBP (**41**) both bind in a similar manner at DAT, yet biological studies have shown DCBP to be more potent. Modeling of DCBP at DAT suggests that there is the potential to form a halogen

bond with the hydroxyl group of S149 and the chloro-substituent of DCBP (see also Table 3). Mutating DAT to the S149A mutant should provide insight on this interaction if it is occurring. Hence, optical isomers of **41** and **42** will be examined at mutant S149A DAT using computational modeling and in vitro fluorescence assays.

Hypothesis: If DMBP and DCBP are binding in a similar manner at DAT and DCBP is in fact forming a halogen bond, then the DAT mutation S149A should abolish this interaction and the activity of DCBP and DMBP should converge due to the similar steric and lipophilic properties of chloro- and methyl-substituents.

E. Determine affinity/activity for α-ETs at 5-HT$_{2A}$ receptors

The stereoisomers of α-ET (**27**) have shown intriguing activity at 5-HT$_{2A}$ receptors. The *S* isomer demonstrates partial agonist activity in the Ca^{2+} mobilization assay whereas the *R* isomer does not show any activity.[124] There are no binding data for these compounds or for any of the methoxy- or bromo-substituted analogs. The introduction of 4- and 5-position substituents tends to enhance potency of tryptamines in binding and behavioral assays (e.g., psilocybin and 5-MeO-DMT, respectively), but it is unknown for the SAR of the α-ET series. Hence, α-ET and its methoxy- and bromo-substituted analogs (Figure 23) will be studied using computational modeling and also prepared and examined in radioligand binding studies.

(±) α-ET   (**27**)
(±) 4-MeO-α-ET (**44**)
(±) 5-MeO-α-ET (**45**)
(±) 4-Br-α-ET   (**46**)
(±) 5-Br-α-ET   (**47**)

(*S*) α-ET   (**27a**)   (*R*) α-ET   (**27b**)
(*S*) 4-MeO-α-ET (**44a**)   (*R*) 4-MeO-α-ET (**44b**)
(*S*) 5-MeO-α-ET (**45a**)   (*R*) 5-MeO-α-ET (**45b**)
(*S*) 4-Br-α-ET   (**46a**)   (*R*) 4-Br-α-ET   (**46b**)
(*S*) 5-Br-α-ET   (**47a**)   (*R*) 5-Br-α-ET   (**47b**)
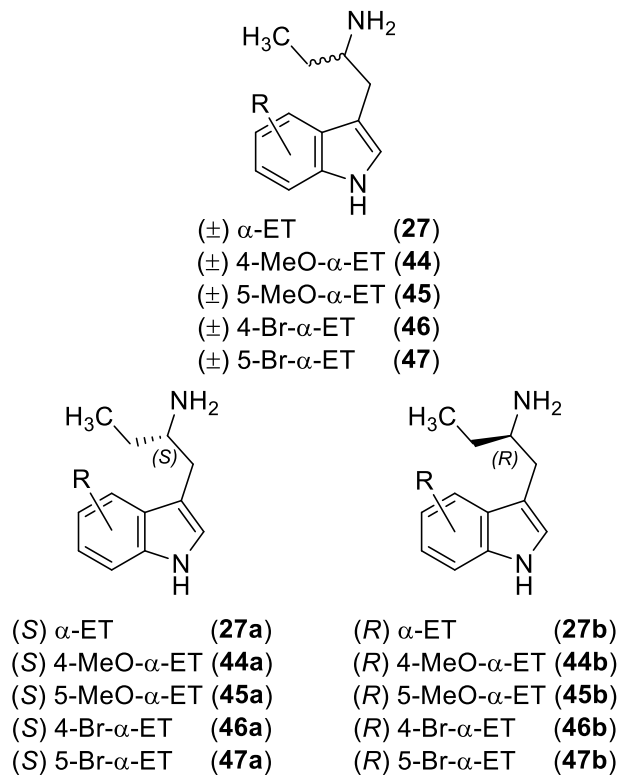
Figure 23. Structure of α-ET analogs to be examined.

Hypothesis: If α-ET and its analogs mimic the behavior of the above-mentioned tryptamines, then the binding affinity of α-ET stereoisomers and methoxy- and bromo-substituted analogs should show that only the *S* isomer of α-ET binds and that the 4- and 5-position substituted analogs should bind with higher affinity than the parent α-ET.

IV. Results and Discussion

A. Determine stereoselectivity of benzoylpiperidines at DAT

1. Homology Modeling of DAT

Over the past 20 years, significant advancements have been made in understanding the structure and mechanism of monoamine transporters (MATs) due in part to X-ray crystallography and cryo-EM. From the initial breakthrough with the crystallization of the orthologous bacterial leucine transporter (LeuT) to more recent structures of the higher-identity *Drosophila* dopamine transporter (dDAT) and human serotonin transporter (hSERT), the development of improved 3D computational models of the human dopamine transporter (hDAT) has been pursued.[188–190] This progress has proven to be crucial for developing new medications for neuropsychiatric disorders associated with dopamine dysregulation. Previous and recent homology models of the yet-to-be-crystallized human dopamine hDAT have relied on a single template for generating an hDAT model. For these studies, a multi-template approach was used to build a 3D homology model of hDAT, where the contributions of individual templates address the missing structural features of single-template models (e.g., extracellular loop 2 (EL2) in dDAT). Based on the primary amino acid sequence similarity (~40%; Figure 24) and mutagenesis studies, it is assumed that all three MATs are structurally similar. Understanding the interaction of hDAT with substrates or inhibitors at the molecular level is crucial for guiding SAR studies in the development of new pharmacological tools and pharmaceutical entities. The functional mechanisms and crystal structures of some MATs have been elucidated over the past two decades. Despite the advancements in structural biology, a crystal structure

of hDAT is still lacking. Nevertheless, homology modeling is used as a surrogate approach to explore hDAT.

Figure 24. Alignment of LeuT, hSERT, dDAT, hDAT, and hNET. Symbols represent: (*) identity, (:) high similarity, (−) similar, and blank space is non similar.

Using the most recent homologs with high identity to hDAT, it is now possible to develop more accurate models than those used in the past. With new crystal structures being solved that are closer to hDAT in terms of identity and total peptide chain length, improved homology models can be generated to study the inner workings of hDAT through docking. The first hDAT homology model, based on the LeuT crystal structure as a template, was

reported in 2007.[191] LeuT has low identity and query coverage (the percentage of contiguous length aligning with the NCBI hit) compared to hDAT. After the crystal structure of dDAT was elucidated in 2013, it served as the next step forward in hDAT 3D homology modeling studies.[190,192] Thus, a DAT crystal structure became available for generating hDAT homology models. The first hDAT homology model using the dDAT crystal structure (PDB ID: 4M48) as a template was reported in 2015.[192] Also, in 2015, a plethora of dDAT crystal structures were elucidated, comprising the remainder of the currently reported dDAT crystal structures.[193,194] The following year, a human MAT, specifically hSERT, was crystallized and its structure reported for the first time.[189] Despite this, most hDAT homology models continued to be developed primarily from the dDAT template. Several homology models had been published using either dDAT PDB ID: 4M48 or 4XPA.[195] Currently, only one hDAT homology model has been reported using hSERT as a template.[196] This model was generated using two crystal structure-bound inhibitors (dDAT PDB: 4XP4 and hSERT PDB: 516X) as templates, and simulated annealing was used to generate EL2. While LeuT, a homolog of MATs, was crucial in understanding the conformational changes in the alternating access model, it is now a poor choice for hDAT homology model generation. This is because there are many more closely related proteins with much higher identity percentages to hDAT than LeuT. Currently, dDAT is the most accurate single template available for hDAT homology modeling.[196] However, dDAT only has outward-open facing crystal structures, which means hDAT homology models of occluded and inward-open facing states cannot be generated using dDAT alone. Another issue that has plagued hDAT homology model development is the inability to properly model EL2 from dDAT due to its removal for single

53

crystal formation in the reported crystal structures. To address this, the crystal structure of hSERT, which possesses an intact EL2, can be used to model this portion of the hDAT homology model.[189] Nevertheless, generating an hDAT homology model using only the hSERT crystal structure as a template is not recommended, as the dDAT crystal structures have a higher percentage identity and use the same endogenous ligand (dopamine) as hDAT.

Using the hDAT target sequence from the NCBI GenPept protein database and the best-fitting dDAT and hSERT crystal structure templates (PDB IDs: 4XPB_A, 4XPT_A, and 6VRH_A), MODELLER was employed to generate 100 homology models.[194,197,198] The best model was selected based on evaluations from scoring functions such as discrete optimized protein energy (DOPE) and GA341.[198,199] Portions of the model that were not properly generated (e.g., residues 1–54) were then truncated. To validate the homology model, both cocaine (**31**) and 3,4-dichlorophenethylamine (**48**, Figure 25) were docked into the model. The docking solutions were compared with the binding modes of **31** and **48** in the co-crystal structures (PDB IDs: 4XPB and 4XPT, respectively).[194] It was found that the new model retained/mimicked the structural features necessary for binding both the blocker and releasing agent (Figure 26). Both test ligands resulted in docking poses that matched the co-crystal structures and retained an essential salt bridge interaction between the nitrogen atom of the ligands and the carboxylate anion of ASP79 in hDAT, corresponding to ASP46 in the dDAT crystal structures. This validated the accuracy of the hDAT homology model.
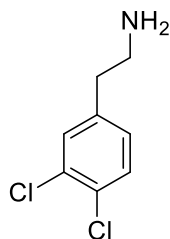
3,4-Dichlorophenylethylamine (**48**)

Figure 25. Structure of 3,4-dichlorophenylethylamine (**48**).

Since the two main types of agents that interact with DAT are blockers and releasing agents, using crystal structure complexes of both types (i.e., PDB IDs: 4XPB for blockers and 4XPT for releasing agents) as templates could enhance docking studies by producing a "dual-purpose" homology model. This should be due to specific molecular interactions between the protein and ligand complex that are characteristic of a particular type of
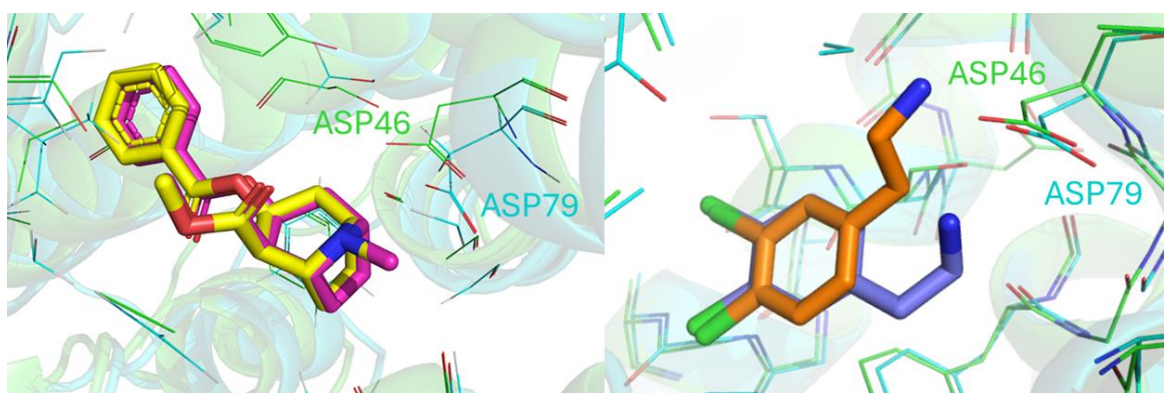
Figure 26. (Left) Validation of the hDAT homology model (cartoon and lines, cyan) with the cocaine (**31**) docking solution (capped sticks, magenta) overlayed with the dDAT crystal structure (PDB ID: 4XPB, cartoon and lines, green) and cocrystallized ligand cocaine (capped sticks, yellow). (Right) Validation of the hDAT homology model (cartoon and lines, cyan) with the 3,4-dichlorophenethylamine (**48**) docking solution (capped sticks, orange) fitted with the dDAT crystal structure (PDB ID: 4XPT, cartoon and lines, green) and cocrystallized ligand 3,4-dichlorophenethylamine (capped sticks, purple).

ligand. Additionally, such a dual-purpose homology model could be useful in studies where the functional activity of chemical entities is unknown, allowing for the docking of both types of agents before determining their function.

Another method used to validate the model was to generate a Ramachandran plot (Figure 27). Approximately 94.6% of the residues in the hDAT homology model are in the most favored regions. A good quality model is expected to have over 90% of the amino acid residues in these regions. No bond lengths, omega torsion angles, or chiral atoms deviated from ideal values. Only a few residues had poor bond angles, but these were close to the 10 Å cutoff and none were within the central binding pocket. The RMSD of the hDAT homology model was compared to the dDAT template for further validation. The RMSD between all atoms of the two proteins was 2.16 Å. An RMSD < 3 Å for the Cα atoms of the backbone is considered a success,[200] indicating that the hDAT homology model is more than satisfactory.
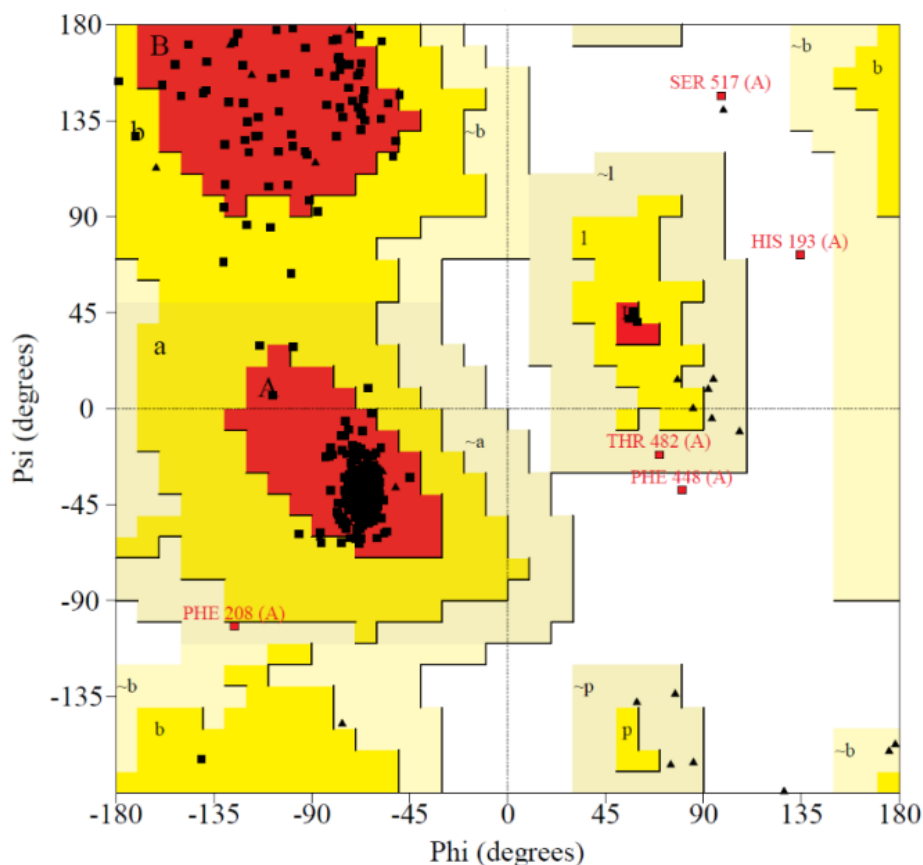
Figure 27. Ramachandran plot of the hDAT homology model. Phi (X-axis) and Psi (Y-axis) represent backbone conformation angles of amino acid residues. Three amino acid residues (HIS193, SER517, and PHE448) were found in the disallowed region (white) of the plot; however, they are not in proximity of the S1 central binding pocket.

Using multiple crystal structures of homologous proteins should produce a more realistic 3D homology model of the proteins of interest compared to using a single crystal structure as a template. By utilizing hSERT and two dDAT crystal structures together, hDAT homology models were generated that account for all extra- and intracellular loops lacking in previous 3D models (Figure 28).[201] With templates that include both a substrate and a blocker, docking studies can be conducted with both types of agents while preserving specific molecular protein/ligand interactions. MODELLER can integrate dDAT and

57

hSERT crystal structures as templates for an hDAT homology model. Additionally, binding

studies can be used to more accurately depict the inner workings of hDAT.
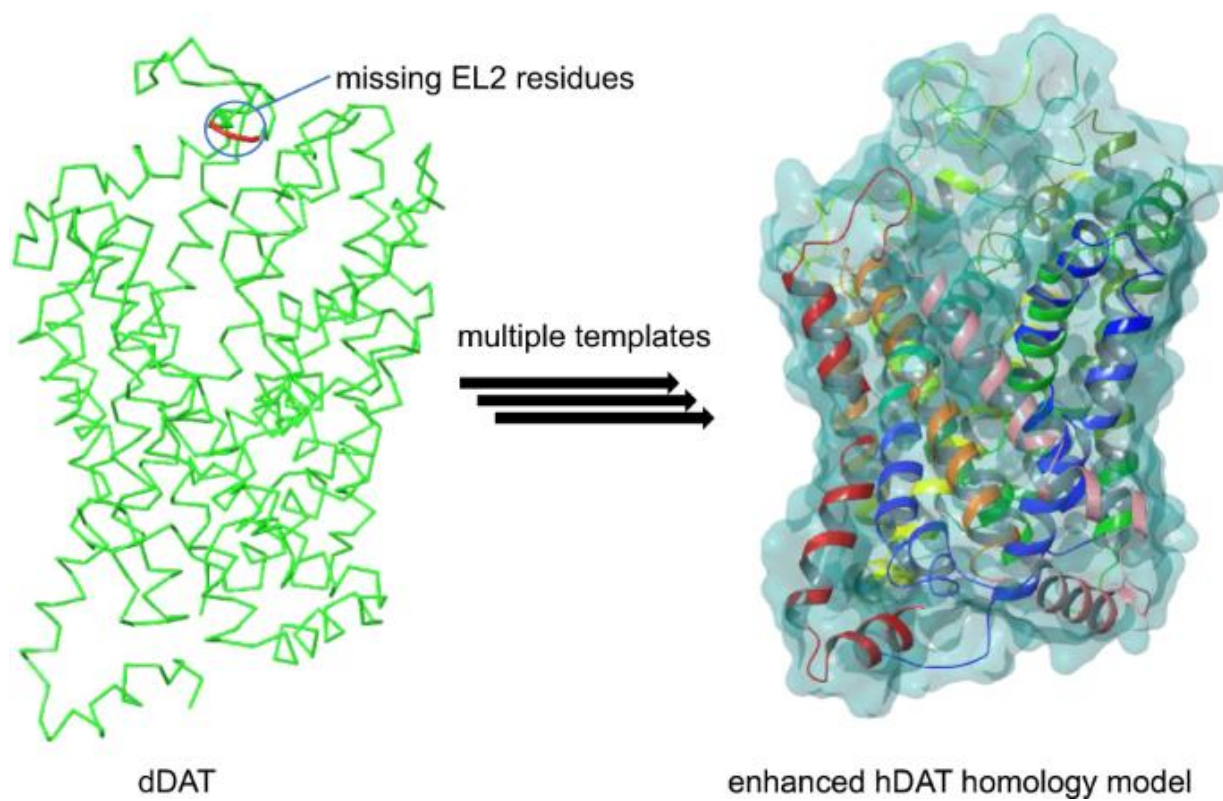
Figure 28. Enhanced homology model of hDAT utilizing multiple templates.[201]

2. Docking BPs at DAT

Docking studies of BPs were conducted with both stereoisomers. The highest-scoring binding poses are oriented similarly within the binding pocket (Figure 29). The aryl and carbonyl portions of the molecules occupy the same areas, with the carbonyl oxygen atoms forming an electrostatic interaction with TYR156. This interaction likely has a stabilizing effect on the compounds within the binding pocket. The only difference between the molecules is the orientation of the piperidine rings: the *S* isomers are farther from the essential ASP79 at 3.5 Å, while the *R* isomers are closer at 2.8 Å, possibly exhibiting stronger salt bridge interactions.
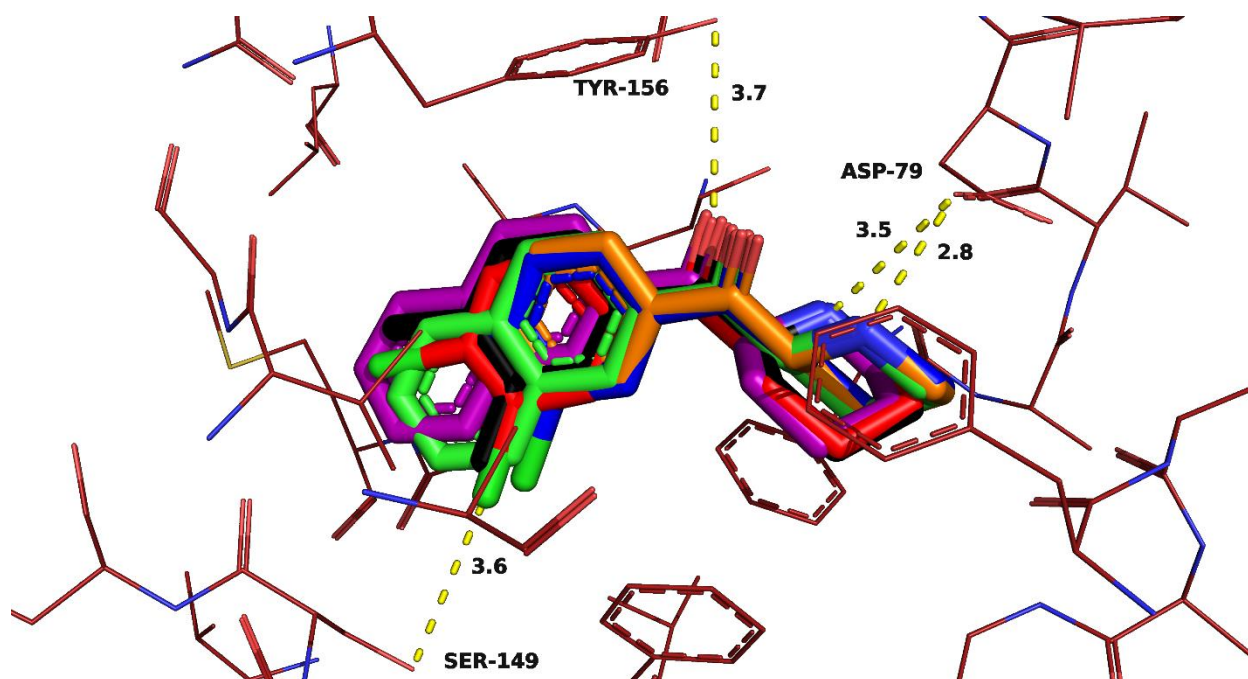
Figure 29. Highest scoring docking solutions of *R* DCBP (capped sticks, blue), *R* DMBP (capped sticks, orange), *R* NP (capped sticks, green), *S* DCBP (capped sticks, red), *S* DMBP (capped sticks, black), and *S* NP (capped sticks, purple) within the binding site of DAT (lines, dark red). Electrostatic interactions and hydrogen bond (yellow dashed lines).

Piperidine rings from each isomer are puckered in such a manner as to be as close as possible to ASP79. One important interaction to note is between SER149 and the *m*-chloro-substituent of DCBP that will be discussed later. It is very likely that all *R* isomer compounds examined bind in a similar manner to each other as well as all *S* isomer compounds binding similarly to one another. This docking then predicts that the same trend in activity should be observed for each set of isomers when tested in vitro. That is to say, the eutomer of each compound should be the same in this series. Scoring wise, all *R* isomers scored higher than their *S* isomer counterparts. ChemPLP scores from GOLD docking indicated that both DCBP and NP likely have a more pronounced affinity for DAT than DMBP (Table 5). DMBP not only has the lowest ChemPLP score but also the highest number of negative interactions from Hydropathic INTeractions (HINT) [202] analysis. These negative interactions are unlikely to be due to steric size or lipophilicity since the chloro- and methyl-substituents are approximately the same size, and all substituents in the series are hydrophobic (see Table 2). However, the chloro- and benz-fused substituents are electron-withdrawing, while the methyl-substituents are electron-donating.

Table 5. ChemPLP Scores and Number of Positive and Negative Interactions for Aryl Substituents of (*R*) and (*S*) **41**-**43** in DAT.

Compound	ChemPLP Score	# Positive HINT Interactions	# Negative HINT Interactions
(*R*) DCBP (**41a**)	52.7	13	7
(*S*) DCBP (**41b**)	48.8	11	9
(*R*) DMBP (**42a**)	52.2	13	10
(*S*) DMBP (**42b**)	47.9	10	10
(*R*) NP (**43a**)	58.5	9	4
(*S*) NP (**43b**)	51.7	10	5

3. Synthesis of Chiral BPs

The stereoisomers of compounds **41**-**43** were asymmetrically synthesized according to previously reported procedures for similar compounds[203] and fully characterized (Scheme 1). Commercially available *D*- or *L*-*N*-Boc-pipecolic acid (**49**) was used as the starting material for each respective stereoisomer. The carboxylic acid was coupled with *N*,*O*-dimethylhydroxylamine using the peptide coupling agent (benzotriazol-1-yloxy)tris(dimethylamino)phosphonium hexafluorophosphate (BOP) to generate the

known chiral Weinreb amide (**50**). This chiral amide served as the common intermediate in the preparation of the chiral BPs.

Scheme 1. Asymmetric synthesis of BPs.
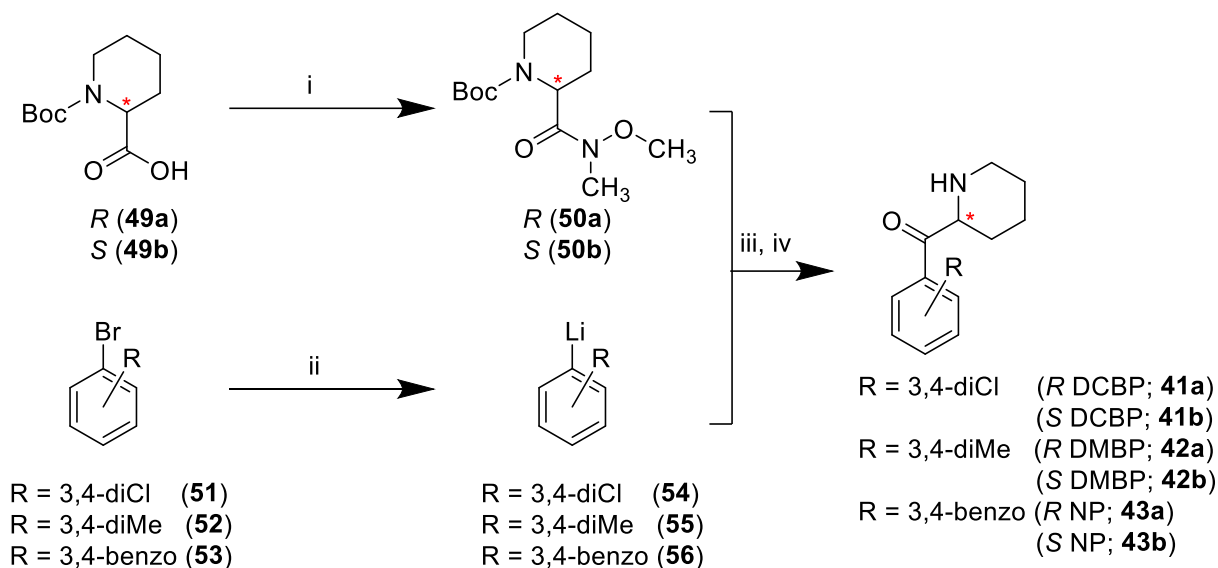
(i) *N,O*-Dimethylhydroxylamine hydrochloride, BOP, Et₃N, DCM, rt, 16 h; (ii) 2.5 M *n*-BuLi in hexanes, anhydrous Et₂O, −78 °C (see text), 3 h; (iii) anhydrous Et₂O, −29 °C, 24 h; (iv) ethereal HCl, anhydrous MeOH, 0 °C.

The aryl portion of the compounds was prepared using organometallic methods. Initially, a lithium–halogen exchange was performed on the mono-brominated aryl ring (**51**-**53**) using 1 equivalent of n-BuLi. The resulting organolithium intermediates (i.e., **54**-**56**) were then reacted with the chiral Weinreb amide intermediates **50** producing the *N*-Boc protected target compounds (i.e., **41**-**43**). During the preparation of the DMBP isomers, it was found that conducting the lithium-halogen exchange reaction at -78 °C caused the starting material (4-bromo-*o*-xylene, **52**) to solidify, preventing the lithium-halogen exchange from occurring. The melting point of 4-bromo-*o*-xylene is reported as -0.2 °C,

and at -78 °C, it is not soluble in anhydrous diethyl ether. Therefore, the reaction was performed at 0 °C to ensure that the reagent remained in solution and the desired organolithium intermediate was generated. Deprotection and hydrochloride salt formation were accomplished by adding an anhydrous HCl-saturated ethereal solution in a dropwise manner to the *N*-Boc protected target compounds dissolved in anhydrous methanol at 0 °C. Each stereoisomer was evaluated for optical rotation using a polarimeter (Table 6). Only the stereoisomers of DCBP showed rotations that differed by approximately 4° in each direction, while the rest of the compounds demonstrated nearly equal and opposite rotations, differing by less than 1° for the respective *R* and *S* isomers.

Table 6. Molecular formula, molecular weight, optical rotation, and melting point of BP target compounds.

Compound	Molecular Formula	MW	Optical Rotation	Melting Point
(R) DCBP (**41a**)	$C_{12}H_{13}NOCl_2 \cdot HCl$	294.60	36.4°	269-271 °C
(S) DCBP (**41b**)	$C_{12}H_{13}NOCl_2 \cdot HCl$	294.60	-40.8°	272-274 °C
(R) DMBP (**42a**)	$C_{14}H_{19}NO \cdot HCl$	253.77	40.0°	267-269 °C
(S) DMBP (**42b**)	$C_{14}H_{19}NO \cdot HCl$	253.77	-40.1°	266-269 °C
(R) NP (**43a**)	$C_{16}H_{17}NO \cdot HCl$	277.78	70.5°	264-266 °C
(S) NP (**43b**)	$C_{16}H_{17}NO \cdot HCl$	277.78	-70.0°	272 °C

4. Activity of Chiral BPs a DAT.

The series was evaluated for its ability to inhibit transport of the fluorescent false neurotransmitter DAT substrate 4-(4-(dimethylamino)phenyl)-1-methylpyridinium (APP+) through DAT expressed in human embryonic kidney (HEK) 293 cells, as measured by epifluorescence microscopy. Nonlinear regression using GraphPad Prism was performed on concentration-response curves for each compound (Figure 30) to generate IC_{50} activity values.
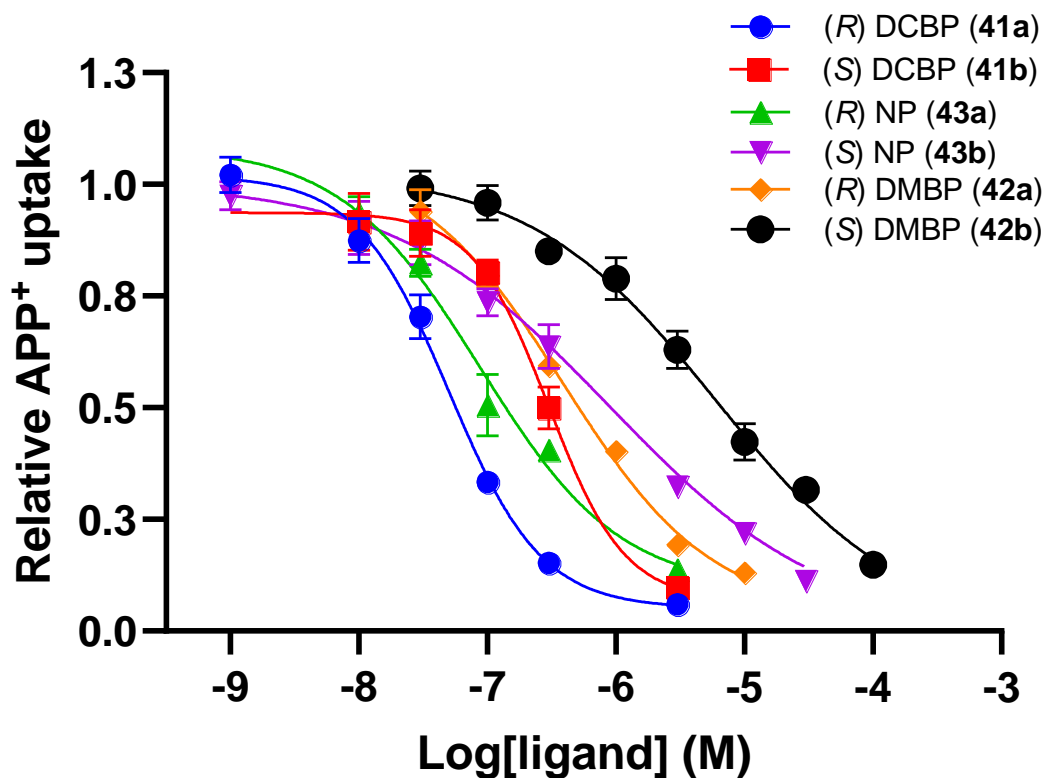
Figure 30. Concentration-response inhibition curves of APP$^+$ transport at DAT by BP stereoisomers.

As predicted by the molecular docking studies, the *R* stereoisomers of each compound were more potent than their *S* stereoisomer counterparts (Table 7). The largest difference between stereoisomer activity was for DMBP where the *R* isomer was over 15 times more potent than the *S* isomer.

Table 7. Inhibition activity (IC_{50}, nM) and 95% confidence intervals for chiral BPs at DAT.

Compound	IC_{50} (nM)	95% CI (nM)
(*R*) DCBP (**41a**)	50	38-65
(*S*) DCBP (**41b**)	300	211-1266
(*R*) DMBP (**42a**)	390	157-617
(*S*) DMBP (**42b**)	6069	2939-9190
(*R*) NP (**43a**)	88	50-215
(*S*) NP (**43b**)	895	335-1427

B. Determine activity and stereoselectivity of benzoylpiperidines at SERT

1. Modeling of SERT

hSERT is the only human MAT crystal structure that has been solved. A model of SERT (Figure 31) was generated using the crystal structure PDB ID: 5I6X as a template.[189] All molecules and antibody fragments were removed and then hydrogens were added to the protein and the model was minimized using the Tripos Force Field with Gasteiger-Hückel charges.
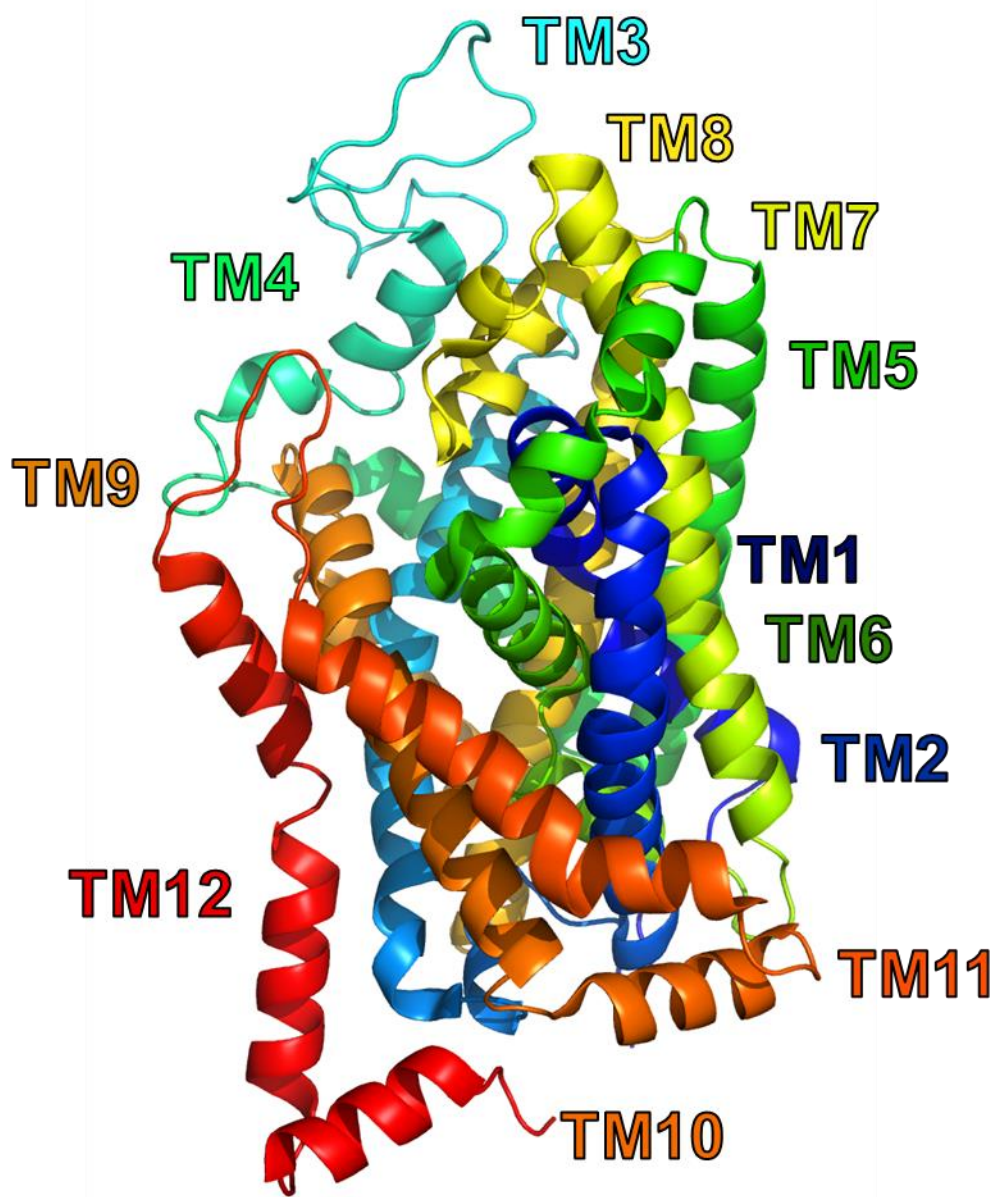
Figure 31. Model of SERT used for docking studies generated from PDB ID: 5I6X.

2. Docking BPs at SERT

The BP stereoisomers were docked 100 times each at the binding site of the transporter. The resultant docking solutions were scored using the ChemPLP scoring function in GOLD2020 and analyzed for molecular interactions within the binding pocket using HINT[202] analysis. For evaluation of racemic compounds, scores and interactions were combined for both stereoisomers of each compound (i.e., **41-43**). The highest ChemPLP scoring solution for each compound in SERT positioned the compounds in a similar orientation and overlapping space, suggesting they might bind in a similar manner. However, the stereoisomers were flipped, maintaining the 3D orientation of the piperidine rings constant but pointing the ketone moieties in opposite directions (Figure 32).
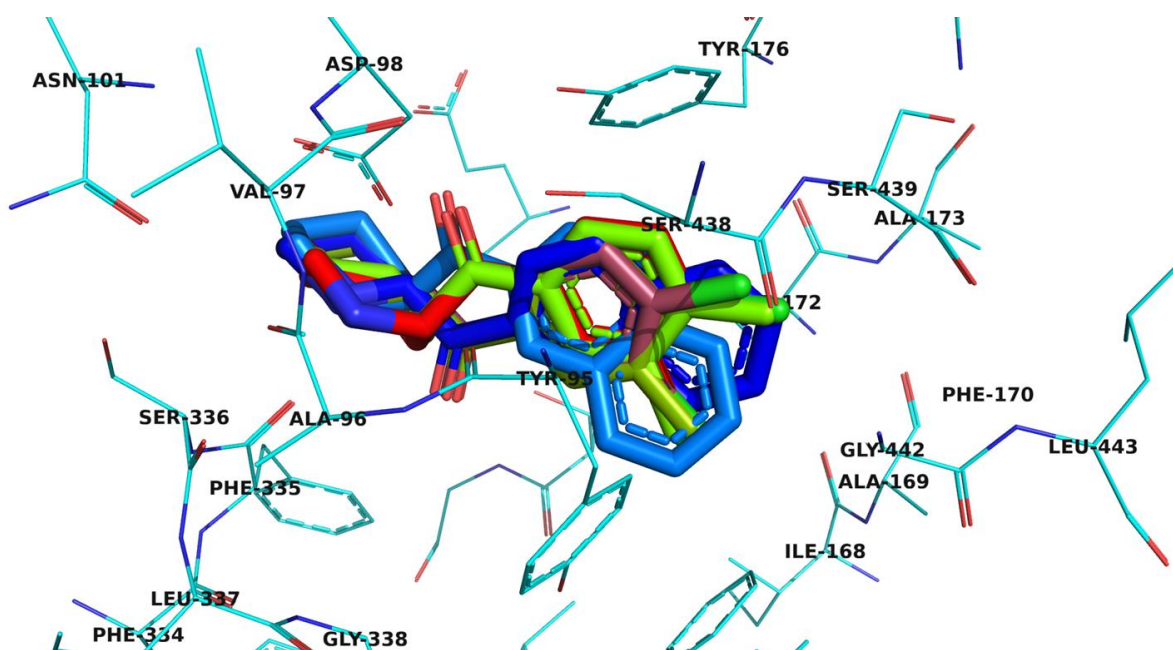
Figure 32. Highest scored docking solutions for DCBP (red and ruby, capped sticks), DMBP (chartreuse and lime green, capped sticks), and NP (dark blue and sky blue, capped sticks) for S and R isomers, respectively, in SERT (PDB ID: 5I6X) model (lines, cyan).

Docking studies resulted in solutions that were analogously and comparably oriented to the SERT crystal structures of paroxetine, sertraline, and fluvoxamine (Figure 33; PDB IDs: 5I6X, 6AWO, and 6AWP, respectively). The protonated nitrogen atom within the heterocyclic piperidine ring of each compound was positioned within 4 Å to form a salt bridge with the essential ASP98 in SERT. The similarity in docking scores and poses, to known crystal structures, indicates that each of the tested compounds likely binds at SERT.
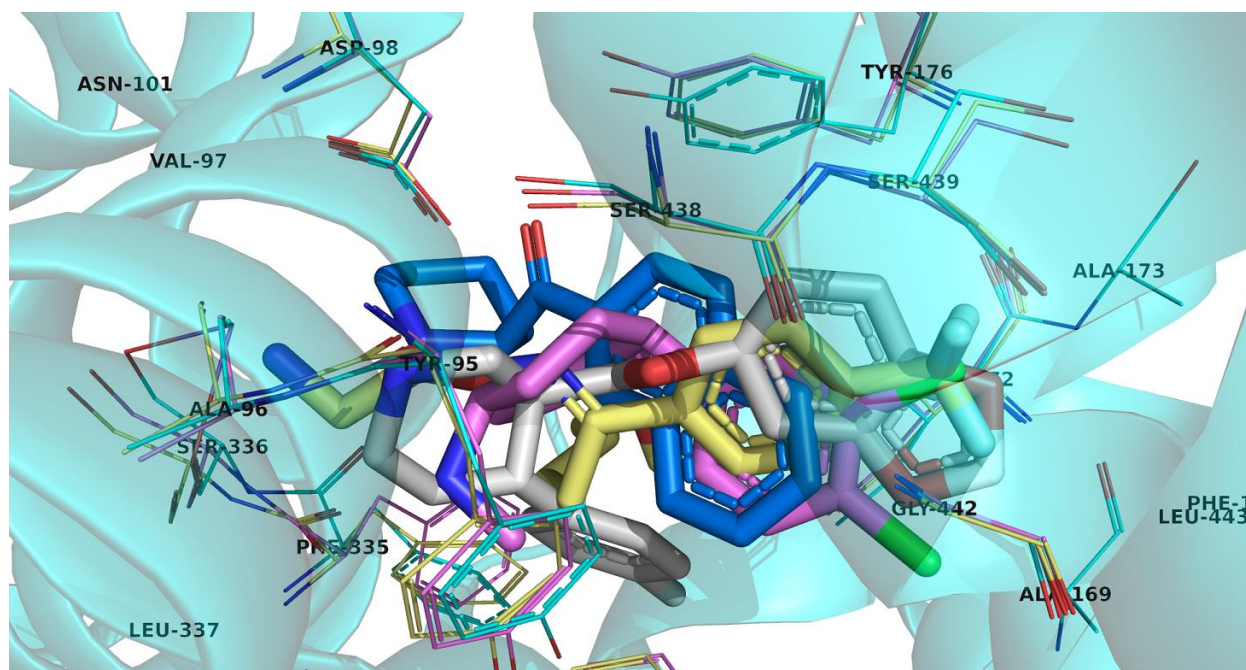
Figure 33. *S* NP (sky blue, capped sticks) in the SERT (PDB ID: 5I6X) model (cyan residues line rendering) mimics the orientation of the aromatic portions of paroxetine (grey, capped sticks) in the crystal structure of SERT (PDB ID: 5I6X; cyan residues line rendering), sertraline (violet, capped sticks) in the crystal structure of SERT (PDB ID: 6AWO; violet residues line rendering), and fluvoxamine (yellow, capped sticks) in the crystal structure of SERT (PDB ID: 6AWP; yellow residues line rendering).

Whether this formation occurs in vitro is unknown. The residues interacting with the aryl substituents, as supported by HINT analysis, were TYR95, ILE172, PHE341, VAL343, SER438, SER439, and GLY442. These favorable interactions are primarily hydrophobic with a few acid/base pairings. Specifically, TYR95 and ILE172 have been previously examined and are known to be vital for transport activity.[204,205] NP exhibited the fewest negative interactions (Table 8) between the "substituent" (i.e., isosteric phenyl) and the surrounding residues, totaling only 2 for the racemic compound, while DCBP and DMBP had 7 and 8 negative interactions, respectively. This suggests that NP should have the greatest activity at SERT compared to the other compounds. Conversely, DMBP, despite not having the fewest positive interactions, exhibited the greatest number of negative interactions at SERT, indicating that DMBP might be the least active compound of the three.

Table 8. ChemPLP scores and number of positive and negative interactions for aryl substituents of racemic **41-43** in SERT.

Compound[a]	ChemPLP Score	# Positive HINT Interactions	# Negative HINT Interactions
DCBP (**41**)	52.56	16	7
DMBP (**42**)	53.20	19	8
NP (**43**)	63.57	15	2

[a]Combined results for both isomers.

3. Activity of BPs at SERT.

Racemic **41-43** were evaluated in APP[+] inhibition assays at SERT with nonlinear regression performed on concentration-response curves (Figure 34) to generate IC_{50} values (Table 9) that demonstrate the remarkable ability for substituents positioned at the aryl ring to influence transporter selectivity and potency.
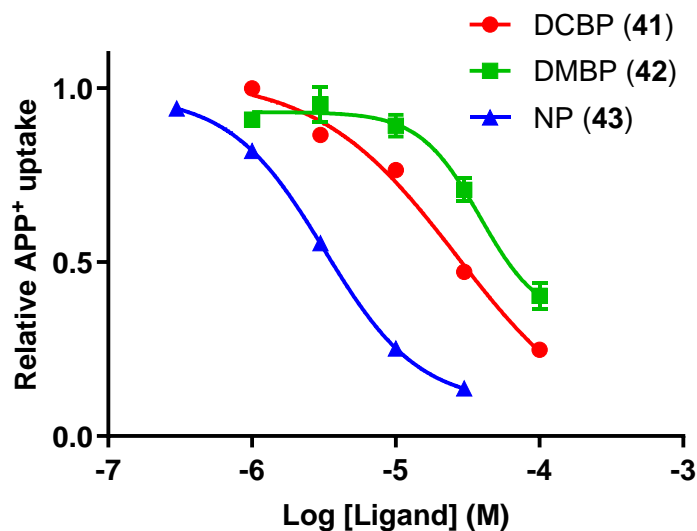
Figure 34. Concentration–response curves of the inhibitory effect of racemic **41**-**43** on APP$^+$ uptake assay in HEK293 cells stably expressing SERT.

As predicted by modeling, DMBP was the least active compound and NP was the most active at SERT (Table 9). NP, with its extended π system due to the naphthyl ring, was approximately 10-fold more potent at SERT than the other compounds examined. This increased potency of NP contrasts with the low potency of DCBP, despite these substituents usually being considered bioisosteres. Similar trends were observed in MPH analogues, where a naphthyl analogue demonstrated an affinity of 71.6 nM, while other examined analogues had K_i values greater than 10,000 nM.[50] This additional data generated at SERT indicates that hybrid cathinone BP compounds likely function in a similar manner to their corresponding methylphenidate counterparts.

Table 9. Functional activity of racemic **41-43** in the APP[+] assay at SERT with selectivity calculated for DAT.

Compound	SERT $IC_{50} \pm$ SEM (nM)	DAT selectivity[a]
DCBP (**41**)	$26,500 \pm 11,000$	1,560
DMBP (**42**)	$38,500 \pm 19,000$	100
NP (**43**)	$3,200 \pm 500$	64

[a]Selectivity calculated using DAT IC_{50} values from Table 4.

The selectivity of the BPs for DAT versus SERT (Table 9) demonstrates that DCBP is highly selective for DAT while NP is the least selective of the series. This could indicate that DCBP might have greater abuse liability compared to NP. Now that stereoselectivity has been established at DAT for BPs, will SERT follow the same trend? Due to the poor activity of DCBP and DMBP at SERT only the stereoisomers of NP were considered to be evaluated at SERT. The modeling studies suggest the only difference in binding modes for (*S*) and (*R*) NP is the 3D orientation of the ketone moiety. Only the carbonyl oxygen of the *S* isomer has any ability for an electrostatic interaction. This interaction possibly takes place with TYR176 (Figure 35) and due to this additional interface, it is thus predicted that (*S*) NP is more selective for SERT than (*R*) NP. The stereoisomers of NP were examined in the APP[+] inhibition assays at SERT with nonlinear regression performed on concentration-response curves (Figure 36) to generate IC_{50} values.
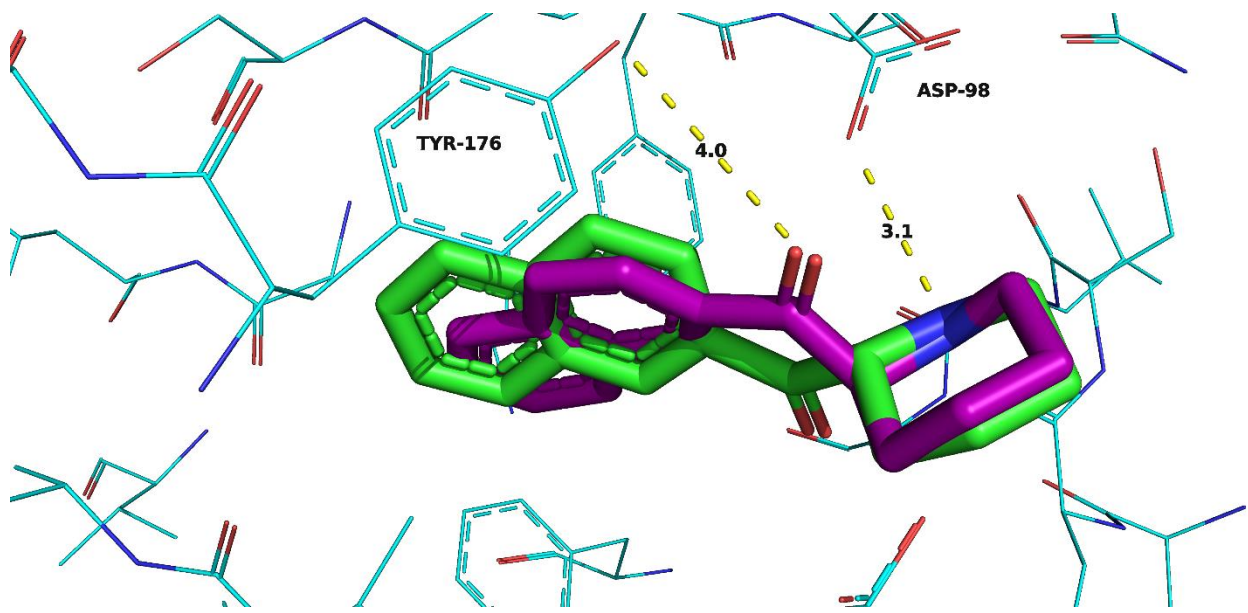
Figure 35. (*S*) and (*R*) NP (purple and green, capped sticks, respectively) in SERT (cyan, lines) exhibiting salt bridge to ASP98 and electrostatic interactions with TYR176 (yellow, dashes).
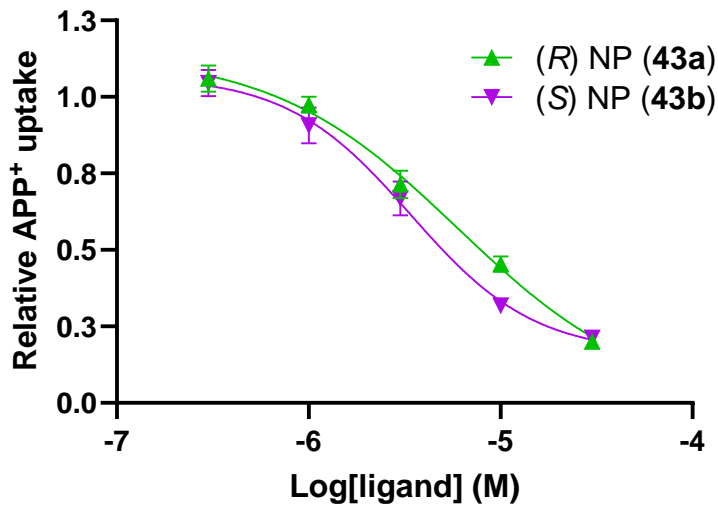
Figure 36. Concentration–response curves of the inhibitory effect of (*R*) and (*S*) NP on APP+ uptake assay in HEK293 cells stably expressing SERT.

Both (*S*) and (*R*) NP exhibited activity at SERT with similar potencies, yet surprisingly, the

S stereoisomer of NP is the eutomer at SERT (Table 10). BPs seem to have opposite

stereoisomer eutomers at DAT and SERT. That is to say the eutomer at DAT is the *R*

stereoisomer whereas the eutomer at SERT is the *S* isomer.

Table 10. Functional activity of (*S*) and (*R*) NP in the APP$^+$ assay at SERT with
selectivity calculated for DAT.

Compound	IC$_{50}$ (µM)	95% CI (µM)	DAT Selectivity[a]
(*R*) NP (**43a**)	5.9	3.5-8.0	67
(*S*) NP (**43b**)	3.3	2.1-5.9	4

[a]Selectivity calculated using DAT IC$_{50}$ values from Table 7.

The selectivity for DAT of (*S*) NP is the lowest in the entire series indicating that (*S*) NP

should have lower abuse liability than the other BPs tested thus far. It is remarkable that

manipulation of stereochemistry and simple aryl substitution can dictate selectivity and

potency between more than one target. From this study that used a small series of

compounds, there were both a highly potent and selective agent for DAT that does not

have physiologically relevant activity at SERT ((*R*) DCBP) and also an agent that shows

physiologically relevant activity at SERT with much less selectivity for DAT ((*S*) NP).

C. Determine function of benzoylpiperidines at SERT

Pentedrone (**40**) is a cathinone stimulant with mixed functionality; it is a DAT reuptake inhibitor but a SERT partial releasing agent. Its ring-substituted analogues retain similar functional activity with greater affinity at SERT.[180] Pentedrone possesses the same number of carbon atoms as the piperidine ring in BPs and can be considered a conformationally unconstrained isomer. While it is established that BPs are reuptake inhibitors at DAT, it was unknown whether they are substrates or reuptake inhibitors at SERT. To address this, substrate activity at SERT using a MAT-Ca^{2+} assay was assessed for compounds **41**-**43**. It is well accepted that substrates at MATs activate an inward current that electrically depolarizes the plasma membrane; [206,207] therefore, co-expressed voltage-gated Ca^{2+} channels can be used to detect such depolarization by increasing intracellular Ca^{2+} concentration.[208–210] In experiments performed in HEK293 cells co-expressing SERT and voltage-gated Ca^{2+} channels, none of the compounds produced a depolarizing current large enough to open Ca^{2+} channels when perfused alone. However, they inhibited the depolarization caused by 5-HT (Figure 37), strongly suggesting that the conformationally constrained cathinones are SERT inhibitors.
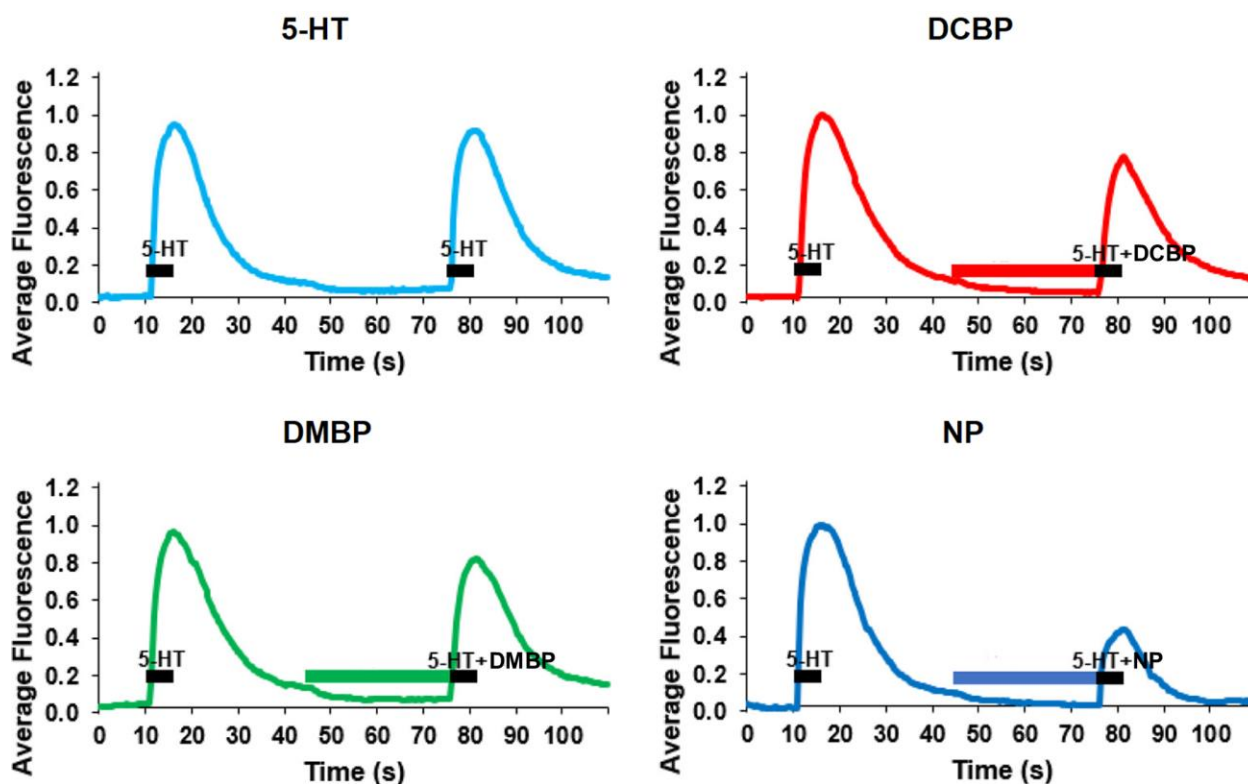
Figure 37. Depolarization induced by SERT activation, electrically coupled to $Ca_v1.2$ for 10 µM 5-HT (cyan), DCBP (red), DMBP (green), and NP (blue). Benzoylpiperidine compounds (25 µM) did not produce a depolarization current when perfused alone.

D. Explore halogen bond formation for DAT S149/DCBP

1. Modeling of Halogen Bond Interactions in DAT

Docking studies of DCBP in DAT indicated that the *m*-chloro-substituent was the proper distance and angle to form a halogen bond with the terminal oxygen atom lone pair of SER149 (Figure 38). Halogen bonding, a non-covalent interaction of halogen atoms, is explained by the presence of a region of positive electrostatic potential, the so-called σ-hole, on the outermost portion of the halogen's surface, centered on the R–X axis

(X = halogen, R = alkyl or aryl carbon). Halogen atoms closely approximate the $s^2p^2 xp^2 yp^1 z$ configuration in molecules that contain Cl, Br, and I atoms, where the *z*-axis is along the R–X bond.[211,212] Due to spin around the R–X bond, the three unshared electron pairs form a doughnut-like cloud of negative electrostatic potential around the halogen atom, leaving the positive potential region at its apex, the σ-hole.[213] The σ-hole differs in size according to the halogen involved (I > Br > Cl) and offers a possibility for an interaction with a Lewis base (e.g., a lone electron pair of a heteroatom such as a carbonyl oxygen atom).[213] Fluoro halogen atoms are not considered under this description because the atom does not have the capacity to form the σ-hole effect without being linked to a strongly electron-withdrawing residue.[214] For modeling, this interaction is difficult to examine because most standard molecular mechanics force fields are unable to model halogen bonds because they represent electrostatic interactions using atom-centered point charges. Neither software employed in the studies (i.e., ChemPLP and HINT) directly measures halogen bonding interactions. ChemPLP relies on "goodness of fit" and shows hydrogen bonding contacts. HINT relies on the cLogP of the ligand and the protein to determine hydropathic interactions between them.[202]
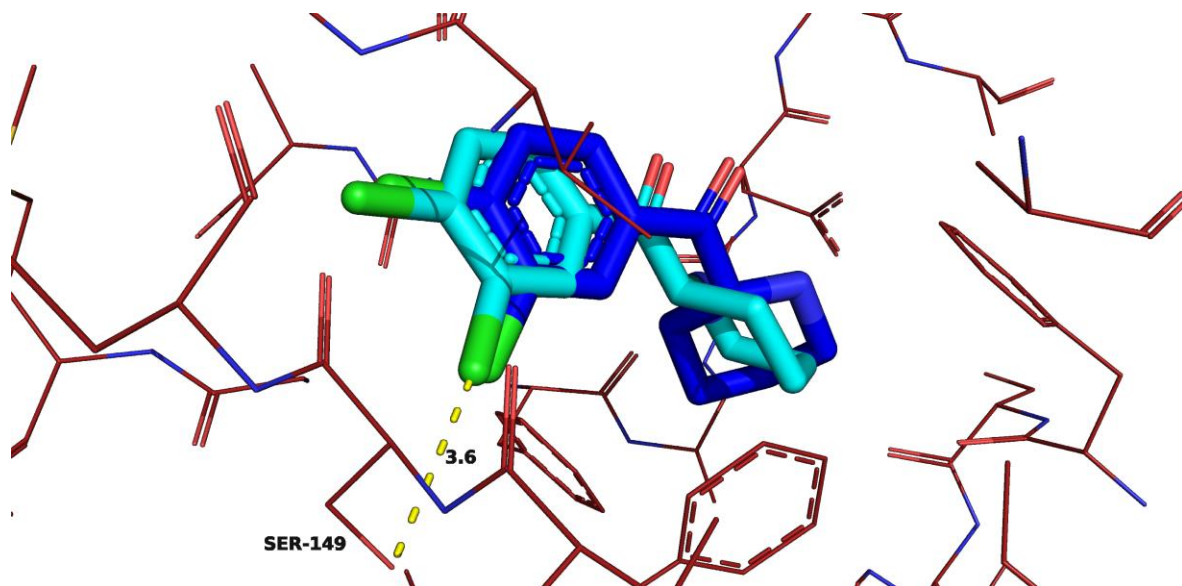
Figure 38. Halogen bond interaction (yellow, dashes) between DAT (red, lines) SER149 and (*S*) and (*R*) DCBP (cyan, blue, capped sticks, respectively).

By its convention, the chloro-SER149 relationship is scored negatively in HINT as a base/base clash. The anisotropic nature of the larger halogens is not considered and therefore other techniques must be employed to investigate the halogen bond possibility. There must be some electrostatic interactions associated with DCBP and DAT due to the potency difference seen between DCBP and DMBP. Employing Schrödinger's Maestro,[215] a software package that shows halogen bonds explicitly, it was found that DCBP likely forms this interaction with DAT's SER149 (Figure 39).
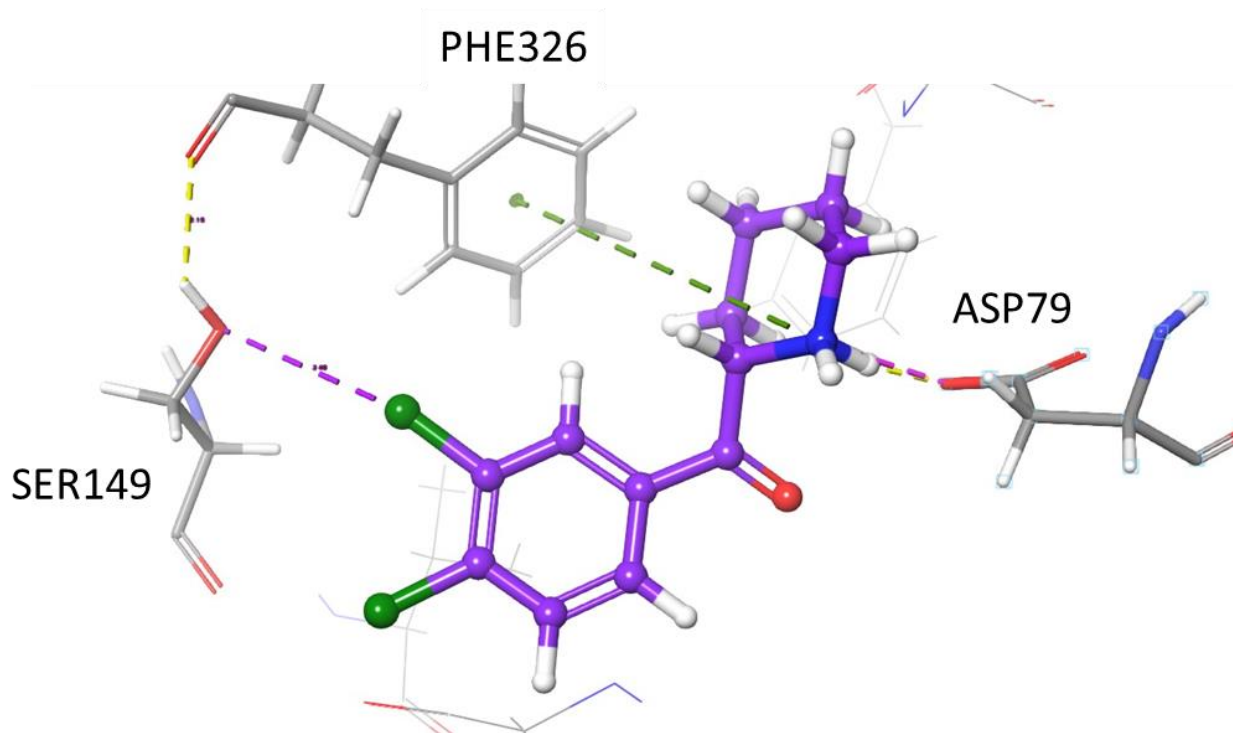
Figure 39. Halogen bond (purple, dashes) between SER149 and DCBP (purple, ball and stick) in DAT (grey, lines) with π-cation (green, dashes), hydrogen bonds (yellow, dashes), and salt bridge (pink, dashes) displayed in Maestro.

2. Modeling of S149A DAT

To assist in validating the halogen bond interaction a mutagenesis study was conducted. By mutating SER149 to ALA149, the potential halogen bond formation with the *m*-chloro-substituent can no longer occur. What should be observed in biological evaluation is a loss in function. Typically, a loss in function alone would not necessarily confirm a particular ligand-protein interaction due to possible misfolding and dysfunction of the protein itself. Fortunately, DMBP can be used to aid in the study. DMBP cannot form a halogen bond and also should have a hydrophobic/polar clash between the *m*-methyl-substituent and the terminal hydroxyl moiety of SER149. Mutation to ALA149 should abolish this clash and instead exhibit hydrophobic interactions between the *m*-methyl-

substituent of DMBP and the methyl group from ALA149. In this case a gain in function or no change in activity should be observed. Both a loss in function and a gain in function would be compelling evidence to corroborate the previous docking studies and other biological activities suggesting halogen bond formation for DCBP.

A model of DAT S149A was generated from the previous DAT model[201] by replacing SER149 with ALA149 followed by a minimization using the Tripos Force Field with Gasteiger-Hückel charges. Both stereoisomers of DCBP and DMBP were each docked 100 times in the mutant transporter resulting in 400 total solutions. The ChemPLP scoring function and HINT analysis were performed to determine the best fitting solutions. It was determined that all four compounds likely bind in a similar manner in mutant DAT compared to WT DAT. All piperidine ring nitrogen atoms were able to form salt bridge interactions with ASP79 and the carbonyl oxygen atoms were able to participate in electrostatic interactions with TYR156 (Figure 40). Surprisingly, the *R* stereoisomers formed salt bridge interactions at 2.8 Å and the *S* stereoisomers formed salt bridge interactions at 3.5 Å in the exact same manner as was seen in the WT DAT docking study. There was no interaction with ALA149 indicating that the *m*-substituents of each compound should have the exact same interactions. That is, only hydrophobic interactions should prevail for both *m*-chloro- and *m*-methyl-substituents in mutant DAT.
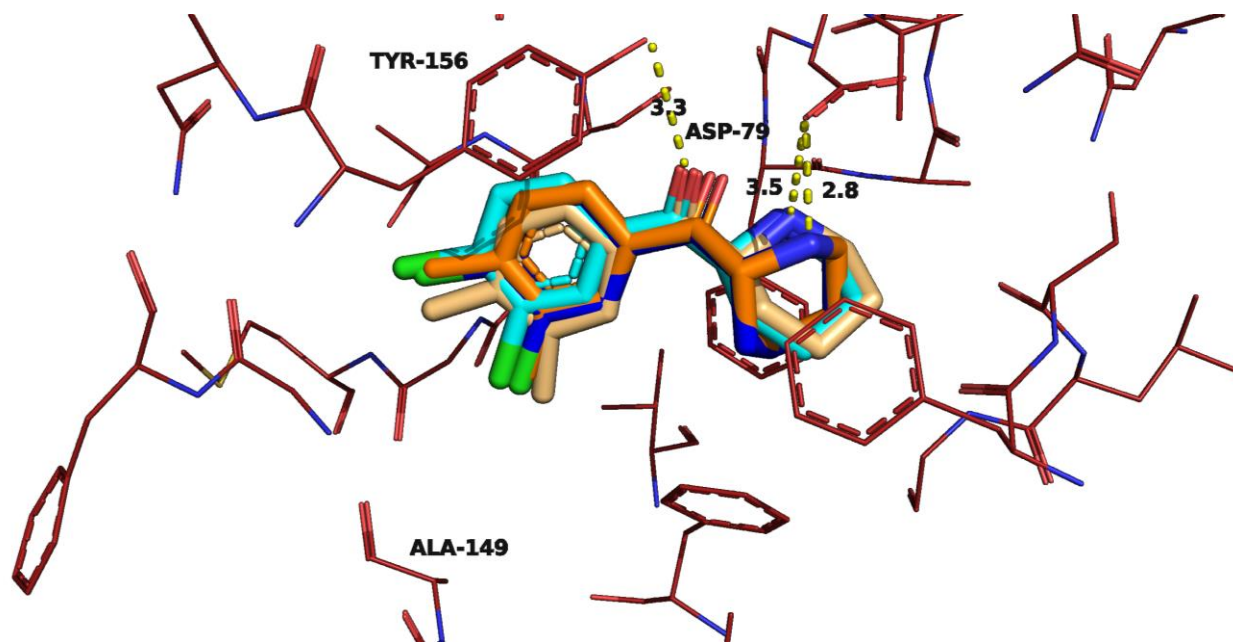
Figure 40. (*S*) and (*R*) DCBP (cyan and blue, capped sticks, respectively) and (*S*) and (*R*) DMBP (cream and orange, capped sticks, respectively) in mutant DAT S149A (red, lines) exhibiting salt bridge to ASP79 and electrostatic interactions with TYR1156 (yellow, dashes).

3. Activity of BPs at Mutant S149A DAT

Biological studies were conducted utilizing HEK293 cells stably expressing the mutant S149A DAT. APP+ inhibition assays were carried out on the cells with nonlinear regression performed on concentration-response curves (Figure 41) to generate IC_{50} activity values. As predicted by modeling and previous studies, both stereoisomers of DCBP (**41a**, **41b**) demonstrated a right-shift whereas the stereoisomers of DMBP (**42a**, **42b**) showed left-shifts. Both *R* stereoisomers continued to be the eutomer at the mutant DAT and demonstrated IC_{50} values nearing each other's measurement at ~100 nM. The loss in function observed for DCBP was found to be statistically significant ($p < 0.05$) but the gain in function for DMBP was not statistically significant ($p > 0.05$). Regardless, the

observed gain in function for DMBP was not necessary for adequate evidence to support

halogen bond formation with DCBP in DAT, only that DMBP did not exhibit a loss in

function at the mutant DAT.
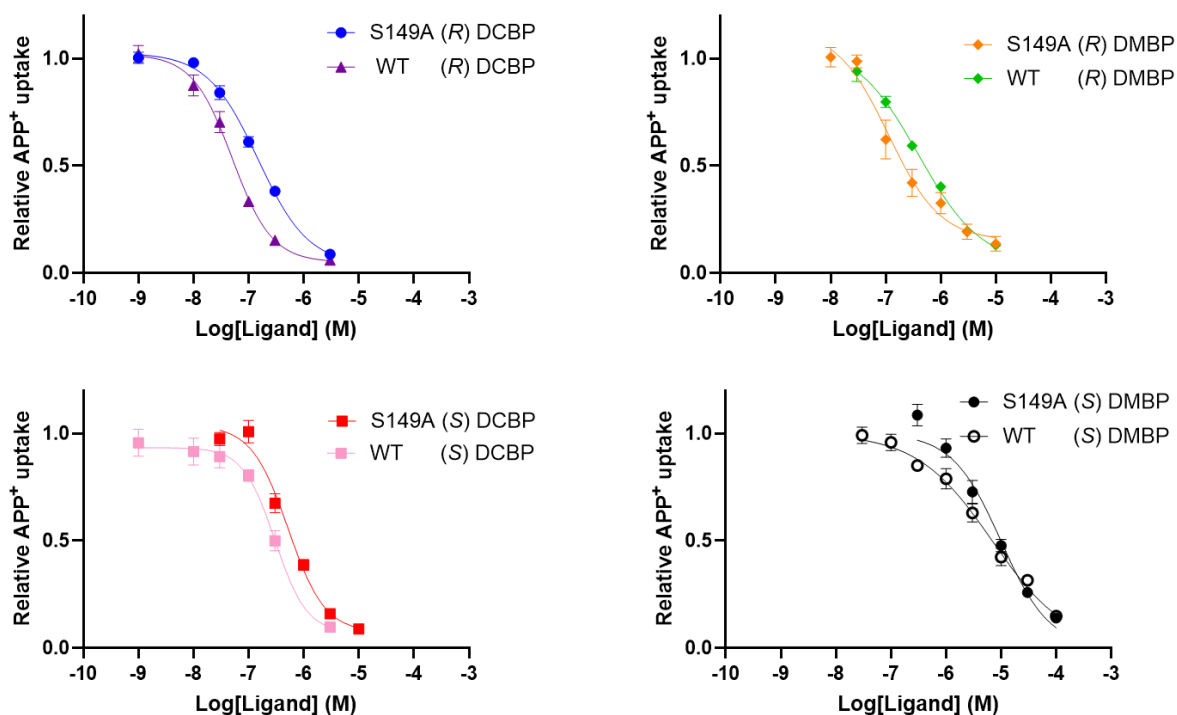
Figure 41. Concentration–response curves of the inhibitory effect of (*R*) and (*S*) DCBP (**41a** and **41b**, respectively) and DMBP (**42a** and **42b**, respectively) on APP$^+$ uptake assay in HEK293 cells stably expressing either WT or S149A DAT.

Table 11. Functional activity of (*S*) and (*R*) DCBP and DMBP in the APP[+] assay at mutant S149A DAT and WT DAT with change in activity calculated.

Compound	S149A IC$_{50}$ (nM)	95% CI (nM)	WT IC$_{50}$ (nM)	95% CI (nM)	Δ Activity
(*R*) DCBP (**41a**)	147	115-195	50	38-65	-97
(*S*) DCBP (**41b**)	522	39-706	300	211-1266	-222
(*R*) DMBP (**42a**)	113	3.4-212	390	157-617	277
(*S*) DMBP (**42b**)	5016	362-14170	6069	2939-9190	1053

E. Determine affinity/activity for α-ETs at 5-HT$_{2A}$ receptors

1. Modeling of 5-HT$_{2A}$ receptor

In the past five years several crystal structures of 5-HT$_{2A}$ receptors have been elucidated. Since that time 5-HT$_{2A}$ receptor structures containing antagonists, partial agonists, and full agonist ligands have been solved. The template chosen for modeling α-ETs in the 5-HT$_{2A}$ receptor was the structure crystallized with the partial agonist LSD (**17**) bound in the orthosteric binding pocket (PDB ID: 6WGT, Figure 42).[216] This structure was chosen due to the fact that the *S* stereoisomer of α-ET (**27a**) demonstrated partial agonist activity in the Ca^{2+} mobilization asssay with an E$_{MAX}$ of 61%.[124] Racemic and (*R*) α-ET (**27** and **27b**, respectively) did not show any activity[124] in the above assay, suggesting that they and might be antagonists or not bind to the receptor at all. All molecules and co-crystallized receptors were removed and then hydrogen atoms were added to the protein. The model was energy minimized using the Tripos Force Field with Gasteiger-Hückel charges.
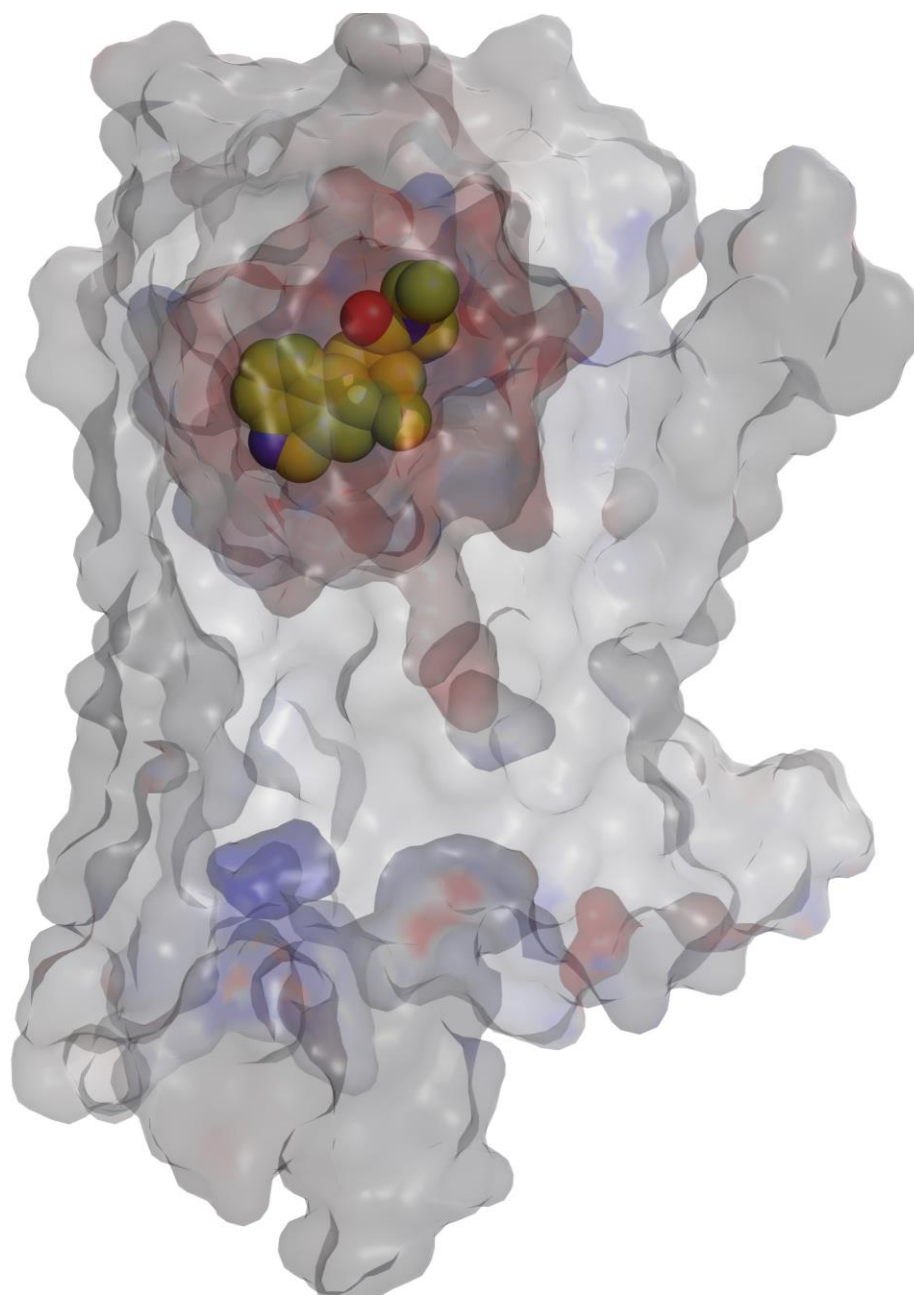
Figure 42. 5-HT$_{2A}$ receptor (PDB ID: 6WGT) [216] model (grey) with LSD (**17**, yellow, spheres) bound in the orthosteric binding pocket (red).

2. Docking α-ETs at 5-HT$_{2A}$ receptor

Compared to the large LSD (**17**) molecule, α-ET (**27**) is quite small and consequently there are many sites in the receptor binding pocket that the molecule could fit. For docking, the strictly conserved ASP155 residue essential for the interaction with ligands in aminergic receptors was chosen as the origin to define a 10 Å-sphere within which α-ETs were docked.[217] Upon docking both stereoisomers of α-ET (**27a** and **27b**), it was found that there are possibly two binding modes for these molecules. The *R* stereoisomer tended to orient in the extended binding pocket (EBP) similarly to the diethylamide moiety of LSD as can be seen in Figure 43. In contrast, (*S*) α-ET had a binding mode in the lower portion of the orthosteric site with the indole portion of the molecule overlapping the indole portion of LSD (Figure 43). LSD will be used in figures as an archetype for binding interactions and 3D orientation of docking solutions.
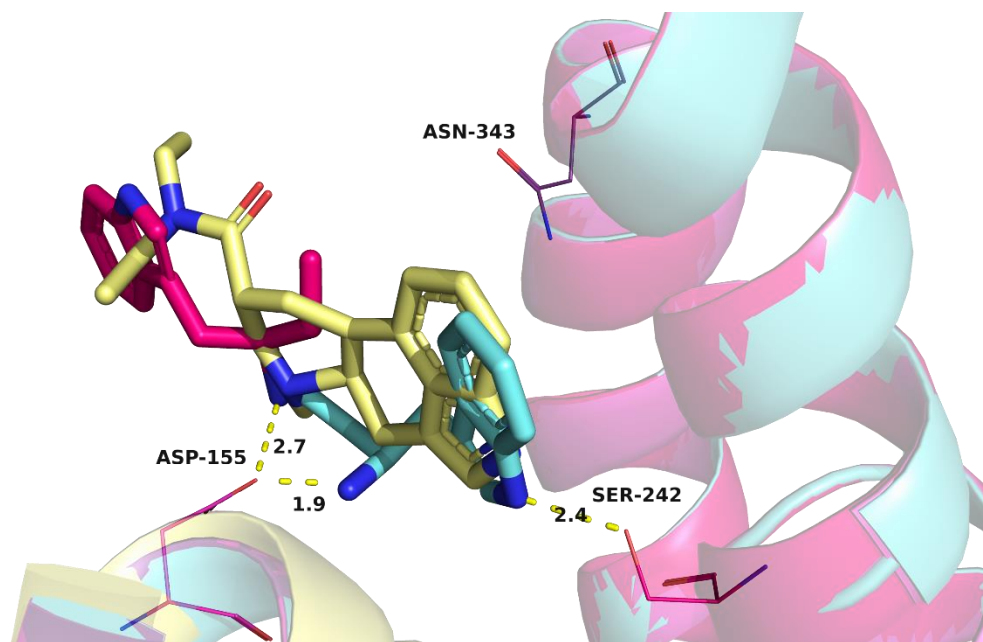
Figure 43. Binding modes of LSD (yellow, sticks), (*R*) α-ET (magenta, sticks), and (*S*) α-ET (cyan, sticks) in the 5-HT$_{2A}$ receptor model (multicolored, cartoon) with salt bridge and electrostatic interactions (yellow, dashes).

Both α-ET stereoisomers were able to make salt bridge interactions with ASP155, but only (*S*) α-ET was able to form a hydrogen bond with SER242. The difference in binding poses as well as hydrogen bonding interactions with SER242 might be the reason that only (*S*) α-ET was able to exhibit partial agonist activity, whereas (*R*) α-ET showed no activity. Regardless that (*R*) α-ET did not show activity,[124] this docking suggests that the molecule could still bind.

Docking solutions for the 4-MeO-α-ET stereoisomers were very similar to (*S*) α-ET. Both stereoisomers demonstrated binding modes in the lower orthosteric pocket with salt bridge interactions with ASP155 and exhibited hydrogen bonding interactions with SER242 (Figure 44). The oxygen atom lone pair from the methoxy substituent is able to

hydrogen bond to the amide nitrogen atom of ASN343. This additional interaction when compared to unsubstituted α-ET might indicate that the 4-methoxy substituted α-ET binds with greater affinity to the 5-HT$_{2A}$ receptor. Also, this interaction might be the reason that both stereoisomers of 4-MeO-α-ET are able to have binding modes in the lower region of the orthosteric binding pocket similarly to (*S*) α-ET while (*R*) α-Et binds in the EBP.
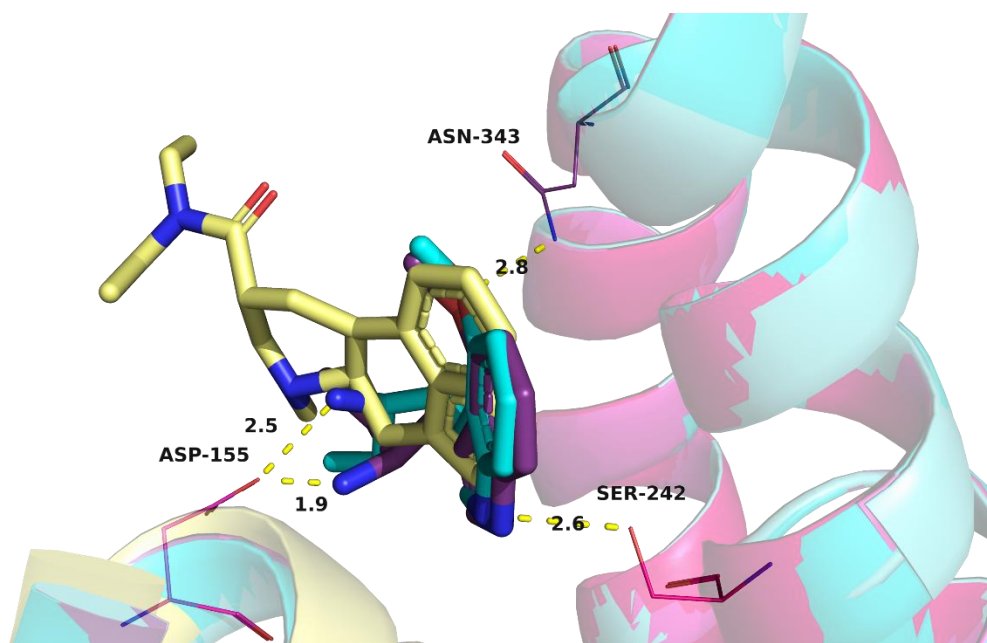
Figure 44. Binding modes of LSD (yellow, sticks), (*R*) 4-MeO-α-ET (cyan, sticks), and (*S*) 4-MeO-α-ET (purple, sticks) in the 5-HT$_{2A}$ receptor model (multicolored, cartoon) with salt bridge and electrostatic interactions (yellow, dashes).

Docking the 5-MeO-α-ET stereoisomers (Figure 45) resulted in almost identical binding modes compared to 4-MeO-α-ET. All the same interactions were observed between these α-ET analogs suggesting they might have similar affinities at 5-HT$_{2A}$ receptors.
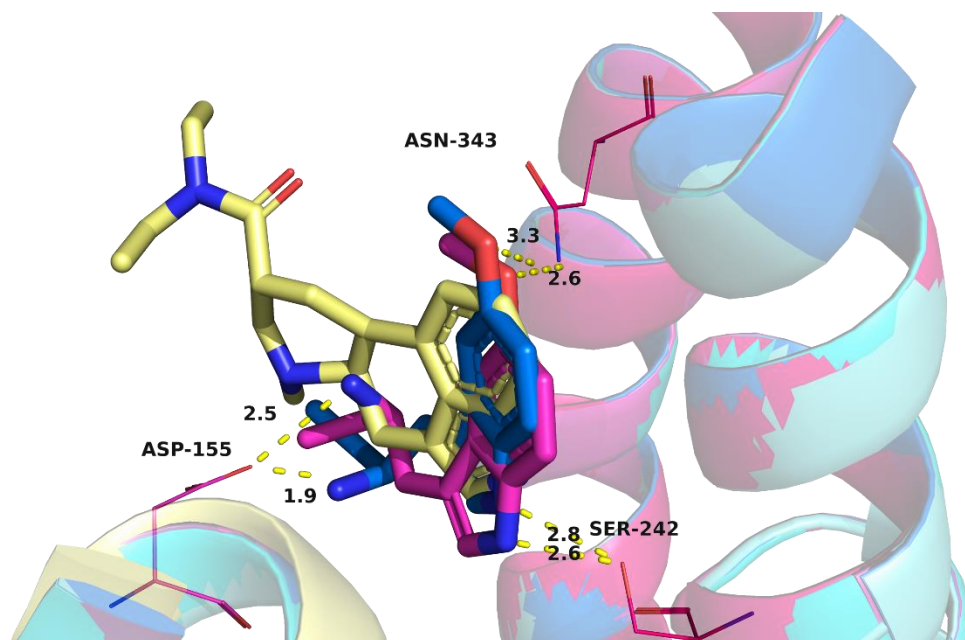
Figure 45. Binding modes of LSD (yellow, sticks), (*R*) 5-MeO-α-ET (pink, sticks), and (*S*) 5-MeO-α-ET (blue, sticks) in the 5-HT$_{2A}$ receptor model (multicolored, cartoon) with salt bridge and electrostatic interactions (yellow, dashes).

For the 4-bromo-substituted α-ET stereoisomer docking, both isomers displayed binding modes in the lower part of the orthosteric binding pocket (Figure 46). A salt bridge was potentially formed between ASP155 and the primary amine nitrogen atoms for both stereoisomers. They were thus able to make electrostatic interactions with the amide nitrogen atom of ASN343 and the bromo-substituent, but only (*S*) 4-Br-α-ET was able to make a hydrogen bond interaction with the indolic nitrogen atom and the hydroxyl group of SER242. The docking then suggests that 4-Br-α-ET might not bind as well as the 4-methoxy-substituted analogs.
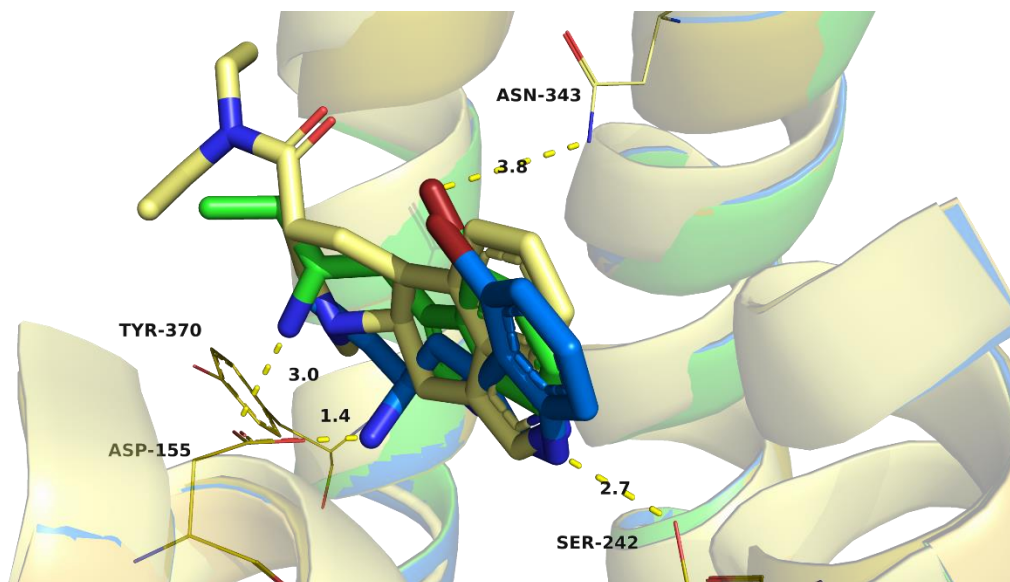
Figure 46. Binding modes of LSD (yellow, sticks), (*R*) 4-Br-α-ET (green, sticks), and (*S*) 4-Br-α-ET (blue, sticks) in the 5-HT$_{2A}$ receptor model (multicolored, cartoon) with salt bridge and electrostatic interactions (yellow, dashes).

5-Br-α-ET docking resulted in palindromic binding modes compared to unsubstituted α-ET in that the *R* stereoisomer was oriented in the lower orthosteric binding pocket and the *S* isomer was situated in the EBP (Figure 47). As seen with the other compounds examined in the 5-HT$_{2A}$ receptor, these two stereoisomers were also able to form a salt bridge with ASP155. The *R* stereoisomer was able to form a hydrogen bond with the amide nitrogen atom of ASN343 as well as the hydroxyl group of SER242 in a similar manner to the 5-MeO-α-ETs analogs. The bromo-substituent of (*S*) 5-Br-α-ET did not make any appreciable electrostatic interactions but the indolic nitrogen was able to form a hydrogen bond with TYR370. With the 4-Br-α-ET analogs binding in the lower orthosteric binding pocket and the 5-Br-α-ET analogs displaying mixed results in the EBP

and orthosteric binding pocket, it might be expected then that 4-Br-α-ET will have greater

affinity/activity compared 5-Br-α-ET.
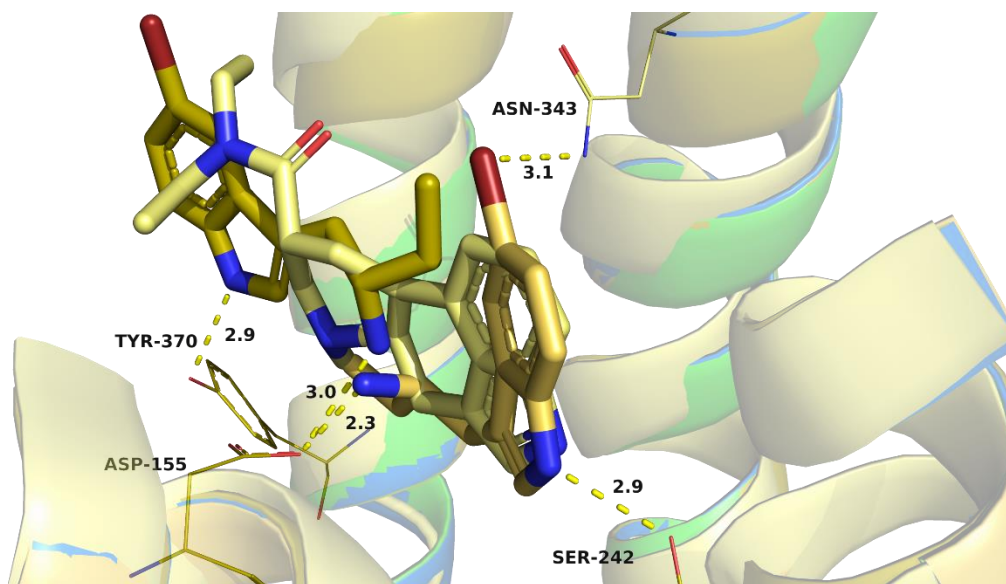
Figure 47. Binding modes of LSD (yellow, sticks), (*R*) 5-Br-α-ET (mustard, sticks), and (*S*) 5-Br-α-ET (gold, sticks) in the 5-HT$_{2A}$ receptor model (multicolored, cartoon) with salt bridge and electrostatic interactions (yellow, dashes).

Taken together the docking studies predict that all α-ETs studied here likely bind in the

5-HT$_{2A}$ receptor.

3. Synthesis of α-ETs

Racemic α-ETs analogs were synthesized according to previously reported procedures

for similar compounds[218] according to the general Scheme 2 and fully characterized. In

some cases, the required gramine was commercially available. Commercially available

indoles and substituted indoles were dissolved in and stirred with dimethylamine, formaldehyde, and acetic acid in a Mannich type condensation reaction resulting in the generation of a gramine intermediate. This intermediate was then reacted with 1-nitropropane in a base catalyzed reaction under reflux to produce a nitrobutyl intermediate. Raney nickel reduction of the nitro group yielded the racemic target compound freebases. Depending on the particular analog either an HCl, oxalate, or acetate salt was formed as the target compound.

Scheme 2. General synthesis of racemic α-ET analogs.

R = -H (**57**)	R = -H (**62**)	R = -H (**67**)	R = -H (**27**)
R = 4-OMe (**58**)	R = 4-OMe (**63**)	R = 4-OMe (**68**)	R = 4-OMe (**44**)
R = 5-OMe (**59**)	R = 5-OMe (**64**)	R = 5-OMe (**69**)	R = 5-OMe (**45**)
R = 4-Br (**60**)	R = 4-Br (**65**)	R = 4-Br (**70**)	R = 4-Br (**46**)
R = 5-Br (**61**)	R = 5-Br (**66**)	R = 5-Br (**71**)	R = 5-Br (**47**)
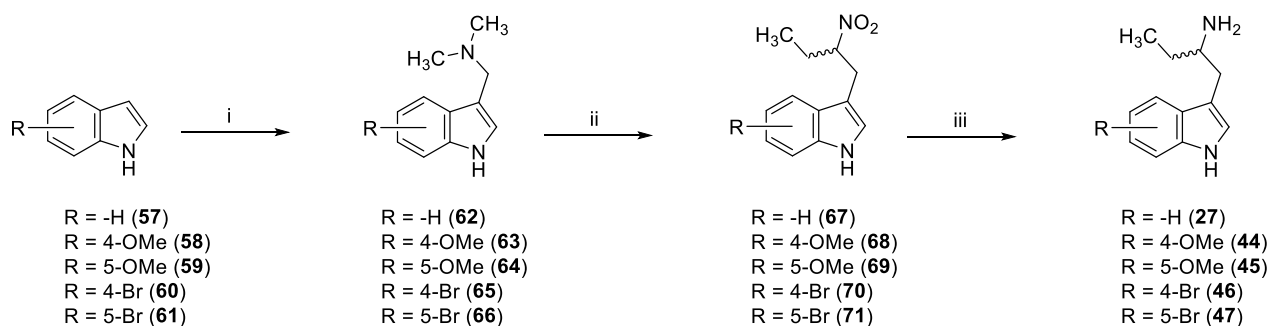
i) $(CH_3)_2NH$, CH_2O, AcOH, 0 °C, 18 h; ii) 1-nitropropane, NaOH, N_2, reflux 18 h; iii) Raney nickel, hydrazine hydrate, EtOH, N_2, reflux 3 h.

Resolution of the stereoisomers was carried out using diastereomeric crystallization (Scheme 3). The racemic α-ET analog freebase was first derivatized using a camphor sulfonic acid stereoisomer. Subsequently, four recrystallizations were performed to isolate one stereoisomer of the α-ET analog. The other isomer could not be isolated from

92

mother liquor so starting from a separate racemic α-ET batch, the same procedure was

followed except using the opposite camphor sulfonic acid stereoisomer for derivatization.

Scheme 3. Chiral resolution of α-ETs stereoisomers.

(±)αET
R = -H (**27**)
R = -OMe (**45**)

R = -H (**27b**)
R = -OMe (**45b**)

R = -H (**27a**)
R = -OMe (**45a**)
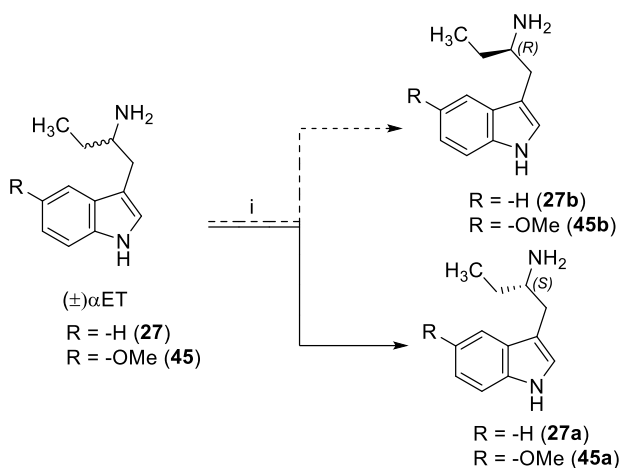
i) (1*S*)-(+)-10-camphorsulfonic acid or (1*R*)-(-)-10-camphorsulfonic acid

Each stereoisomer was evaluated for optical rotation using a polarimeter (Table 12) and

chiral HPLC was used as an additional method to determine purity of each enriched 5-

MeO-α-ET stereoisomer (Figure 48). The *S* isomer had an enantiomeric excess (*ee*) of

95% whereas the *R* isomer had an *ee* of 75.6%. Regardless, each stereoisomer was

substantially enriched and should be expected to behave in biological assays as if

enantiopure.

Table 12. Molecular formula, molecular weight, optical rotation, and melting point of chiral α-ET and 5-MeO-α-ET target compounds.

Compound	Molecular Formula	MW	Optical Rotation	Melting Point
(*S*) α-ET (**27a**)	$C_{12}H_{16}N_2 \cdot C_2H_4O_2$	248.33	49.8°	166-168 °C
(*R*) α-ET (**27a**)	$C_{12}H_{16}N_2 \cdot C_2H_4O_2$	248.33	-39.8°	168-170 °C
(*S*) 5-MeO-α-ET (**27a**)	$C_{13}H_{18}N_2O \cdot HCl$	254.76	40.7°	224-226 °C
(*R*) 5-MeO-α-ET (**27a**)	$C_{13}H_{18}N_2O \cdot HCl$	254.76	-46.0°	224-226 °C

(±) 5-MeO-α-ET 47.4% *R* 52.6% *S*
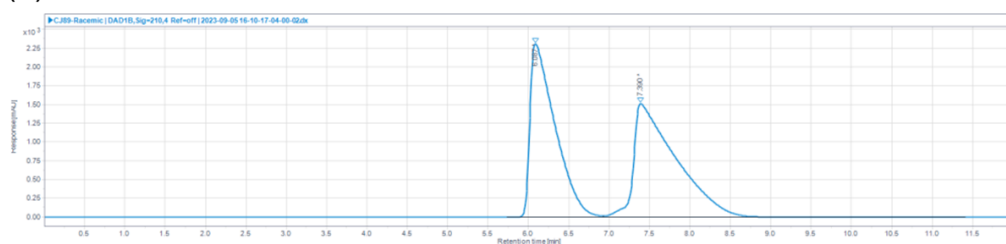
(*S*) 5-MeO-α-ET 2.5% *R* 97.5% *S*
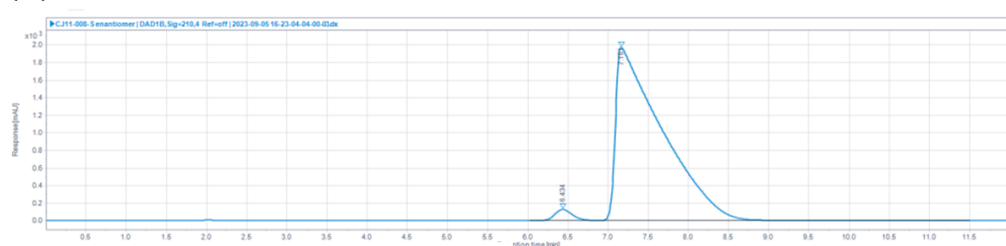
(*R*) 5-MeO-α-ET 88.3% *R* 11.7% *S*
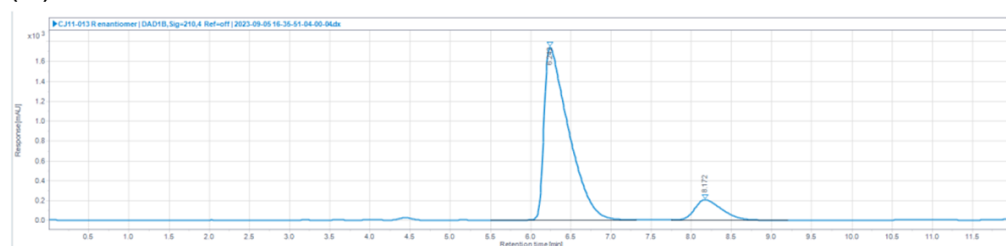
Figure 48. Chiral HPLC resolution of 5-MeO-α-ET.

This separation by recrystallization method used for resolving the stereoisomers of α-ETs is highly inefficient. Even in the patent that the procedure was adopted from started with 51.8 g of racemic α-ET to only obtain 6.8 g of one stereoisomer.[120] With that in mind an asymmetric synthetic route would appear to be warranted for future studies regarding α-ETs. Following are several proposed methods for the synthesis of chiral α-ETs.

Scheme 4 starts from commercially available tryptophan (**72**). First, an Arndt-Eistert synthesis forms a homologated carboxylic acid resulting in a β-amino acid **75**. This is accomplished by activation of the tryptophan carboxylic acid with thionyl chloride to form acid halide **73** that then acylates the carbon atom from diazomethane generating α-diazoketone **74**. Using a silver catalyst, a Wolff-rearrangement occurs forming a ketene intermediate from the diazoketone. In the presence of water as a nucleophile the ketene transitions to carboxylic acid **75**. Reduction of the carboxylic acid yields primary alcohol **76**. Protection of the amine is afforded by reaction with benzyl chloroformate, forming **77** followed by protection of the alcohol with 4-toluenesulfonyl chloride, yielding **78**. A final reduction removes the tosyl group and deprotects the amine, yielding the target chiral α-ET. Both stereoisomers of tryptophan are readily available but the one drawback for this method is only unsubstituted α-ET can be synthesized.

Scheme 4. Proposed asymmetric synthesis of α-ET.
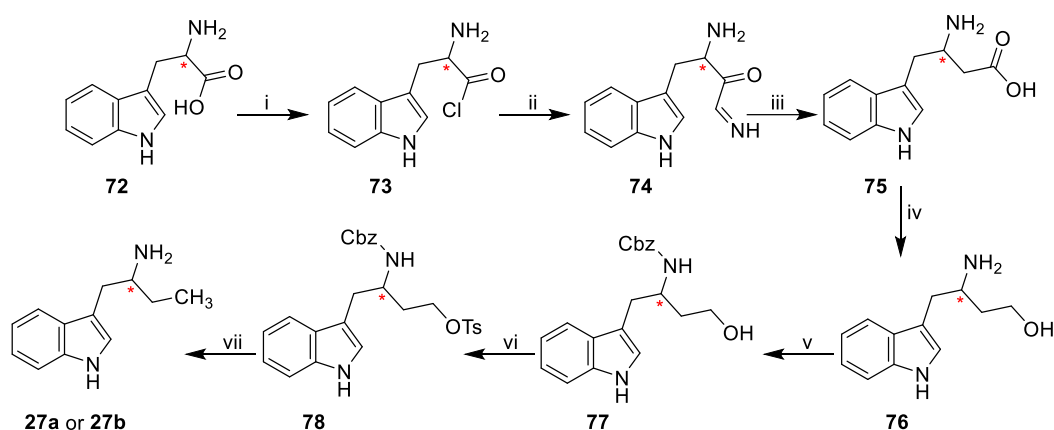
i) SOCl$_2$, DCM, DMF, 0 °C; ii) CH$_2$N$_2$, CH$_3$Cl, N$_2$; iii) PhCO$_2$Ag, H$_2$O, dioxane; iv) LAH, Et$_2$O; v) CbzCl, dioxane, 10% AcOH; vi) TsCl, CH$_2$CN; vii) LAH, Et$_2$O.

Another asymmetric method to obtain chiral α-ETs is to start with commercially available fluorenylmethoxycarbonyl (Fmoc) protected 2-aminobutyric acid **79** and a substituted indole **81**. This method (Scheme 5) can yield substituted chiral α-ETs. The carboxylic acid of Fmoc-2-aminobutyric acid is transformed into acid halide **80**, utilizing thionyl chloride. Then, an *N*-metallated indole **82** is obtained by reaction of indole or substituted indole **81** with a Grignard reagent. Activated nucleophile **82** is reacted with the acid chloride electrophile **80,** yielding ketone **83**. Deprotection of the amine generates **84,** followed by reduction of the ketone, yielding the target chiral α-ET **27a** or **27b**.

Scheme 5. Proposed asymmetric synthesis of substituted α-ETs.
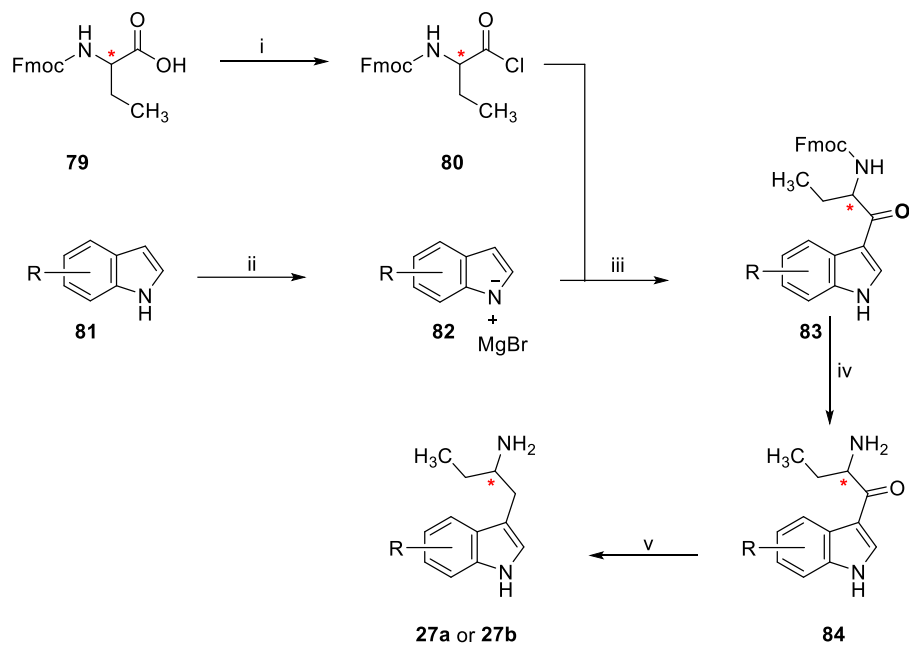
i) SOCl$_2$, DCM, DMF, 0 °C; ii) EtMgBr, DCM, 0 °C; iii) DCM, 0 °C, 1 M HCl; iv) 10% piperidine, DMF, rt; v) NaBH$_4$, CH$_3$CN, *i*-PrOH, reflux.

An additional asymmetric method that has been reported[219] involves preparation of the indole nucleophile **89** with a Grignard reagent in the presence of CuCl (Scheme 6). The nucleophile is then reacted with *N*-Boc protected chiral cyclic sulfamidate **87** that is prepared from commercially available *N*-Boc-2-aminobutanol **85**. This method can also yield substituted α-ETs as with the previous one, but also has the benefit of greater atom economy.

Scheme 6. Alternative proposed asymmetric synthesis of substituted α-ETs.
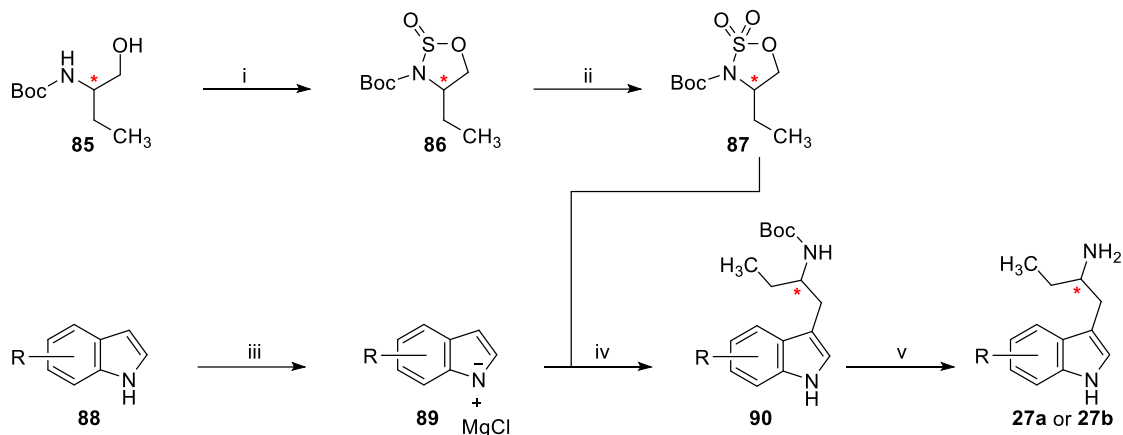
i) SOCl$_2$, pyridine, DCM, -40 °C; ii) RuCl$_3$, NaIO$_4$, CH$_3$CN, H$_2$O, 0 °C; iii) MeMgCl, CuCl, DCM, -20 °C; iv) DCM -20 °C v) HCl, MeOH 0 °C.

4. Affinity and activity of α-ET at 5-HT$_{2A}$ Receptors

As predicted, binding affinity increased for all substituted racemic compounds tested compared to unsubstituted α-ET (Table 13). The 4-methoxy substituted α-ET had the greatest binding affinity out of the series. Interestingly, 4- and 5-substitution patterns for the halogen had the same effect and both had approximately the same affinity.

Table 13. Binding affinity for α-ETs at 5-HT$_{2A}$ receptors expressed in HEK293 cells with [^{3}H]ketanserin as the radioligand.[a]

Compound	K_i (nM)	pK_i ± SEM
α-ET (**27**)	56234	4.25 ± 4.05
4-MeO-α-ET (**44**)	154	6.81 ± 0.39
5-MeO-α-ET (**45**)	4073	5.39 ± 0.36
4-Br-α-ET (**46**)	1698	5.77 ± 0.20
5-Br-α-ET (**47**)	1737	5.76 ± 0.16

[a]Data generated and provided by Dr. González -Maeso's laboratory, VCU.

When testing the stereoisomers of α-ET and 5-MeO-α-ET, it was found that all isomers bind at 5-HT$_{2A}$ receptors with the unsubstituted *S* isomer having the greatest affinity (Table 14). The racemic unsubstituted α-ET demonstrated poor binding yet each of the stereoisomers exhibited binding affinities similarly to 5-MeO-α-ET and its two stereoisomers. Although the modeling predicted that both isomers of α-ET should bind and this biological data supports that prediction, it is surprising that (*R*) α-ET did not have any activity in the Ca^{+2} mobilization activity assay as previously reported.[124] This prompted the evaluation of the α-ET series in the Ca^{+2} mobilization activity assay.

Table 14. Binding affinity for α-ET and 5-MeO-α-ET stereoisomers at 5-HT$_{2A}$ receptors expressed in HEK293 cells with [^{3}H]ketanserin as the radioligand.[a]

Compound	K_i (nM)	pK_i ± SEM
(±) α-ET (**27**)	56234	4.25 ± 4.05
(*S*) α-ET (**27a**)	1096	5.96 ± 0.17
(*R*) α-ET (**27b**)	5370	5.27 ± 0.45
(±) 5-MeO-α-ET (**45**)	4073	5.39 ± 0.36
(*S*) 5-MeO-α-ET (**45a**)	6166	5.21 ± 0.23
(*R*) 5-MeO-α-ET (**45b**)	9772	5.01 ± 0.19

[a]Data generated and provided by Dr. González
-Maeso's laboratory, VCU.

All substituted racemic compounds demonstrated agonist activity with 4-Br-α-ET displaying full agonism of 5-HT$_{2A}$ receptors (Table 15). As was previously reported[124] α-ET was not active in the assay. 4-MeO-α-ET had the lowest maximal response but was the most potent of the series. The bromo-substituted α-ETs had low potency (EC$_{50}$ > 10000 nM) contrasting their greater binding affinity. Racemic and both stereoisomers of 5-MeO-α-ET had the opposite occur with greater activity compared to lower binding affinity. However, 4-Br-α-ET (**46**) displayed full agonism (Table 15)

Table 15. Activity of racemic α-ETs at 5-HT$_{2A}$ receptors expressed in HEK293 cells in Ca^{+2} mobilization assay.[a]

Compound	EC$_{50}$ (nM)	pEC$_{50}$ ± SEM	E$_{MAX}$[%]
α-ET (**27**)	Inactive[b]	Inactive[b]	Inactive[b]
4-MeO-α-ET (**44**)	24	7.61 ± 0.78	11
5-MeO-α-ET (**45**)	166	6.78 ± 0.31	34
4-Br-α-ET (**46**)	51286	4.29 ± 0.50	100
5-Br-α-ET (**47**)	15488	4.81 ± 0.26	58

[a]Data generated and provided by Dr. González -Maeso's laboratory, VCU. [b]No activity up to 100 µM.

Evaluation of the stereoisomers of α-ETs demonstrated similar results to previously published data. The *S* stereoisomer of unsubstituted α-ET displayed partial agonist activity and the *R* stereoisomer as well as racemic α-ET were inactive (Table 16) in agreement with data published by Blough et al.[124] Two different experiments were performed to validate the previously reported activity for (*S*) α-ET, one using a FlexStation and the other employing epifluorescence microscopy. Testing the methoxy-substituted stereoisomers exhibited somewhat surprising results; racemic and both stereoisomers were all active as partial agonists. This biological data is in agreement with and supports the computational modeling studies, but is nonetheless interesting as it demonstrates the addition of a substituent can overcome stereospecific activity.

Table 16. Activity of chiral α-ETs at 5-HT$_{2A}$ receptors expressed in HEK293 cells in Ca^{+2} mobilization assay.[a]

Compound	EC$_{50}$ (nM)	pEC$_{50}$ ± SEM	E$_{Max}$[%]
(±) α-ET (**27**)	Inactive[c]	Inactive[c]	Inactive[c]
(S) α-ET (**27a**)	16218	4.79 ± 0.38	25
(S) α-ET (**27a**)[b]	4314	5.36 ± 0.42	56
(R) α-ET (**27b**)	Inactive[c]	Inactive[c]	Inactive[c]
(±) 5-MeO-α-ET (**45**)	166	6.78 ± 0.31	34
(S) 5-MeO-α-ET (**45a**)	316	6.50 ± 0.37	49
(R) 5-MeO-α-ET (**45b**)	794	6.10 ± 0.58	29

[a]Data obtained from the González-Maeso laboratory. [b]Data obtained using epifluorescence microscopy. [c]No signal up to 100 μM.

The affinity data coupled with activity data then posits the question: Could (R) α-ET be an antagonist? If so, it would explain why racemic α-ET did not show any activity. Two separate possible explanations are presented here:

1. Both stereoisomers can bind at the same time, both agonist and antagonist, overall resulting in the receptor taking on an antagonist/low affinity conformation as observed with antagonist and agonist ligands for 5-HT$_2$ receptors.[220]

2. The stereoisomers do not bind at the same time, resulting in competitive inhibition and racemic α-ET is weakly active at >>10,000 nM.

It has been recently speculated that for a 5-HT$_{2A}$ receptor agonist to induce hallucinogenic activity in humans a threshold E$_{MAX}$ of 70% must be achieved.[221] In our α-ET series examined thus far, only 4-Br-α-ET displayed an E$_{MAX}$ that exceeds this hypothetical threshold. The remainder of the agents in the series might then prove to be attractive as leads in the design of fast-acting non-hallucinogenic 5-HT$_{2A}$ receptor agonist antidepressants. This series of α-ET compounds is well suited to test the 70% E$_{MAX}$ hypothesis and serve as molecular tools in future studies.

V. Summary of Conclusions

It has now been determined that BPs do not behave identically to abused cathinones and instead act in closer relation to MPH analogs. In this manner, it seems that BPs are, in fact, a novel class of compounds with a unique pharmacology that warrants future studies. The generated homology model of DAT was shown to be adequate for modeling BP reuptake inhibitor interactions as the docking studies were able to predict the eutomer as well as implicate halogen bond interactions despite software limitations. Not only has it now been established that BPs show *R* stereoselectivity at DAT but also it has now been determined how these agents interact with SERT. Docking studies at SERT predicted the stereoselectivity that the BPs displayed in biological assays but were unable to predict their action as a substrate or a reuptake inhibitor. Using pentedrone as a comparison, conformationally constraining its α-alkyl chain by ligating it back onto the methylamine moiety forming a piperidine ring (BP) renders a substrate at SERT into a reuptake inhibitor. BPs also displayed opposite stereoselectivity at SERT compared to DAT as it was shown the *S* isomer is the eutomer. In addition, aryl substitution has now been shown to possess moderate influence over activity at SERT for BPs. By simple substitution, BPs exhibited the spectrum of exceedingly weak inhibition activity at greater than 25 µM transitioning to low micromolar activity at SERT. New insights on MATs have also been discovered. In DAT, the amino acid SER149 is very likely implicated in the enhanced potency of DCBP (**41**) due to halogen bond formation. Utilizing computational modeling, chemical agents as tools, and mutagenesis studies, evidence establishes the impact that SER149 can present. Taken together these studies demonstrate medicinal chemistry drug design principles on how activity and stereoselectivity between DAT and SERT can

be fine-tuned for drug development and lead optimization. It is thus suggested that this series of BPs and related BP analogs be used in future animal studies to determine abuse liability and to what extent the ratio of DAT to SERT activity has on abuse liability for related MAT reuptake inhibitors. These agents are likely to show utility in low abuse-liability ADHD treatments, new antidepressants with fewer side effects, and the development of stimulant abuse treatments through understanding SAR and molecular mechanisms of MATs.

Studies into α-ETs and the 5-HT$_{2A}$ receptor revealed for the first time the affinity these agents have for 5-HT$_{2A}$ receptors. Prepared and examined were α-ET, analogs bearing 4- and 5-position methoxy substituents, and their optical isomers. The most enigmatic revelation was that racemic and (R) α-ET bind to the receptor but have no activity in a 5-HT$_{2A}$ receptor functional assay. It might be possible that the chiral center is actually a molecular switch for agonist/antagonist activity. Docking studies utilizing the 5-HT$_{2A}$ receptor in a partial agonist conformation were not able to predict the activity of the α-ET series but they did predict that all α-ETs examined would bind to the receptor. If a molecular switch does exist for α-ET it has yet to be determined through modeling. With some differences in pharmacology for the stereoisomers being elucidated it is very possible that a difference in agranulocytosis liability for these agents could also exist. Interestingly, enough the puzzling affinity/activity data only held true for unsubstituted α-ET. While computational studies did demonstrate a juxtaposition in binding modes for 5-Br-α-ET and unsubstituted α-ET stereoisomers, racemic 5-Br-α-ET showed agonist activity at 5-HT$_{2A}$ receptors yet racemic unsubstituted α-ET showed no activity. All substituted α-ETs demonstrated the predicted increases in affinity and activity. Future

studies on this series of molecules should include animal studies to elucidate abuse liability, the onset and duration of antidepressant like activity, and potential hallucinogenic activity with HTR. Future investigations into these molecules for therapeutic potential is thoroughly warranted.

All in all, this work has provided a means in which to expand the understanding of SAR at target sites of ADHD, depression, and drugs of abuse (see Figure 21). These are the first studies of BP isomers at MATs, and binding modes/affinities of α-ETs at 5-HT$_{2A}$ receptors. Additionally, synthetic strategies have been proposed as to prepare chiral α-ETs to be used in further animal studies, as well as drug development in the case of potential therapeutics.

VI. Experimentals

DAT Homology Modeling

One hundred homology models of hDAT were generated using MODELLER 9.24 and three crystal structures as a template. The two highest identity dDAT crystal structures (PDB ID: 4XPB and 4XPT) at 55.35% identity as well as the greatest query coverage hSERT crystal structure (PDB ID: 6VRH) at 92% coverage were used. The original alignment of the structures was conducted using BLAST. The sequences of dDAT, hSERT, and hDAT were obtained from genpept (accession codes 4XPB_A, 6VRH_A, and BAA22511, respectively). Due to the lack of corresponding residues, the first 54 residues from the N-terminus were not modeled. The homology model with the lowest discrete optimized protein energy DOPE score and highest GA341 score was then selected for further analysis and validation. GA341 is a multivariate scoring function that depends on compactness and combined statistical potential z-score of the model as well as the percentage sequence identity of the target-template alignment that was used to build the model. Candidate model was subjected to analysis through a PROCHECK, and ProTable, and then validated by the docking.

Protein Structure Analysis

PROCHECK and ProTable were used to analyze the lead hDAT homology model. PROCHECK examines the stereochemical quality of the hDAT structure, producing a number of plots analyzing its overall and residue-by-residue geometry. The Ramachandran plot (Figure 27) generated by PROCHECK has 94.6% of the residues

from the hDAT homology model in the most favored regions. The test ligands cocaine and 3,4-dichlorophenethylamine were sketched using SYBYL-X 2.1.1 and energy-minimized using Powell Method and the Tripos Force Field with Gasteiger–Hückel charges and a distance-dependent dielectric constant of 1.0 D/Å to an energy gradient cutoff of 0.05 kcal $(\text{mol} \times \text{Å})^{-1}$.

Molecular docking was conducted using the GOLD scoring function from GOLD 2020. GOLD is an optimized scoring function for the prediction of the binding orientation of small-molecules that takes into account protein-ligand hydrogen bond energy, protein-ligand van der Waals energy, ligand internal vdW energy, and ligand torsional strain energy. The test ligands cocaine and 3,4-dichlorophenethylamine were docked 100 times each into the hDAT homology model and the resultant 200 docking solutions were analyzed. The GOLD docking solutions were ranked according to their overall fitness function scores. The binding site was defined to include all atoms within 10 Å of the carboxylic acid portion of the key amino acid residue ASP79 which makes an essential salt bridge interaction with the nitrogen atom of hDAT agents.

SERT Model

A model of SERT was generated using the crystal structure PDB ID: 5I6X. All molecules and antibody fragments were removed and then hydrogen atoms were added to the protein and the model was minimized using the Tripos Force Field with Gasteiger-Hückel charges.

5-HT$_{2A}$ Receptor Model

A model of a 5-HT$_{2A}$ receptor was generated using the crystal structure PDB ID: 6WGT as a template.[189] All molecules and other co-crystallized receptors were removed and then hydrogen atoms were added to the protein and the model was minimized using the Tripos Force Field with Gasteiger-Hückel charges.

Docking Studies

The GOLD2020 docking suite was used for docking all compounds. The binding pocket was defined by a 10 Å radius surrounding the essential amino acid residues ASP79 for DAT, ASP98 for SERT, and ASP155 for 5-HT$_{2A}$. Each compound was first sketched in SybylX 2.1.1 and energy minimized using the Tripos Force Field with Gasteiger-Hückel charges, and then 100 docking solutions were generated, using default parameters.

Hydropathic Analysis

Each docking solution was then merged into the model protein, minimized, and extracted, and HINT analysis[202] was performed using Sybyl 8.1's and Sybyl's Programing Language (spl) scripts. The HINT scores for each docking solution were ranked from the highest to lowest, with the highest scored solution being used to tabulate the specific atomic interactions between the test compound and the amino acids of the protein. All instances of a positive interaction or negative interaction between the test compound and all amino

acid residues identified by HINT were added together for a qualitative analysis of the overall influence on affinity/activity.

Synthesis

Melting points were taken on MEL TEMP melting point apparatus in glass capillary tubes and are uncorrected. ^{1}H NMR spectra were recorded using a Bruker AXR 400 MHz spectrometer with tetramethylsilane (TMS) as an internal standard. Signal positions are given in parts per million (δ) downfield from TMS, together with their splitting pattern (s = singlet, d = doublet, t = triplet, q = quartet, dd = doublet of doublets, m = multiplet), coupling constant (J, Hz) and integration. HRMS were recorded using a Waters Acquity tandem quadrupole (TQD) instrument with electrospray ionization. Optical rotation was measured on a Jasco P-2000 polarimeter. HPLC analysis was performed on an Agilent 1260 Infinity II SFC with a diode array detector and Chiralpak-CBH (4.0 x 150 mm; 5.0 µm) column. Microanalyses were performed by Atlantic Microlab Inc. (Norcross, GA) for the indicated elements and results are within 0.4% of calculated values. Reactions were routinely monitored by thin-layer 105 chromatography (TLC) using silica gel GHLF plates (250 mm, 2.5 x 10 cm; Analtech Inc. Newark, DE), and flash chromatography was performed on a CombiFlash Companion/TS (Teledyne Isco Inc. Lincoln, NE). All final compounds were prepared either as hydrochloride, oxalate, or acetate water-soluble salts. Compound **27** and both of its stereoisomers as their acetate salts were available from earlier studies in the laboratory. Racemic compounds **41-43** were prepared as their

HCl salt and available from a previous study.[183] Compound **44** was previously prepared by Dr. Carmen Abate and compounds **46** and **47** were prepared by Dr. Ajay Bansode.

(*R*)-(+)-2-(3,4-Dichlorobenzoyl)-piperidine Hydrochloride (41a). 4-Bromo-1,2-dichlorobenzene (0.67 g, 2.97 mmol) was added to a solution of anhydrous Et_2O (5 mL) under an N_2 atmosphere and cooled to -78 °C (acetone : dry ice bath) and then 2.5 M n-BuLi in hexane (2.37 mL, 5.93 mmol) was added in a dropwise manner over 15 min. The reaction mixture was stirred at -78 °C (acetone : dry ice bath) for 3 h to give intermediate **54**. In another flask a stirred solution of **50a** (0.81 g, 2.96 mmol) in Et_2O (5 mL) under an N_2 atmosphere was cooled to -29 °C (o-xylene : dry ice bath) and then **54** was added in a dropwise manner over 15 min. The reaction mixture was stirred at -29 °C (o-xylene : dry ice bath) for 3 h and then allowed to warm to room temperature with continued stirring for 12 h. The reaction mixture was quenched using cold 1M KH_2PO_4 (30 mL), extracted with EtOAc (3 x 20 mL), dried over $MgSO_4$, filtered, and evaporated under reduced pressure to yield a yellow oil that was chromatographed on silica gel 9.5:0.5 hexane:EtOAc. The collected pure fractions were combined, and solvent was removed under reduced pressure to yield a crude yellow oil. The oil was dissolved in anhydrous MeOH and cooled in an ice bath. Anhydrous methanolic HCl was added in a dropwise manner until pH=1. The solution was stirred overnight and evaporated to dryness. Recrystallization from MeOH gave 0.25 g (23% yield) of **41a** as a white solid: mp 269-271 °C; $[\alpha]_D^{25}$36.4° (c = 0.176, MeOH); ^{1}H NMR (DMSO-d_6, 400 MHz): δ 1.43 (m, 1H, CH_2), 1.77 (m, 4H, 2 x CH_2), 2.06 (d, 1H, *J* = 16 Hz, CH_2), 2.91 (m, 1H, CH_2), 3.33 (d, 1H,

J = 16 Hz, CH$_2$), 5.16 (m, 1H, CH), 7.90 (m, 1H, ArH), 8.02 (m, 1H, ArH), 8.31 (s, 1H, ArH), 9.00 (br s, 1H, NH), 9.75 (br s, 1H, NH$^+$); HRMS (ESI-TOF) m/z [M + H]$^+$ calcd for C$_{12}$H$_{14}$NOCl$_2$, 258.0452; found, 258.0435.

(*S*)-(-)-2-(3,4-Dichlorobenzoyl)-piperidine Hydrochloride (41b). 4-Bromo-1,2-dichlorobenzene (0.45 mL, 3.5 mmol) was added to a solution of anhydrous Et$_2$O (5 mL) under an N$_2$ atmosphere and cooled to -78 °C (acetone : dry ice bath) and then 2.5 M n-BuLi in hexane (1.43 mL, 3.5 mmol) was added in a dropwise manner over 15 min. The reaction mixture was stirred at -78 °C (acetone : dry ice bath) for 3 h to give intermediate **54**. In another flask a stirred solution of **50b** (0.50 g, 1.8 mmol) in Et$_2$O (5 mL) under an N$_2$ atmosphere was cooled to -29 °C (o-xylene : dry ice bath) and then **54** was added in a dropwise manner over 15 min. The reaction mixture was stirred at -29 °C (o-xylene : dry ice bath) for 3 h and then allowed to warm to room temperature with continued stirring for 12 h. The reaction mixture was quenched using cold 1 M KH$_2$PO$_4$ (30 mL), extracted with EtOAc (3 x 20 mL), dried over MgSO$_4$, filtered, and evaporated under reduced pressure to yield a yellow oil that was chromatographed on silica gel 9.5:0.5 hexane:EtOAc. The collected pure fractions were combined, and solvent was removed under reduced pressure to yield a crude yellow oil. The oil was dissolved in anhydrous MeOH and cooled in an ice bath. Anhydrous methanolic HCl was added in a dropwise manner until pH=1. The solution was stirred overnight and evaporated to dryness. Recrystallization from MeOH gave 0.16 g of **41b** (29% yield) as a white solid: mp 272-274 °C; [α]$_D^{25}$-40.8° (c = 0.114, MeOH); ^{1}H NMR (DMSO-*d$_6$*, 400 MHz): δ 1.43 (m, 1H, CH$_2$), 1.77 (m, 4H, 2 x CH$_2$), 2.06 (d, 1H, *J* = 16 Hz, CH$_2$), 2.94 (m, 1H, CH$_2$), 3.32 (d, 1H,

J = 16 Hz, CH₂), 5.16 (m, 1H, CH), 7.89 (m, 1H, ArH), 8.02 (m, 1H, ArH), 8.31 (s, 1H, ArH), 9.00 (br s, 1H, NH), 9.80 (br s, 1H, NH⁺); HRMS (ESI-TOF) m/z [M + H]⁺ calcd for $C_{12}H_{14}NOCl_2$, 258.0452; found, 258.0451.

(*R*)-(+)-2-(3,4-Dimethylbenzoyl)-piperidine Hydrochloride (42a). 4-Bromo-o-xylene (0.35 mL, 2.6 mmol) was added to a solution of anhydrous Et_2O (5 mL) under an N_2 atmosphere and cooled to 0 °C (ice bath) and then 2.5 M n-BuLi in hexane (1.26 mL, 3.1 mmol) was added in a dropwise manner over 15 min. The reaction mixture was stirred at 0 °C (ice bath) for 3 h to give intermediate **55**. In another flask a stirred solution of **50a** (0.50 g, 1.8 mmol) in Et_2O (5 mL) under an N_2 atmosphere was cooled to -29 °C (o-xylene : dry ice bath) and then **55** was added in a dropwise manner over 15 min. The reaction mixture was stirred at -29 °C (o-xylene : dry ice bath) for 3 h and then allowed to warm to room temperature with continued stirring for 12 h. The reaction mixture was quenched using cold 1 M KH_2PO_4 (30 mL), extracted with EtOAc (3 x 20 mL), dried over $MgSO_4$, filtered, and evaporated under reduced pressure to yield a yellow oil that was chromatographed on silica gel 9.5:0.5 hexane:EtOAc. The collected pure fractions were combined, and solvent was removed under reduced pressure to yield a crude yellow oil. The oil was dissolved in anhydrous MeOH and cooled in an ice bath. Anhydrous methanolic HCl was added in a dropwise manner until pH=1. The solution was stirred overnight and evaporated to dryness. Recrystallization from MeOH gave 0.20 g (45% yield) of **42a** as a white solid: mp 267-269 °C; [α]$_D^{25}$40.0° (c = 0.132, MeOH); ¹H NMR (DMSO-*d₆*, 400 MHz): δ 1.45 (m, 1H, CH₂), 1.76 (m, 4H, 2 x CH₂), 2.05 (d, 1H, *J* = 16 Hz, CH₂), 2.31 (s, 6H, 2 x CH₃), 2.96 (m, 1H, CH₂), 3.30 (d, 1H, *J* = 16 Hz, CH₂), 5.07 (m, 1H,

CH), 7.36 (m, 1H, ArH), 7.79 (m, 1H, ArH), 7.83 (s, 1H, ArH), 8.88 (br s, 1H, NH), 9.79 (br s, 1H, NH$^+$); HRMS (ESI-TOF) m/z [M + H]$^+$ calcd for $C_{14}H_{20}NO$, 218.1545; found, 218.1535.

(*S*)-(-)-2-(3,4-Dimethylbenzoyl)-piperidine Hydrochloride (42b). 4-Bromo-o-xylene (0.35 mL, 2.6 mmol) was added to a solution of anhydrous Et$_2$O (5 mL) under an N$_2$ atmosphere and cooled to 0 °C (ice bath) and then 2.5 M n-BuLi in hexane (1.26 mL, 3.1 mmol) was added in a dropwise manner over 15 min. The reaction mixture was stirred at 0 °C (ice bath) for 3 h to give intermediate **55**. In another flask a stirred solution of **50b** (0.50 g, 1.8 mmol) in Et$_2$O (5 mL) under an N$_2$ atmosphere was cooled to -29 °C (o-xylene : dry ice bath) and then **55** was added in a dropwise manner over 15 min. The reaction mixture was stirred at -29 °C (o-xylene : dry ice bath) for 3 h and then allowed to warm to room temperature with continued stirring for 12 h. The reaction mixture was quenched using cold 1 M KH$_2$PO$_4$ (30 mL), extracted with EtOAc (3 x 20 mL), dried over MgSO$_4$, filtered, and evaporated under reduced pressure to yield a yellow oil that was chromatographed on silica gel 9.5:0.5 hexane:EtOAc. The collected fractions were combined, and solvent was removed under reduced pressure to yield a crude yellow oil. The oil was dissolved in anhydrous MeOH and cooled in an ice bath. Anhydrous methanolic HCl was added in a dropwise manner until pH=1. The solution was stirred overnight and evaporated to dryness. Recrystallization from MeOH gave 0.27 g (57% yield) of **42b** as a white solid: mp 266-269 °C; [α]$_D^{25}$-40.1° (c = 0.120, MeOH); ^{1}H NMR (DMSO-*d$_6$*, 400 MHz): δ 1.45 (m, 1H, CH$_2$), 1.75 (m, 4H, 2 x CH$_2$), 2.06 (d, 1H, *J* = 16 Hz, CH$_2$), 2.32 (s, 6H, 2 x CH$_3$), 2.97 (m, 1H, CH$_2$), 3.30 (d, 1H, *J* = 16 Hz, CH$_2$), 5.05 (m, 1H,

CH), 7.36 (m, 1H, ArH), 7.79 (m, 1H, ArH), 7.83 (s, 1H, ArH), 8.87 (br s, 1H, NH), 9.70 (br s, 1H, NH$^+$); HRMS (ESI-TOF) m/z [M + H]$^+$ calcd for $C_{14}H_{20}NO$, 218.1545; found, 218.1536.

(*R*)-(+)-2-(Naptho-2-yl)-piperidine Hydrochloride (43a). 2-Bromonapthalene (0.43 g, 2.1 mmol) was added to a solution of anhydrous Et$_2$O (5 mL) under an N$_2$ atmosphere and cooled to -78 °C (acetone : dry ice bath) and then 2.5 M n-BuLi in hexane (1.68 mL, 4.18 mmol) was added in a dropwise manner over 15 min. The reaction mixture was stirred at -78 °C (acetone : dry ice bath) for 3 h to give intermediate **56**. In another flask a stirred solution of **50a** (0.57 g, 2.0 mmol) in Et$_2$O (5 mL) under an N$_2$ atmosphere was cooled to -29 °C (o-xylene : dry ice bath) and then **56** was added in a dropwise manner over 15 min. The reaction mixture was stirred at -29 °C (o-xylene : dry ice bath) for 3 h and then allowed to warm to room temperature with continued stirring for 12 h. The reaction mixture was quenched using cold 1 M KH$_2$PO$_4$ (50 mL), extracted with EtOAc (3 x 20 mL), dried over MgSO$_4$, filtered, and solvent was evaporated under reduced pressure to produce a yellow oil that was chromatographed on silica gel 9.5:0.5 hexane:EtOAc. The collected pure fractions were combined, and solvent was removed under reduced pressure to yield a crude yellow oil. The oil was dissolved in anhydrous MeOH and cooled in an ice bath. Anhydrous methanolic HCl was added in a dropwise manner until pH=1. The solution was stirred overnight and evaporated to dryness to yield a beige solid. Recrystallization from EtOH/Et$_2$O gave 0.06 g of **43a** as a white solid (11% yield): mp 264-266 °C; $[\alpha]_D^{25}$70.5° (c = 0.114, MeOH); ^{1}H NMR (DMSO-*d$_6$*, 400 MHz): δ 1.51 (m, 1H, CH$_2$), 1.69 (m, 1H, CH$_2$), 1.72 (m, 3H, CH$_2$), 2.21 (d, 1H, *J* = 16 Hz, CH$_2$), 3.02 (m,

2H, CH$_2$), 5.26 (m, 1H, CH), 7.69 (m, 2H, ArH), 8.02 (m, 4H, ArH), 8.81 (s, 1H, ArH), 8.97 (br s, 1H, NH), 9.27 (br s, 1H, NH$^+$); HRMS (ESI-TOF) m/z [M + H]$^+$ calcd for C$_{16}$H$_{18}$NO, 240.1388; found, 240.1380.

(*S*)-(-)-2-(Naptho-2-yl)-piperidine Hydrochloride (43b). 2-Bromonapthalene (0.46 g, 2.2 mmol) was added to a solution of anhydrous Et$_2$O (5 mL) under an N$_2$ atmosphere and cooled to -78 °C (acetone : dry ice bath) and then 2.5 M n-BuLi in hexane (1.77 mL, 4.4 mmol) was added in a dropwise manner over 15 min. The reaction mixture was stirred at -78 °C (acetone : dry ice bath) for 3 h to give intermediate **56**. In another flask a stirred solution of **50b** (0.59 g, 2.19 mmol) in Et$_2$O (5 mL) under an N$_2$ atmosphere was cooled to -29 °C (o-xylene : dry ice bath) and then **56** was added in a dropwise manner over 15 min. The reaction mixture was stirred at -29 °C (o-xylene : dry ice bath) for 3 h and then allowed to warm to room temperature with continued stirring for 12 h. The reaction mixture was quenched using cold 1 M KH$_2$PO$_4$ (50 mL), extracted with EtOAc (3 x 20 mL), dried over MgSO$_4$, filtered, and solvent was evaporated under reduced pressure to yield a yellow oil that was chromatographed on silica gel 9.5:0.5 hexane:EtOAc. The collected pure fractions were combined, and solvent was removed under reduced pressure to yield a crude yellow oil. The oil was dissolved in anhydrous MeOH and cooled in an ice bath. Anhydrous methanolic HCl was added in a dropwise manner until pH=1. The solution was stirred overnight and evaporated to dryness. Recrystallization from MeOH/Et$_2$O gave 0.16 g (27% yield) of **43b** as a white solid: mp 272 °C; [α]$_D^{25}$-70.0° (c = 0.109, MeOH); ^{1}H NMR (DMSO-*d$_6$*, 400 MHz): δ 1.52 (m, 1H, CH$_2$), 1.82 (m, 4H, 2 x CH$_2$), 2.21 (d, 1H, *J* = 16 Hz, CH$_2$), 3.03 (m, 1H, CH$_2$), 3.38 (d, 1H, *J* = 16 Hz, CH$_2$), 5.26 (m, 1H, CH), 7.70 (m, 2H,

ArH), 8.05 (m, 4H, ArH), 8.83 (s, 1H, ArH), 8.98 (br s, 1H, NH), 9.49 (br s, 1H, NH+);

HRMS (ESI-TOF) m/z [M + H]+ calcd for $C_{16}H_{18}NO$, 240.1388; found, 240.1374.

4-Methoxy-α-ethyltryptamine Oxalate (44). The compound was prepared in our laboratory by Dr. Carmen Abate (as CA-55). 4-Methoxygramine (**63**) was obtained from 4-methoxyindole (**58**) following a literature procedure.[222] A solution of 4-methoxygramine (**63**) (1.05 g, 5.14 mmol) and NaOH (0.230 g, 5.75 mmol) in 1-nitropropane (10 mL) was allowed to stir under N_2 atmosphere for few minutes and then heated at reflux overnight. A solution of CH_3COOH (10 %, 10 mL) was added to the cooled (ice bath) mixture. The mixture was extracted with Et_2O (3 x 15 mL). The organic phases were combined, dried over Na_2SO_4 and then evaporated under reduced pressure to give a dark oil. Purification of the crude oil via column chromatography using CH_2Cl_2 as eluent afforded **68** (1.02 g, 80% yield) as a viscous orange oil: ^{1}H NMR ($CDCl_3$, 400 MHz): δ 1.03 (t, 3H, CH_3), 1.82-2.15 (m, 2H, CH_2CH_3), 3.39-3.43 (m, 2H, $ArCH_2$), 3.96 (s, 3H, OCH_3), 4.85-4.99 (m, 1H, $CHNO_2$), 6.52-7.14 (m, 4H, ArH), 8.00 (bs, 1H, NH).

A solution of 1-(4-methoxyindol-3-yl)-2-nitrobutane (**68**) (1.05 g, 4.2 mmol) in anhydrous Et_2O (20 mL) was added to a stirred suspension of $LiAlH_4$ (0.70 g, 18.6 mmol) in anhydrous Et_2O (30 mL) cooled at 0° C and kept under N_2 atmosphere. The mixture was then heated at reflux for 6 h and allowed to stand overnight at room temperature. The reaction mixture was cooled (ice bath) and H_2O and then 15% NaOH (8 mL of each) were added; the mixture was filtered through a Celite pad. The filtrate was extracted with Et_2O (3 x 30 mL); the organic phases were collected, dried over Na_2SO_4 and then evaporated

under reduced pressure. Purification of the crude mixture was achieved by filtration through silica gel using CH_2Cl_2 and MeOH (85/15) as eluent affording the final amine (0.50 g, 55%) as a white solid: mp 129-130 °C; ^{1}H NMR (CDCl$_3$, 400 MHz): δ 1.03 (t, 3H, CH$_3$), 1.26-1.65 (m, 2H, CH$_2$CH$_3$), 2.58-2.65 (m, 1H, CH), 2.90-3.08 (m, 2H, ArCH$_2$), 3.98 (s, 3H, OCH$_3$), 6.63-7.27 (m, 4H, ArH), 8.38 (bs, 1H, NH). The corresponding oxalate salt was obtained and recrystallized from anhydrous MeOH/anhydrous Et$_2$O to afford **44** (0.36 g, 52%) as beige crystals: mp 209-210 °C; ^{1}H NMR (DMSO-d_6, 400 MHz): δ 0.96 (t, 3H, CH$_3$), 1.52-1.62 (m, 2H, CH$_2$CH$_3$), 2.87-3.17 (m, 2H, ArCH$_2$), 3.26-3.34 (m, 1H, CH), 3.85 (s, 3H, OCH$_3$), 6.46-7.05 (m, 4H, ArH), 11.00 (bs, 1H, NH). Anal. Calcd for $C_{13}H_{18}N_2O \cdot C_2O_4H_2$ (C, H, N).

5-Methoxy-α-ethyltryptamine Hydrochloride (45). Raney nickel 50% solution in EtOH (0.34 g, 5.80 mmol) was added to a solution of absolute EtOH (10 mL) and 5-methoxy-3-(2-nitrobutyl)-1H-indole (**69**) (0.2 g, 0.81 mmol) under an N_2 atmosphere followed by the addition of hydrazine hydrate 20% solution in absolute EtOH (10 mL). The reaction mixture was heated at reflux for 3 h with stirring, allowed to cool to room temperature, filtered through Celite, and concentrated via reduced pressure. The resultant oil was taken up in DCM and cooled to 0 °C using an ice bath. Ethereal HCl was added in a dropwise manner until pH ~3. The formed precipitate was recrystallized using MeOH/Et$_2$O to yield 0.076 g of **45** (37% yield) as brown crystals: mp 224-226 °C (lit.[218] mp 226-227 °C); ^{1}H NMR (DMSO-d_6, 400 MHz): δ 0.9 (t, 3H, J = 8 Hz, CH$_3$), 1.33 (m, 1H, CH$_2$), 1.47 (m, 1H, CH$_2$), 1.81 (s, 3H, CH$_3$), 2.73 (m, 2H, CH$_2$), 2.96 (m, 1H, CH), 3.75 (s, 3H, CH$_3$), 6.48 (br s, 3H, NH$_3^+$ D$_2$O exchangeable), 6.62 (d, 1H, J = 8 Hz, ArH), 6.85 (s, 1H, ArH),

7.01 (s, 1H, ArH), 7.38 (d, 1H, J = 8 Hz, ArH), 10.69 (s, 1H, NH D_2O exchangeable); HRMS (ESI-TOF) m/z [M + H]$^+$ calcd for $C_{13}H_{19}N_2O$, 219.1497; found, 219.1500.

(S)-(+)-5-Methoxy-α-ethyltryptamine Hydrochloride (45a). Upjohn Co. prepared (S) α-ET by resolution of the racemate using camphorsulfonic acid.[223] Dr. Carmen Abate of our laboratory prepared the previously unreported HCl salt of the target compound (**45a**) via a similar route: mp 215-217 °C; $[\alpha]_D^{25}$36.5° (c = 0.8, MeOH); Anal. Calcd for ($C_{13}H_{18}$ $N_2O \cdot HCl \cdot 0.25H_2O$) C, H, N. Because an insufficient quantity of the isomer was on hand for the necessary studies, her synthesis was replicated.

The freebase of 5-methoxy-α-ethyltryptamine hydrochloride (**45**) (1.0 g) was prepared using sat. $NaHCO_3$ that was extracted with EtOAc (3 x 30 mL) and concentrated under reduced pressure. The freebase was dissolved in hot i-PrOH (10 mL) with (R)-(-)-camphorsufonic acid (0.94 g) and then recrystallized 4 times using i-PrOH. The crystals were then collected by filtration and dried under vacuum. The dried salt was dissolved in H_2O (10 mL) and 1.2 eq of 0.08 M NaOH was added in a dropwise manner. DCM (3 x 10 mL) was used to extract the freebase that was dried over $MgSO_4$ and concentrated under reduced pressure. The freebase was converted to the HCl salt using ethereal HCl to yield 0.04 g of **45a** (4% yield) as brown crystals: 95% ee; freebase $[\alpha]_D^{25}$40.7° (c = 0.108, MeOH); mp 224-226 °C (lit.[218] mp 226-227 °C); ^{1}H NMR (DMSO-d_6, 400 MHz): δ 0.9 (t, 3H, J = 8 Hz, CH_3), 1.33 (m, 1H, CH_2), 1.47 (m, 1H, CH_2), 1.81 (s, 3H, CH_3), 2.73 (m, 2H, CH_2), 2.96 (m, 1H, CH), 3.75 (s, 3H, CH_3), 6.48 (br s, 3H, NH_3^+ D_2O exchangeable), 6.62 (d, 1H, J = 8 Hz, ArH), 6.85 (s, 1H, ArH), 7.01 (s, 1H, ArH), 7.38 (d, 1H, J = 8 Hz, ArH),

10.69 (s, 1H, NH D_2O exchangeable); HRMS (ESI-TOF) m/z [M + H]+ calcd for $C_{13}H_{19}N_2O$, 219.1497; found, 219.1500.

(*R*)-(-)-5-Methoxy-α-ethyltryptamine hydrochloride (45b). Upjohn Co. prepared (*R*) α-ET by resolution of the racemate using camphorsulfonic acid.[223] Dr. Carmen Abate of our laboratory used a similar resolution procedure and prepared the previously unreported HCl salt of the target (**45b**): mp 216-218 °C; $[\alpha]_D^{25}$-38.6° (c = 0.8, MeOH); Anal. Calcd for ($C_{13}H_{18}$ N_2O·HCl·H_2O) C, H, N. Because an insufficient quantity of the isomer was available for the necessary biological studies, her synthesis was replicated.

A freebase of 5-methoxy-α-ethyltryptamine hydrochloride (**45**) (1.0 g) was prepared using sat. $NaHCO_3$ that was then extracted with EtOAc (3 x 30 mL) and concentrated under reduced pressure. The freebase was dissolved in hot *i*-PrOH (10 mL) with (*S*)-(+)-camphorsufonic acid (0.94 g) and then recrystallized 4 times using *i*-PrOH. The crystals were collected by filtration and dried under vacuum. The dried salt was then dissolved in H_2O (10 mL) and 1.2 eq of 0.08 M NaOH was added in a dropwise manner. DCM (3 x 10 mL) was used to extract the freebase that was then dried over $MgSO_4$, filtered, and concentrated under reduced pressure. The freebase was converted to the HCl salt using ethereal HCl to yield 0.1 g of **45b** (10% yield) as brown crystals: 76.6% ee; freebase $[\alpha]_D^{25}$-46° (c = 0.266, MeOH); mp 224-226 °C (lit.[218] mp 226-227 °C); ^1H NMR (DMSO-*d6*, 400 MHz): δ 0.9 (t, 3H, *J* = 8 Hz, CH_3), 1.33 (m, 1H, CH_2), 1.47 (m, 1H, CH_2), 1.81 (s, 3H, CH_3), 2.73 (m, 2H, CH_2), 2.96 (m, 1H, CH), 3.75 (s, 3H, CH_3), 6.48 (br s, 3H, NH_3^+ D_2O exchangeable), 6.62 (d, 1H, *J* = 8 Hz, ArH), 6.85 (s, 1H, ArH), 7.01 (s, 1H, ArH), 7.38

(d, 1H, J = 8 Hz, ArH), 10.69 (s, 1H, NH D$_2$O exchangeable); HRMS (ESI-TOF) m/z [M + H]$^+$ calcd for C$_{13}$H$_{19}$N$_2$O, 219.1497; found, 219.1500.

4-Bromo-α-ethyltryptamine hydrochloride (46) The target compound was prepared by Dr. Ajay Bansode, a postdoctioral fellow in our laboratory with whom I worked. Formaldehyde (37% in H$_2$O) (0.37 mL, 5.1 mmol) and glacial acetic acid (0.58 mL, 10.2 mmol) were added in a dropwise manner to cold dimethylamine (40% in H$_2$O) (0.64 mL, 5.1 mmol) maintaining the temperature at 0 °C (ice bath) under an inert atmosphere (N$_2$ gas). The reaction mixture was allowed to stir for 10 min, then a solution of 4-bromoindole (**60**) (1.00 g, 5.1 mmol) in glacial acetic acid (5 mL) was added in a dropwise manner and stirring was continued at room temperature for 12 h. The reaction mixture was poured into ice-cold water and basified to pH~12 using 2N aq. NaOH. The precipitate was collected by filtration and the solid residue was washed with H$_2$O and dried under high vacuum to afford 0.98 g (76%) of 4-bromogramine (**65**) as a white solid; mp 142-144 °C (lit.[224] 146-147 °C); ^{1}H NMR (CDCl$_3$, 400 MHz): δ 2.27 (s, 6H, 2 x CH$_3$), 3.79 (s, 2H, CH$_2$), 6.85 (t, 1H, J = 7.95 Hz, ArH), 6.88 (s, 1H, ArH), 7.08 (d, 1H, J = 7.64 Hz, ArH), 7.14 (d, 1H, J = 7.34 Hz, ArH), 9.04 (br s, 1H, NH).

Solid NaOH (0.21 g, 5.3 mmol) was added to a mixture of 4-bromogramine (**65**) (1.00 g, 4.0 mmol) and 1-nitropropane (3.57 mL, 40.0 mmol) at room temperature under an inert atmosphere (N$_2$ gas) and the reaction mixture was heated to reflux for 12 h. During the first 10 min, formation of a precipitate was observed and an additional 10 mL of 1-nitropropane was added. The reaction mixture was allowed to cool to room temperature

and extracted with H_2O (20 mL) and EtOAc (3 x 5 mL). The combined organic portion was washed with brine, dried over Na_2SO_4, and evaporated under reduced pressure. The crude residue was purified by column chromatography using hexane/EtOAc (100:0 to 80:20) and the combined fraction was evaporated to dryness to afford 0.92 g (78%) of 4-bromo-3-(2-nitrobutyl)-1*H*-indole (**70**) as a white solid; mp 111-113 °C; ^{1}H NMR (CDCl$_3$, 400 MHz): δ 0.96 (t, 3H, J = 7.34 Hz, CH$_3$), 1.86-2.05 (m, 2H, CH$_2$), 3.30 (dd, 1H, J = 9.88 & 15.65 Hz, CH), 3.59 (dd, 1H, J = 3.95 & 15.29 Hz, CH), 4.83-4.90 (m, 1H), 6.93-6.96 (m, 2H, ArH), 7.21 (d, 1H, J = 2.61 Hz, ArH), 7.23 (d, 1H, J = 3.34 Hz, ArH), 8.08 (br s, 1H, NH).

Raney Nickel (50% in H_2O) (0.24 g, 4.1 mmol) was added to a solution of 4-bromo-3-(2-nitrobutyl)-1*H*-indole (**70**) (0.30 g, 1.0 mmol) in EtOH (15 mL) at room temperature under an inert atmosphere (N$_2$ gas), followed by 20% hydrazine hydrate in EtOH (10 mL; i.e., 2 mL of hydrazine hydrate in 8 mL of EtOH) and the reaction mixture was heated at reflux for 12 h. The reaction mixture was allowed to cool to room temperature and filtered through a Celite pad. The filtrate was evaporated under reduced pressure to yield 4-bromo-α-ethyltryptamine as a yellow oil, that was dissolved in dry MeOH (5 mL) and cooled to 0 °C (ice bath). A saturated solution of HCl in Et$_2$O was added in a dropwise manner to pH~1-2 and further stirred for 5 min at 0 °C (ice bath). The solvent was evaporated under reduced pressure, and the solid residue was recrystallized from MeOH/Et$_2$O to yield 0.26 g (76%) of 4-bromo-α-ethyltryptamine hydrochloride (**46**) as a white solid; mp 288-290 °C (dec.) (MeOH/Et$_2$O); ^{1}H NMR (DMSO-*d*$_6$, 400 MHz): δ 0.98 (t, 3H, J = 7.44 Hz, CH$_3$), 1.67 (q, 2H, J = 7.28 Hz, CH$_2$), 3.08 (dd, 1H, J = 7.65 & 14.35

Hz, CH), 3.27 (dd, 1H, J = 6.33 & 14.45 Hz, CH), 3.37 (m, 1H), 6.99 (t, 1H, J = 7.74 Hz, ArH), 7.19 (d, 1H, J = 7.74 Hz, ArH), 7.39-7.42 (m, 2H, ArH), 8.02 (br s, 2H, NH_2, D_2O exchangable), 11.29 (br s, 1H, NH, D_2O non-exchangable); HRMS (ESI-TOF) m/z [M+H]$^+$ calcd for $C_{12}H_{16}N_2Br$, 267.0491. Found: 267.0481; Anal. Calcd for ($C_{12}H_{15}N_2Br\cdot HCl$) C, 47.47; H, 5.31; N, 9.23. Found: C, 47.50; H, 5.36; N, 9.26.

5-Bromo-α-ethyltryptamine hydrochloride (47) The target compound was prepared by Dr. Ajay Bansode in our laboratory. Formaldehyde (37% in H_2O) (1.91 mL, 25.5 mmol) and glacial acetic acid (2.91 mL, 51.0 mmol) were added in a dropwise manner to cold dimethylamine (40% in H_2O) (3.30 mL, 25.5 mmol) maintaining the temperature at 0 °C (ice bath) under an inert atmosphere (N_2 gas). The reaction mixture was stirred for 10 min, then a solution of 5-bromoindole (**61**) (5.00 g, 25.5 mmol) in glacial acetic acid (25 mL) was added in a dropwise manner and the reaction mixture was stirred at room temperature for 12 h. The reaction mixture was poured into ice-cold water and basified to pH~12 using 2N aq. NaOH. The precipitate was collected by filtration and the solid residue was washed with H_2O and dried under high vacuum to afford 4.50 g (70%) of 5-bromogramine (**66**) as a white solid; mp 136-138 °C (lit.[225] 134-137 °C); ^{1}H NMR (CDCl$_3$, 400 MHz): δ 2.19 (s, 6H, 2 x CH_3), 3.49 (s, 2H, CH_2), 7.03 (s, 1H, ArH), 7.12-7.18 (m, 2H, ArH), 7.75 (s, 1H, ArH), 8.28 (br s, 1H, NH).

Solid NaOH (0.42 g, 10.6 mmol) was added to a mixture of 5-bromogramine (**66**) (2.00 g, 7.9 mmol) and 1-nitropropane (7.10 mL, 79.4 mmol) at room temperature under an inert atmosphere (N_2 gas) and the reaction mixture was heated at reflux for 12 h. During the

first 10 min, formation of a precipitate was observed and an additional 10 mL of 1-nitropropane was added. The reaction mixture was allowed to cool to room temperature and extracted with H_2O (30 mL) and EtOAc (3 x 10 mL). The combined organic portion was washed with brine, dried over Na_2SO_4, and evaporated under reduced pressure. The crude residue was purified by column chromatography using hexane/EtOAc (100:0 to 80:20) and the combined fraction was evaporated to dryness to afford 1.80 g (86%) of 5-bromo-3-(2-nitrobutyl)-1*H*-indole (**71**) as a white solid; mp 84-86 °C; ^1H NMR ($CDCl_3$, 400 MHz): δ 0.94 (t, 3H, *J* = 7.08 Hz, CH_3), 1.78-1.86 (m, 1H, CH), 1.93-2.03 (m, 1H, CH), 3.06 (dd, 1H, *J* = 5.14 & 15.28 Hz, CH), 3.30 (dd, 1H, *J* = 8.93 & 15.68 Hz, CH), 4.59-4.66 (m, 1H, CH), 6.93 (d, 1H, *J* = 2.35 Hz, ArH), 7.17 (d, 1H, *J* = 6.71 Hz, ArH), 7.21 (dd, 1H, *J* = 8.89 and 1.84 Hz, ArH), 7.59 (d, 1H, *J* = 1.75 Hz, ArH), 8.03 (br s, 1H, NH).

Raney Nickel (50% in H_2O) (0.24 g, 4.1 mmol) was added to a solution of 5-bromo-3-(2-nitrobutyl)-1*H*-indole (**71**) (0.30 g, 1.0 mmol) in EtOH (15 mL) at room temperature under an inert atmosphere (N_2 gas), followed by 20% hydrazine hydrate in EtOH (10 mL; i.e., 2 mL of hydrazine hydrate in 8 mL of EtOH) and the reaction mixture was heated at reflux for 5 h. The reaction mixture was allowed to cool to room temperature and filtered through a Celite pad. The filtrate was evaporated under reduced pressure to yield 5-bromo-α-ethyltryptamine as a yellow oil, which was dissolved in dry MeOH (5 mL) and cooled to 0 °C (ice bath). A saturated solution of HCl in Et_2O was added in a dropwise manner until pH~1-2 and further stirred for 5 min at 0 °C (ice bath). The solvent was evaporated under reduced pressure, and the solid residue was recrystallized from MeOH/Et_2O to yield 0.19 g (62%) of 5-bromo-α-ethyltryptamine hydrochloride (**47**) as a white solid; mp 241-243 °C

(dec.) (MeOH/Et$_2$O); ^{1}H NMR (DMSO-d_6, 400 MHz): δ 0.94 (t, 3H, J = 7.63 Hz, CH$_3$), 1.51-1.62 (m, 2H, CH$_2$), 2.92 (dd, 1H, J = 7.63 & 15.25 Hz, CH), 3.02 (dd, 1H, J = 5.73 & 14.16 Hz, CH), 3.25 (br s, 1H, CH), 7.20 (dd, 1H, J = 8.88 and 1.74 Hz, ArH), 7.35 (d, 2H, J = 8.59 Hz, ArH), 7.81 (d, 1H, J = 1.51 Hz, ArH), 8.02 (br s, 3H, NH$_3^+$, D$_2$O exchangable), 11.30 (br s, 1H, NH, D$_2$O non-exchangable); HRMS (ESI-TOF) m/z [M+H]$^+$ calcd for C$_{12}$H$_{16}$N$_2$Br, 267.0491. Found: 267.0499; Anal. Calcd for (C$_{12}$H$_{15}$N$_2$Br·HCl) C, 47.47; H, 5.31; N, 9.23. Found: C, 47.81; H, 5.30; N, 8.95.

(*R*)-(+)-*N*-Boc-pipecolate *N*-(methylmethoxyl)amide (50a). *N,O*-dimethylhydroxylamine hydrochloride (0.90 g, 9.4 mmol), Et$_3$N (3.29 mL, 23.6 mmol), and PyBOP (4.5 g, 8.6 mmol) were successively added to a stirred solution of (*R*)-*N*-Boc-2-pipecolic acid (**49a**) (1.8 g, 7.8 mmol) in DCM (50 mL) and the mixture was stirred at room temperature for 16 h. The reaction mixture was then diluted with DCM (50 mL) and added to a separatory funnel containing 1 M HCl (50 mL). The organic layer was washed with sat. NaHCO$_3$ (3 x 30 mL), brine (3 x 30 mL), H$_2$O (3 x 30 mL), dried over MgSO$_4$, filtered, and solvent was evaporated under reduced pressure. The resultant oil was then chromatographed on silica gel 4:1 hexanes:EtOAc to afford 1.44 g (68% yield) of **50a** as a light-yellow oil.

(*S*)-(-)-*N*-Boc-pipecolate *N*-(methylmethoxyl)amide (50b). *N,O*-Dimethylhydroxylamine hydrochloride (0.80 g, 8.2 mmol), Et$_3$N (2.85 mL, 20.5 mmol), and PyBOP (3.92 g, 7.5 mmol) were successively added to a stirred solution of (*S*)-*N*-boc-2-pipecolic acid (**49b**) (1.57 g, 6.8 mmol) in DCM (50 mL) and the mixture was stirred at

room temperature for 16 h. The reaction mixture was then diluted with DCM (50 mL) and added to a separatory funnel containing 1 M HCl (50 mL). The organic portion was washed with sat. NaHCO$_3$ (3 x 30 mL), brine (3 x 30 mL), H$_2$O (3 x 30 mL), dried over MgSO$_4$, filtered, and solvent was evaporated under reduced pressure. The resultant oil was chromatographed on silica gel 4:1 hexanes:EtOAc to afford 1.08 g (58% yield) of **50b** as a colorless oil.

5-Methoxygramine (64). Dimethylamine 40% in H$_2$O (0.43 mL, 3.39 mmol) was cooled to 0 °C using an ice bath followed by the addition of formaldehyde 37% in H$_2$O (0.26 mL, 3.39 mmol) and glacial acetic acid (0.45 mL, 7.81 mmol). The reaction mixture was stirred at 0 °C for 10 min then 5-methoxyindole (**59**) (0.5 g, 3.39 mmol) in glacial acetic acid (~3 mL) was added in a dropwise manner. The reaction mixture was allowed to warm to room temperature and stirred overnight. Water (10 mL) was used to dilute the mixture then an ice bath was used for cooling while 2 M NaOH was slowly added until pH = 12. The precipitated solid was collected by filtration, washed with water (3 x 20 mL), and recrystallized using EtOAc/hexane to afford 0.50 g (72% yield) of **64** as a light brown solid: mp 124-126 °C (lit.[226] mp 124-125 °C).

5-Methoxy-3-(2-nitrobutyl)-1*H*-indole (69). 5-Methoxygramine (**64**) (0.50 g, 2.46 mmol) was added to a solution of 1-nitropropane (6.51 mL, 72.92 mmol) and NaOH (0.13 g, 3.27 mmol) under an N$_2$ atmosphere. The reaction mixture was stirred and heated at reflux overnight then allowed to cool to room temperature and diluted with water (10 mL) and

acidified to pH ~2 using 1 M HCl. The reaction mixture was extracted with EtOAc (3 x 10 mL) and the organic phase was concentrated under reduced pressure. Hexanes (3 x 30 mL) was then used to wash the resultant oil that was flash chromatographed on silica gel using 5% EtOAc:Hexanes. The collected fractions were combined, and solvent was removed under reduced pressure to yield 0.43 g of **69** (70% yield) as a brown oil.

Biological Studies

S149A DAT Mutation

To obtain hDAT S149A, hDAT cDNA sequence subcloned in an intermediate vector (pGEM 3Zf) was cut between BglII and BamHI site and that cDNA segment was replaced by a synthetic sequence having the mutation (tca to gcc). The resulting plasmid was sequenced using the Sanger method. Then the full hDATS149A sequence was subcloned into the pcDNA™5/FRT/TO vector (KpnI/XhoI sites) and used for the generation of stable cell lines using the Flp-In™ T-REx™ system as previously described.[209]

APP⁺ Inhibition Assays

The assay was performed on HEK Flp-In™ T-REx™ 293 cells stably expressing hDAT, mutant S149A DAT, or hSERT available from previous experiments. The cells were plated in 96-well flat-bottom imaging plates and were transfected with a red fluorescent protein (DsRed) coding plasmid for focusing on the fluorescent microscope. The cultured

cells were supplemented with 1 mg/mL doxycycline 3 days before experiments to upregulate the expression of the transporters. Epifluorescence microscopy was used to measure fluorescent intensity of the cells. APP$^+$, a fluorescent substrate for MATs, was excited at 460 nm, and emission was detected at a wavelength of 540 nm, using an Olympus IX71 microscope, equipped with a 20× NA 0.80 NA objective, and attached to a PTI EasyRatioPro system (HORIBA scientific). APP$^+$ uptake was inhibited by increasing concentrations of agents that interact with the transporter of interest, and concentration–response curves were obtained. The tested compound (at a single concentration) was pre-perfused for 40 s before applying it in combination with APP$^+$ for an additional 30 s. Each concentration was tested in triplicate, and each experiment was repeated on three separate days to reduce error (analyzing at least 9 wells in total per concentration). All data were analyzed using EasyRatioPro 3 and then plotted with GraphPad Prism 10.0. For each well analyzed, 40 separate cells were chosen as regions of interest (ROI). The mean maximal APP$^+$ signal after 30 s uptake for each concentration of compound tested was used to generate the IC$_{50}$ inhibition curves. Each data set was background-subtracted and normalized by the mean signal of a positive APP$^+$ control in the absence of any competing compound for the experimental day.

SERT Activity Using Ca^{+2} Channel Sensors

Stable HEK293 cell lines expressing hSERT were previously developed in the laboratory and cells were plated in 96-well imaging plates. The culture media was Dulbecco's modified eagle medium, which was supplemented with fetal bovine serum. Cells were plated in 96-well flat-bottom plates.

Plated cells were transfected with the cardiac isoform of voltage-gated Ca^{2+} channel $Ca_{v1.2}$, its auxiliary subunits, and transfection marker DsRed. Plasmids α1, β3, α2δ1, and DsRed in a ratio of 0.9:0.5:0.75:0.25, in µg, along with Fugene 6 (Promega) in OptiMEM media. The media was later supplemented with doxycycline (1 µg/mL) in culture media to induce expression of transporters. Ca^{2+} determinations were made with Fluo4, a Ca^{2+} sensor. Experiments performed in imaging solution (IS; 130 mM NaCl, 4 mM KCl, 2 mM $CaCl_2$, 1 mM $MgCl_2$, 10 mM Hepes, 10 mM glucose, pH = 7.4). Test compounds or controls were exposed to the cells under constant perfusion at 35 °C (ThermoClamp-1, Automate Scientific). Fluorescence was observed using an Olympus IX70 microscope using a 20× 0.75 numerical aperture objective with a fluorescence imaging attachment (Till Photonics). Images were obtained at 490 nm excitation, then recorded for off-line analysis. Each well was used for a single concentration of test agent. Three wells were collected per concentration per compound per experiment, and three experiments were conducted for each compound at multiple concentrations. Each well contained multiple cells, which were individually evaluated for either substrate or blocker activity using the following protocol.

Cells were perfused with IS for 10 s, followed by perfusion of a positive control (5-HT; 10 µM) for 5 s. Following a 30 s washout with IS, the test compound was perfused for 30 s, followed by the test compound at a given concentration with the positive control for 5 s, and a final washout of 30 s with IS.

Concentration-response curves were generated using GraphPad Prism 10.0.

Binding Affinity and Ca^{2+} Mobilization at 5-HT$_{2A}$ Receptors

All binding affinity and functional data for 5-HT$_{2A}$ receptors not utilizing fluorescence microscopy were obtained from the laboratory of Dr. González-Maeso in the VCU Department of Physiology and Biophysics and the experiments were performed as previously described.[227]

Ca^{2+} Mobilization Assay for 5-HT$_{2A}$ Receptors Utilizing Fluorescence Microscopy

The assay was performed on HEK Flp-In T-REx 293 cells stably expressing 5-HT$_{2A}$ receptors available from previous experiments. The cells were plated in 96-well flat-bottom imaging plates and were transfected with enhanced green fluorescent protein (EGFP) coding plasmid for focusing on the fluorescent microscope. The cultured cells were supplemented with 1 µg/mL doxycycline 3 days before experiments to upregulate the expression of the receptors. Epifluorescence microscopy was used to measure fluorescent intensity of the cells. The cells were incubated with 50 µL of 3 µM Fura2 supplemented with pluronic acid (10% solution in DMSO) for 45 min at 37 °C then washed with imaging solution (4 mM KCl, 130 mM NaCl, 2 mM CaCl$_2$, 1 mM MgCl$_2$, 10 mM glucose, 10 mM HEPES, pH 7.4). Changes in fluorescence due to intracellular Ca^{2+} mobilization were measured using an Olympus IX71 microscope, equipped with a 20× NA 0.80 NA objective, and attached to a PTI EasyRatioPro system (HORIBA scientific) with an excitation wavelength of 340 and 380 nm. The experiment was performed in three phases over 110 seconds. First, the cells transfected with EGFP were identified and the baseline of Fura2 signal was recorded for 10 seconds using IS. Next the cells were

exposed to a perfusion of a single concentration of the compound of interest for 30 seconds followed by 30 seconds of washing with IS. Third, a single concentration of 100 nM 5-HT was perfused for 30 seconds and lastly a final wash with IS for 10 seconds. The fluorescence was a measure of intracellular calcium mobilization and was background-subtracted and normalized by the mean signal of a positive 5-HT control for the experimental day. Each concentration was tested in triplicate, and each experiment was repeated on three separate days to reduce error (analyzing at least 9 wells in total per concentration). Additional experiments were performed with cells preincubated with 100 nM ketanserin to determine if signals were induced by a non-5-HT$_{2A}$ receptor pathway as well as experiments on cells not expressing 5-HT$_{2A}$ receptors. All data were analyzed using EasyRatioPro 3 and then plotted with GraphPad Prism 10.0 to generate concentration-response curves using non-linear regression analysis.

VII. Bibliography

1. American Psychiatric Association, ed. (2022). *Diagnostic and Statistical Manual of Mental Disorders, Fifth Edition, Text Revision (DSM-5-TR).* Washington, DC, USA: American Psychiatric Publishing.

2. Yadav, S. K.; Bhat, A. A.; Hashem, S.; Nisar, S.; Kamal, M.; Syed, N.; Temanni, M.-R.; Gupta, R. K.; Kamran, S.; Azeem, M. W.; Srivastava, A. K.; Bagga, P.; Chawla, S.; Reddy, R.; Frenneaux, M. P.; Fakhro, K.; Haris, M. Genetic Variations Influence Brain Changes in Patients with Attention-Deficit Hyperactivity Disorder. *Transl. Psychiatry* **2021**, *11*, 349.

3. PereiraI, S.; FerreiraII, A. M.; AzevedoII, A.; BarrosoIII, C.; MonteiroII, V. Illicit Use of Methylphenidate: The Other Side of the Medical Prescription. *REVNEC* **2018**, *27*, 98–104.

4. Katzman, M. A.; Bilkey, T. S.; Chokka, P. R.; Fallu, A.; Klassen, L. J. Adult ADHD and Comorbid Disorders: Clinical Implications of a Dimensional Approach. *BMC Psychiatry* **2017**, *17*, 302.

5. Kenter, R. M. F.; Lundervold, A. J.; Nordgreen, T. A Self-Guided Internet-Delivered Intervention for Adults with ADHD: A Protocol for a Randomized Controlled Trial. *Internet Interv.* **2021**, *26*, 100485.

6. Song, P.; Zha, M.; Yang, Q.; Zhang, Y.; Li, X.; Rudan, I. The Prevalence of Adult Attention-Deficit Hyperactivity Disorder: A Global Systematic Review and Meta-Analysis. *J. Glob. Health* **2021**, *11*, 04009.

7. Posner, J.; Polanczyk, G. V; Sonuga-Barke, E. Attention-Deficit Hyperactivity Disorder. *Lancet* **2020**, *395*, 450–462.

8. Young, S.; Adamo, N.; Ásgeirsdóttir, B. B.; Branney, P.; Beckett, M.; Colley, W.; Cubbin, S.; Deeley, Q.; Farrag, E.; Gudjonsson, G.; Hill, P.; Hollingdale, J.; Kilic, O.; Lloyd, T.; Mason, P.; Paliokosta, E.; Perecherla, S.; Sedgwick, J.; Skirrow, C.; Tierney, K.; van Rensburg, K.; Woodhouse, E. Females with ADHD: An Expert Consensus Statement Taking a Lifespan Approach Providing Guidance for the Identification and Treatment of Attention-Deficit/ Hyperactivity Disorder in Girls and Women. *BMC Psychiatry* **2020**, *20*, 404.

9. Wilens, T. E.; Biederman, J.; Faraone, S. V.; Martelon, M.; Westerberg, D.; Spencer, T. J. Presenting ADHD Symptoms, Subtypes, and Comorbid Disorders in Clinically Referred Adults With ADHD. *J. Clin. Psychiatry* **2009**, *70*, 1557–1562.

10. Retz-Junginger, P.; Rösler, M.; Giesen, L.; Philipp-Wiegmann, F.; Römer, K.; Zinnow, T.; Retz, W. Der Einfluss Des ADHS-Subtyps Auf Den Leidensdruck Bei Erwachsenen ADHS-Patienten. *Psychiatr. Prax.* **2015**, *43*, 279–282.

11. Liebrenz, M.; Gamma, A.; Ivanov, I.; Buadze, A.; Eich, D. Adult Attention-Deficit/Hyperactivity Disorder: Associations between Subtype and Lifetime Substance Use – A Clinical Study. *F1000Res* **2016**, *4*, 407.

12. Soendergaard, H. M.; Thomsen, P. H.; Pedersen, E.; Pedersen, P.; Poulsen, A. E.; Winther, L.; Nielsen, J. M.; Henriksen, A.; Rungoe, B.; Soegaard, H. J. Associations of Age, Gender, and Subtypes with ADHD Symptoms and Related Comorbidity in a Danish Sample of Clinically Referred Adults. *J. Atten. Disord.* **2016**, *20*, 925–933.

13. Ghosh, A.; Ray, A.; Basu, A. Oppositional Defiant Disorder: Current Insight. *Psychol. Res. Behav. Manag.* **2017**, *10*, 353–367.

14. Williams, O. C.; Prasad, S.; McCrary, A.; Jordan, E.; Sachdeva, V.; Deva, S.; Kumar, H.; Mehta, J.; Neupane, P.; Gupta, A. Adult Attention Deficit Hyperactivity Disorder: A Comprehensive Review. *Ann. Med. Surg.* **2023**, *85*, 1802–1810.

15. Barkley, R. A.; Fischer, M.; Smallish, L.; Fletcher, K. Young Adult Outcome of Hyperactive Children: Adaptive Functioning in Major Life Activities. *J. Am. Acad. Child Adolesc. Psychiatry* **2006**, *45*, 192–202.

16. Eakin, L.; Minde, K.; Hechtman, L.; Ochs, E.; Krane, E.; Bouffard, R.; Greenfield, B.; Looper, K. The Marital and Family Functioning of Adults with ADHD and Their Spouses. *J. Atten. Disord.* **2004**, *8*, 1–10.

17. Christiansen, M. S.; Labriola, M.; Kirkeskov, L.; Lund, T. The Impact of Childhood Diagnosed ADHD versus Controls without ADHD Diagnoses on Later Labour Market Attachment—a Systematic Review of Longitudinal Studies. *Child Adolesc. Psychiatry Ment. Health* **2021**, *15*, 34.

18. Engelhardt, P. E.; Nobes, G.; Pischedda, S. The Relationship between Adult Symptoms of Attention-Deficit/Hyperactivity Disorder and Criminogenic Cognitions. *Brain Sci.* **2019**, *9*, 128.

19. Tsai, F.-J.; Tseng, W.-L.; Yang, L.-K.; Gau, S. S.-F. Psychiatric Comorbid Patterns in Adults with Attention-Deficit Hyperactivity Disorder: Treatment Effect and Subtypes. *PLoS One* **2019**, *14*, e0211873.

20. Reimherr, F. W.; Marchant, B. K.; Gift, T. E.; Steans, T. A.; Wender, P. H. Types of Adult Attention-Deficit Hyperactivity Disorder (ADHD): Baseline Characteristics, Initial Response, and Long-Term Response to Treatment with Methylphenidate. *ADHD Atten. Deficit Hyperact. Disord.* **2015**, *7*, 115–128.

21. Corbisiero, S.; Stieglitz, R.-D.; Retz, W.; Rösler, M. Is Emotional Dysregulation Part of the Psychopathology of ADHD in Adults? *ADHD Atten. Deficit Hyperact. Disord.* **2013**, *5*, 83–92.

22. Bjerrum, M. B.; Pedersen, P. U.; Larsen, P. Living with Symptoms of Attention Deficit Hyperactivity Disorder in Adulthood: A Systematic Review of Qualitative Evidence. *JBI Database System Rev. Implement. Rep.* **2017**, *15*, 1080–1153.

23. Fayyad, J.; De Graaf, R.; Kessler, R.; Alonso, J.; Angermeyer, M.; Demyttenaere, K.; De Girolamo, G.; Haro, J. M.; Karam, E. G.; Lara, C.; Lépine, J.-P.; Ormel, J.; Posada-Villa, J.; Zaslavsky, A. M.; Jin, R. Cross-National Prevalence and Correlates of Adult Attention-Deficit Hyperactivity Disorder. *Br. J. Psychiatry* **2007**, *190*, 402–409.

24. Gustavsson, A.; Svensson, M.; Jacobi, F.; Allgulander, C.; Alonso, J.; Beghi, E.; Dodel, R.; Ekman, M.; Faravelli, C.; Fratiglioni, L.; Gannon, B.; Jones, D. H.; Jennum, P.; Jordanova, A.; Jönsson, L.; Karampampa, K.; Knapp, M.; Kobelt, G.; Kurth, T.; Lieb, R.; Linde, M.; Ljungcrantz, C.; Maercker, A.; Melin, B.; Moscarelli, M.; Musayev, A.; Norwood, F.; Preisig, M.; Pugliatti, M.; Rehm, J.; Salvador-Carulla, L.; Schlehofer, B.; Simon, R.; Steinhausen, H.-C.; Stovner, L. J.; Vallat, J.-M.; den Bergh, P. Van; van Os, J.; Vos, P.; Xu, W.; Wittchen, H.-U.; Jönsson, B.; Olesen,

J. Cost of Disorders of the Brain in Europe 2010. *Eur. Neuropsychopharmacol.* **2011**, *21*, 718–779.

25. Deberdt, W.; Thome, J.; Lebrec, J.; Kraemer, S.; Fregenal, I.; Ramos-Quiroga, J. A.; Arif, M. Prevalence of ADHD in Nonpsychotic Adult Psychiatric Care (ADPSYC): A Multinational Cross-Sectional Study in Europe. *BMC Psychiatry* **2015**, *15*, 242.

26. Salvi, V.; Ribuoli, E.; Servasi, M.; Orsolini, L.; Volpe, U. ADHD and Bipolar Disorder in Adulthood: Clinical and Treatment Implications. *Medicina* **2021**, *57*, 466.

27. Torgersen, T.; Gjervan, B.; Rasmussen, K. Treatment of Adult ADHD: Is Current Knowledge Useful to Clinicians? *Neuropsychiatr. Dis. Treat.* **2008**, 177-186.

28. Castells, X.; Blanco-Silvente, L.; Cunill, R. Amphetamines for Attention Deficit Hyperactivity Disorder (ADHD) in Adults. *Cochrane Database Syst. Rev.* **2018**, CD007813.

29. Faraone, S. V. The Pharmacology of Amphetamine and Methylphenidate: Relevance to the Neurobiology of Attention-Deficit/Hyperactivity Disorder and Other Psychiatric Comorbidities. *Neurosci. Biobehav. Rev.* **2018**, *87*, 255–270.

30. Steingard, R.; Taskiran, S.; Connor, D. F.; Markowitz, J. S.; Stein, M. A. New Formulations of Stimulants: An Update for Clinicians. *J. Child Adolesc. Psychopharmacol.* **2019**, *29*, 324–339.

31. Kolar, D.; Keller, A.; Golfinopoulos, M.; Cumyn, L.; Syer, C.; Hechtman, L. Treatment of Adults with Attention-Deficit/Hyperactivity Disorder. *Neuropsychiatr. Dis. Treat.* **2008**, *4*, 389–403.

32. Underhill, S. M.; Colt, M. S.; Amara, S. G. Amphetamine Stimulates Endocytosis of the Norepinephrine and Neuronal Glutamate Transporters in Cultured Locus Coeruleus Neurons. *Neurochem. Res.* **2020**, *45*, 1410–1419.

33. Underhill, S. M.; Hullihen, P. D.; Chen, J.; Fenollar-Ferrer, C.; Rizzo, M. A.; Ingram, S. L.; Amara, S. G. Amphetamines Signal through Intracellular TAAR1 Receptors Coupled to Gα13 and GαS in Discrete Subcellular Domains. *Mol. Psychiatry* **2021**, *26*, 1208–1223.

34. Miller, G. M. The Emerging Role of Trace Amine-Associated Receptor 1 in the Functional Regulation of Monoamine Transporters and Dopaminergic Activity. *J. Neurochem.* **2011**, *116*, 164–176.

35. Weisler, R. H.; Biederman, J.; Spencer, T. J.; Wilens, T. E.; Faraone, S. V.; Chrisman, A. K.; Read, S. C.; Tulloch, S. J. Mixed Amphetamine Salts Extended-Release in the Treatment of Adult ADHD: A Randomized, Controlled Trial. *CNS Spectr.* **2006**, *11*, 625–639.

36. Heal, D. J.; Smith, S. L.; Gosden, J.; Nutt, D. J. Amphetamine, Past and Present – a Pharmacological and Clinical Perspective. *J. Psychopharmacol.* **2013**, *27*, 479–496.

37. Swanson, J. M. Long-Acting Stimulants: Development and Dosing. *Can. Child Adolesc. Psychiatr. Rev.* **2005**, *14*, 4–9.

38. Raman, S. R.; Man, K. K. C.; Bahmanyar, S.; Berard, A.; Bilder, S.; Boukhris, T.; Bushnell, G.; Crystal, S.; Furu, K.; KaoYang, Y.-H.; Karlstad, Ø.; Kieler, H.; Kubota, K.; Lai, E. C.-C.; Martikainen, J. E.; Maura, G.; Moore, N.; Montero, D.; Nakamura,

H.; Neumann, A.; Pate, V.; Pottegård, A.; Pratt, N. L.; Roughead, E. E.; Macias Saint-Gerons, D.; Stürmer, T.; Su, C.-C.; Zoega, H.; Sturkenbroom, M. C. J. M.; Chan, E. W.; Coghill, D.; Ip, P.; Wong, I. C. K. Trends in Attention-Deficit Hyperactivity Disorder Medication Use: A Retrospective Observational Study Using Population-Based Databases. *Lancet Psychiatry* **2018**, *5*, 824–835.

39.   Piper, B. J.; Ogden, C. L.; Simoyan, O. M.; Chung, D. Y.; Caggiano, J. F.; Nichols, S. D.; McCall, K. L. Trends in Use of Prescription Stimulants in the United States and Territories, 2006 to 2016. *PLoS One* **2018**, *13*, e0206100.

40.   Hartmann, M.; Panizzon, L. Pyridine and Piperidine Compounds and Process of Making Same. US2507631A, May 16, 1950.

41.   Ticktin, H.; Epstein, J.; Shea, J. C.; Fazekas, J. F. Effect of Methylphenidate Hydrochloride in Antagonizing Barbiturate-induced Depression. *Neurology* **1958**, *8*, 267–267.

42.   Panizzon, L. La Preparazione Di Piridil- e Piperidil-arilacetonitrili e Di Alcuni Prodotti Di Trasformazione (Parte Iª). *Helv. Chim. Acta.* **1944**, *27*, 1748–1756.

43.   Challman, T. D.; Lipsky, J. J. Methylphenidate: Its Pharmacology and Uses. *Mayo Clin. Proc.* **2000**, *75*, 711–721.

44.   Di Miceli, M.; Derf, A.; Gronier, B. Consequences of Acute or Chronic Methylphenidate Exposure Using Ex Vivo Neurochemistry and In Vivo Electrophysiology in the Prefrontal Cortex and Striatum of Rats. *Int. J. Mol. Sci.* **2022**, *23*, 8588.

45.   Gatley, S. J.; Pan, D.; Chen, R.; Chaturvedi, G.; Ding, Y.-S. Affinities of Methylphenidate Derivatives for Dopamine, Norepinephrine and Serotonin Transporters. *Life Sci.* **1996**, *58*, PL231–PL239.

46.   Zhang, F.; Li, B.; Sun, Y.; Li, J. Synthesis of Demethylphenidate Hydrochloride and Its Related Optical Isomers. *Chin. J. Org. Chem.* **2016**, *36*, 2162–2167.

47.   Li, C.; Ji, Y.; Cao, Q.; Li, J.; Li, B. Concise and Facile Synthesis of (*R, R*)-Dexmethylphenidate Hydrochloride and Its Three Stereoisomers. *Synth. Commun.* **2017**, *47*, 1301–1306.

48.   Froimowitz, M.; Patrick, K. S.; Cody, V. Conformational Analysis of Methylphenidate and Its Structural Relationship to Other Dopamine Reuptake Blockers Such as CFT. *Pharm. Res.* **1995**, *12*, 1430–1434.

49.   Heal, D. J.; Pierce, D. M. Methylphenidate and Its Isomers. *CNS Drugs* **2006**, *20*, 713–738.

50.   Davies, H. M. L.; Hopper, D. W.; Hansen, T.; Liu, Q.; Childers, S. R. Synthesis of Methylphenidate Analogues and Their Binding Affinities at Dopamine and Serotonin Transport Sites. *Bioorg. Med. Chem. Lett.* **2004**, *14*, 1799–1802.

51.   Misra, M.; Shi, Q.; Ye, X.; Gruszecka-Kowalik, E.; Bu, W.; Liu, Z.; Schweri, M. M.; Deutsch, H. M.; Venanzi, C. A. Quantitative Structure–Activity Relationship Studies of Threo-Methylphenidate Analogs. *Bioorg. Med. Chem.* **2010**, *18*, 7221–7238.

52. Childress, A. C.; Komolova, M.; Sallee, F. R. An Update on the Pharmacokinetic Considerations in the Treatment of ADHD with Long-Acting Methylphenidate and Amphetamine Formulations. *Expert Opin. Drug Metab. Toxicol.* **2019**, *15*, 937–974.

53. Weiss, M. D.; Childress, A. C.; Donnelly, G. A. E. Efficacy and Safety of PRC-063, Extended-Release Multilayer Methylphenidate in Adults with ADHD Including 6-Month Open-Label Extension. *J. Atten. Disord.* **2021**, *25*, 1417–1428.

54. Wigal, S. B.; Wigal, T.; Childress, A.; Donnelly, G. A. E.; Reiz, J. L. The Time Course of Effect of Multilayer-Release Methylphenidate Hydrochloride Capsules: A Randomized, Double-Blind Study of Adults with ADHD in a Simulated Adult Workplace Environment. *J. Atten. Disord.* **2020**, *24*, 373–383.

55. Cândido, R. C. F.; Menezes de Padua, C. A.; Golder, S.; Junqueira, D. R. Immediate-Release Methylphenidate for Attention Deficit Hyperactivity Disorder (ADHD) in Adults. *Cochrane Database of Syst. Rev.* **2021**, *2021*.

56. Harmless, W.; Fitzgerald, R. R. The Sapphire Light of the Mind: The *Skemmata* of Evagrius Ponticus. *Theol. Stud.* **2001**, *62*, 498–529.

57. Ervin, R. B. Prevalence of Metabolic Syndrome Among Adults 20 Years of Age and Over, by Sex, Age, Race and Ethnicity, and Body Mass Index: United States, 2003–2006. *Natl. Health Stat. Rep.* **2009**, *5*, 1–7.

58. Moreno-Agostino, D.; Wu, Y.-T.; Daskalopoulou, C.; Hasan, M. T.; Huisman, M.; Prina, M. Global Trends in the Prevalence and Incidence of Depression: A Systematic Review and Meta-Analysis. *J. Affect. Disord.* **2021**, *281*, 235–243.

59. Gautam, S.; Jain, A.; Gautam, M.; Vahia, V.; Grover, S. Clinical Practice Guidelines for the Management of Depression. *Indian J. Psychiatry* **2017**, *59*, 34.

60. Duval, F.; Lebowitz, B. D.; Macher, J.-P. Treatments in Depression. *Dialogues Clin. Neurosci.* **2006**, *8*, 191–206.

61. Brown, S.; Rittenbach, K.; Cheung, S.; McKean, G.; MacMaster, F. P.; Clement, F. Current and Common Definitions of Treatment-Resistant Depression: Findings from a Systematic Review and Qualitative Interviews. *Can. J. Psychiatry* **2019**, *64*, 380–387.

62. McIntyre, R. S.; Filteau, M.-J.; Martin, L.; Patry, S.; Carvalho, A.; Cha, D. S.; Barakat, M.; Miguelez, M. Treatment-Resistant Depression: Definitions, Review of the Evidence, and Algorithmic Approach. *J. Affect. Disord.* **2014**, *156*, 1–7.

63. Rush, A. J.; Sackeim, H. A.; Conway, C. R.; Bunker, M. T.; Hollon, S. D.; Demyttenaere, K.; Young, A. H.; Aaronson, S. T.; Dibue, M.; Thase, M. E. Research Challenges in Chronic Diseases: Difficult to Treat Depression. *Brain Stimul.* **2021**, *14*, 1724.

64. Pérez-Sola, V.; Roca, M.; Alonso, J.; Gabilondo, A.; Hernando, T.; Sicras-Mainar, A.; Sicras-Navarro, A.; Herrera, B.; Vieta, E. Economic Impact of Treatment-Resistant Depression: A Retrospective Observational Study. *J. Affect. Disord.* **2021**, *295*, 578–586.

65. Barnes, N. M.; Ahern, G. P.; Becamel, C.; Bockaert, J.; Camilleri, M.; Chaumont-Dubel, S.; Claeysen, S.; Cunningham, K. A.; Fone, K. C.; Gershon, M.; Di Giovanni, G.; Goodfellow, N. M.; Halberstadt, A. L.; Hartley, R. M.; Hassaine, G.; Herrick-

Davis, K.; Hovius, R.; Lacivita, E.; Lambe, E. K.; Leopoldo, M.; Levy, F. O.; Lummis, S. C. R.; Marin, P.; Maroteaux, L.; McCreary, A. C.; Nelson, D. L.; Neumaier, J. F.; Newman-Tancredi, A.; Nury, H.; Roberts, A.; Roth, B. L.; Roumier, A.; Sanger, G. J.; Teitler, M.; Sharp, T.; Villalón, C. M.; Vogel, H.; Watts, S. W.; Hoyer, D. International Union of Basic and Clinical Pharmacology. CX. Classification of Receptors for 5-Hydroxytryptamine; Pharmacology and Function. *Pharmacol. Rev.* **2021**, *73*, 310–520.

66. Ayd, F. J. Amitriptyline (Elavil) Therapy for Depressive Reactions. *Psychosomatics* **1960**, *1*, 320–325.

67. Kasper, S. Is Treatment-Resistant Depression Really Resistant? *Eur. Neuropsychopharmacol.* **2022**, *58*, 44–46.

68. Zhdanava, M.; Pilon, D.; Ghelerter, I.; Chow, W.; Joshi, K.; Lefebvre, P.; Sheehan, J. J. The Prevalence and National Burden of Treatment-Resistant Depression and Major Depressive Disorder in the United States. *J. Clin. Psychiatry* **2021**, *82*.

69. Souery, D.; Oswald, P.; Massat, I.; Bailer, U.; Bollen, J.; Demyttenaere, K.; Kasper, S.; Lecrubier, Y.; Montgomery, S.; Serretti, A.; Zohar, J.; Mendlewicz, J. Clinical Factors Associated with Treatment Resistance in Major Depressive Disorder. *J. Clin. Psychiatry* **2007**, *68*, 1062–1070.

70. Svensson, T. H. Brain Noradrenaline and the Mechanisms of Action of Antidepressant Drugs. *Acta Psychiatr. Scand.* **2000**, *101*, 18–27.

71. Glennon, R. A.; Iversen, L. Antidepressants. In *Burger's Medicinal Chemistry and Drug Discovery,* 8th ed; Glennon, R. A., Ed.; Wiley: Hoboken, NJ, 2021; pp 1–56.

72. Bloch, R. G.; Dooneief A. S.; Buchberg, A. S.; Spellman, S. The Clinical Effect of Isoniazid and Iproniazid in the Treatment of Pulmonary Tuberculosis. *Ann. Intern. Med.* **1954**, *40*, 881–900.

73. Kline, N. S. Clinical Experience with Iproniazid (Marsilid). *J. Clin. Exp. Psychopathol.* **1958**, *19*, 72–79.

74. Crane, G. E. Iproniazid (Marsilid) Phosphate, a Therapeutic Agent for Mental Disorders and Debilitating Diseases. *Psychiatr. Res. Rep. Am. Psychiatr. Assoc.* **1957**, *8*, 142–152.

75. Zeller, E. A.; Barsky, J.; Fouts, J. R.; Kirchheimer, W. F.; Van Orden, L. S. Influence of Isonicotinic Acid Hydrazide (INH) and 1-Isonicotinyl-2-isopropyl Hydrazide (IIH) on Bacterial and Mammalian Enzymes. *Experientia* **1952**, *8*, 349–350.

76. Kuhn, R. The Treatment of Depressive States with G 22355 (Imipramine Hydrochloride). *Am. J. Psychiatry* **1958**, *115*, 459–464.

77. Kuhn, R. Treatment of Depressive States with an Iminodibenzyl Derivative (G 22355). *Schweiz. Med. Wochenschr.* **1957**, *87*, 1135–1140.

78. Holm, K. J.; Markham, A. Mirtazapine. *Drugs* **1999**, *57*, 607–631.

79. Feighner, J. P. Mechanism of Action of Antidepressant Medications. *J. Clin. Psychiatry* **1999**, *60 Suppl 4*, 4–11; discussion 12-3.

80. Wong, D. T.; Perry, K. W.; Bymaster, F. P. The Discovery of Fluoxetine Hydrochloride (Prozac). *Nat. Rev. Drug Discov.* **2005**, *4*, 764–774.

81. Anderson, I. M. SSRIs versus Tricyclic Antidepressants in Depressed Inpatients: A Meta-Analysis of Efficacy and Tolerability. *Depress. Anxiety* **1998**, *7 Suppl 1*, 11–17.

82. Edwards, J. G.; Anderson, I. Systematic Review and Guide to Selection of Selective Serotonin Reuptake Inhibitors. *Drugs* **1999**, *57*, 507–533.

83. Rosen, R. C.; Lane, R. M.; Menza, M. Effects of SSRIs on Sexual Function. *J. Clin. Psychopharmacol.* **1999**, *19*, 67–85.

84. Wilkinson, T. J.; Begg, E. J.; Winter, A. C.; Sainsbury, R. Incidence and Risk Factors for Hyponatraemia Following Treatment with Fluoxetine or Paroxetine in Elderly People. *Br. J. Clin. Pharmacol.* **1999**, *47*, 211–217.

85. Gumpper, R. H.; Roth, B. L. SnapShot: Psychedelics and Serotonin Receptor Signaling. *Cell* **2023**, *186*, 232-232.e1.

86. Wacker, D.; Wang, S.; McCorvy, J. D.; Betz, R. M.; Venkatakrishnan, A. J.; Levit, A.; Lansu, K.; Schools, Z. L.; Che, T.; Nichols, D. E.; Shoichet, B. K.; Dror, R. O.; Roth, B. L. Crystal Structure of an LSD-Bound Human Serotonin Receptor. *Cell* **2017**, *168*, 377-389.e12.

87. Allen, J. A.; Yadav, P. N.; Roth, B. L. Insights into the Regulation of 5-HT$_{2A}$ Serotonin Receptors by Scaffolding Proteins and Kinases. *Neuropharmacology* **2008**, *55,* 961–968.

88. Kwan, A. C.; Olson, D. E.; Preller, K. H.; Roth, B. L. The Neural Basis of Psychedelic Action. *Nat. Neurosci.* **2022**, *25,* 1407–1419.

89.   Meltzer, H. Y. Serotonergic Mechanisms as Targets for Existing and Novel Antipsychotics. In *Current Antipsychotics. Handbook of Experimental Pharmacology,* Vol. 212; Gross, G., Geyer, M., Eds.; Springer: Berlin, Heidelberg. 2012; pp 87–124.

90.   Carpenter, L. L.; Jocic, Z.; Hall, J. M.; Rasmussen, S. A.; Price, L. H. Mirtazapine Augmentation in the Treatment of Refractory Depression. *J. Clin. Psychiatry* **1999**, *60*, 45–49.

91.   Gerber, D. J.; Tonegawa, S. Psychotomimetic Effects of Drugs — A Common Pathway to Schizophrenia? *N. Engl. J. Med.* **2004**, *350*, 1047–1048.

92.   Curran, H. V.; D'Souza, D. C.; Robbins, T. W.; Fletcher, P. Modelling Psychosis. *Psychopharmacology* **2009**, *206*, 513–514.

93.   Carhart-Harris, R. L.; Goodwin, G. M. The Therapeutic Potential of Psychedelic Drugs: Past, Present, and Future. *Neuropsychopharmacology* **2017**, *42*, 2105–2113.

94.   Titeler, M.; Lyon, R. A.; Glennon, R. A. Radioligand Binding Evidence Implicates the Brain 5-HT2 Receptor as a Site of Action for LSD and Phenylisopropylamine Hallucinogens. *Psychopharmacology* **1988**, *94*, 213–216.

95.   Glennon, R. A.; Young, R.; Jacyno, J. M.; Slusher, M.; Rosecrans, J. A. DOM-Stimulus Generalization to LSD and Other Hallucinogenic Indolealkylamines. *Eur. J. Pharmacol.* **1983**, *86*, 453–459.

96. Glennon, R. A.; Titeler, M.; McKenney, J. D. Evidence for 5-HT2 Involvement in the Mechanism of Action of Hallucinogenic Agents. *Life Sci.* **1984**, *35*, 2505–2511.

97. van Amsterdam, J.; Nutt, D.; Phillips, L.; van den Brink, W. European Rating of Drug Harms. *J. Psychopharmacol.* **2015**, *29*, 655–660.

98. Hendricks, P. S.; Thorne, C. B.; Clark, C. B.; Coombs, D. W.; Johnson, M. W. Classic Psychedelic Use Is Associated with Reduced Psychological Distress and Suicidality in the United States Adult Population. *J. Psychopharmacol.* **2015**, *29*, 280–288.

99. Bouso, J. C.; González, D.; Fondevila, S.; Cutchet, M.; Fernández, X.; Ribeiro Barbosa, P. C.; Alcázar-Córcoles, M. Á.; Araújo, W. S.; Barbanoj, M. J.; Fábregas, J. M.; Riba, J. Personality, Psychopathology, Life Attitudes and Neuropsychological Performance among Ritual Users of Ayahuasca: A Longitudinal Study. *PLoS One* **2012**, *7*, e42421.

100. Wilkie, M. J. V; Smith, G.; Day, R. K.; Matthews, K.; Smith, D.; Blackwood, D.; Reid, I. C.; Wolf, C. R. Polymorphisms in the SLC6A4 and HTR2A Genes Influence Treatment Outcome Following Antidepressant Therapy. *Pharmacogenomics J.* **2009**, *9*, 61–70.

101. Carhart-Harris, R. L.; Bolstridge, M.; Rucker, J.; Day, C. M. J.; Erritzoe, D.; Kaelen, M.; Bloomfield, M.; Rickard, J. A.; Forbes, B.; Feilding, A.; Taylor, D.; Pilling, S.; Curran, V. H.; Nutt, D. J. Psilocybin with Psychological Support for Treatment-Resistant Depression: An Open-Label Feasibility Study. *Lancet Psychiatry* **2016**, *3*, 619–627.

102. Goodwin, G. M.; Aaronson, S. T.; Alvarez, O.; Arden, P. C.; Baker, A.; Bennett, J. C.; Bird, C.; Blom, R. E.; Brennan, C.; Brusch, D.; Burke, L.; Campbell-Coker, K.; Carhart-Harris, R.; Cattell, J.; Daniel, A.; DeBattista, C.; Dunlop, B. W.; Eisen, K.; Feifel, D.; Forbes, M.; Haumann, H. M.; Hellerstein, D. J.; Hoppe, A. I.; Husain, M. I.; Jelen, L. A.; Kamphuis, J.; Kawasaki, J.; Kelly, J. R.; Key, R. E.; Kishon, R.; Knatz Peck, S.; Knight, G.; Koolen, M. H. B.; Lean, M.; Licht, R. W.; Maples-Keller, J. L.; Mars, J.; Marwood, L.; McElhiney, M. C.; Miller, T. L.; Mirow, A.; Mistry, S.; Mletzko-Crowe, T.; Modlin, L. N.; Nielsen, R. E.; Nielson, E. M.; Offerhaus, S. R.; O'Keane, V.; Páleníček, T.; Printz, D.; Rademaker, M. C.; van Reemst, A.; Reinholdt, F.; Repantis, D.; Rucker, J.; Rudow, S.; Ruffell, S.; Rush, A. J.; Schoevers, R. A.; Seynaeve, M.; Shao, S.; Soares, J. C.; Somers, M.; Stansfield, S. C.; Sterling, D.; Strockis, A.; Tsai, J.; Visser, L.; Wahba, M.; Williams, S.; Young, A. H.; Ywema, P.; Zisook, S.; Malievskaia, E. Single-Dose Psilocybin for a Treatment-Resistant Episode of Major Depression. *N. Engl. J. Med.* **2022**, *387*, 1637–1648.

103. Carhart-Harris, R. L.; Bolstridge, M.; Day, C. M. J.; Rucker, J.; Watts, R.; Erritzoe, D. E.; Kaelen, M.; Giribaldi, B.; Bloomfield, M.; Pilling, S.; Rickard, J. A.; Forbes, B.; Feilding, A.; Taylor, D.; Curran, H. V.; Nutt, D. J. Psilocybin with Psychological Support for Treatment-Resistant Depression: Six-Month Follow-Up. *Psychopharmacology* **2018**, *235*, 399–408.

104. Grob, C. S.; Danforth, A. L.; Chopra, G. S.; Hagerty, M.; McKay, C. R.; Halberstadt, A. L.; Greer, G. R. Pilot Study of Psilocybin Treatment for Anxiety in Patients with Advanced-Stage Cancer. *Arch. Gen. Psychiatry* **2011**, *68*, 71.

105. Griffiths, R. R.; Johnson, M. W.; Carducci, M. A.; Umbricht, A.; Richards, W. A.; Richards, B. D.; Cosimano, M. P.; Klinedinst, M. A. Psilocybin Produces Substantial and Sustained Decreases in Depression and Anxiety in Patients with Life-Threatening Cancer: A Randomized Double-Blind Trial. *J. Psychopharmacol.* **2016**, *30*, 1181–1197.

106. Sanches, R. F.; de Lima Osório, F.; dos Santos, R. G.; Macedo, L. R. H.; Maia-de-Oliveira, J. P.; Wichert-Ana, L.; de Araujo, D. B.; Riba, J.; Crippa, J. A. S.; Hallak, J. E. C. Antidepressant Effects of a Single Dose of Ayahuasca in Patients with Recurrent Depression. *J. Clin. Psychopharmacol.* **2016**, *36*, 77–81.

107. Freedland, C. S.; Mansbach, R. S. Behavioral Profile of Constituents in Ayahuasca, an Amazonian Psychoactive Plant Mixture. *Drug Alcohol Depend.* **1999**, *54*, 183–194.

108. Rosell, D. R.; Thompson, J. L.; Slifstein, M.; Xu, X.; Frankle, W. G.; New, A. S.; Goodman, M.; Weinstein, S. R.; Laruelle, M.; Abi-Dargham, A.; Siever, L. J. Increased Serotonin 2A Receptor Availability in the Orbitofrontal Cortex of Physically Aggressive Personality Disordered Patients. *Biol. Psychiatry* **2010**, *67*, 1154–1162.

109. Bhagwagar, Z.; Hinz, R.; Taylor, M.; Fancy, S.; Cowen, P.; Grasby, P. Increased 5-HT_{2A} Receptor Binding in Euthymic, Medication-Free Patients Recovered From Depression: A Positron Emission Study With [^{11}C]MDL 100,907. *Am. J. Psychiatry* **2006**, *163*, 1580–1587.

110. Frokjaer, V. G.; Mortensen, E. L.; Nielsen, F. Å.; Haugbol, S.; Pinborg, L. H.; Adams, K. H.; Svarer, C.; Hasselbalch, S. G.; Holm, S.; Paulson, O. B.; Knudsen, G. M. Frontolimbic Serotonin 2A Receptor Binding in Healthy Subjects Is Associated with Personality Risk Factors for Affective Disorder. *Biol. Psychiatry* **2008**, *63*, 569–576.

111. Carhart-Harris, R. L.; Kaelen, M.; Bolstridge, M.; Williams, T. M.; Williams, L. T.; Underwood, R.; Feilding, A.; Nutt, D. J. The Paradoxical Psychological Effects of Lysergic Acid Diethylamide (LSD). *Psychol. Med.* **2016**, *46*, 1379–1390.

112. Shelton, R. C.; Sanders-Bush, E.; Manier, D. H.; Lewis, D. A. Elevated 5-HT$_{2A}$ Receptors in Postmortem Prefrontal Cortex in Major Depression Is Associated with Reduced Activity of Protein Kinase A. *Neuroscience* **2009**, *158*, 1406–1415.

113. Stanley, M.; Mann, J. J. Increased Serotonin-2 Binding Sites in Frontal Cortex Of Suicide Victims. *Lancet* **1983**, *321*, 214–216.

114. Muguruza, C.; Miranda-Azpiazu, P.; Díez-Alarcia, R.; Morentin, B.; González-Maeso, J.; Callado, L. F.; Meana, J. J. Evaluation of 5-HT$_{2A}$ and MGlu$_{2/3}$ Receptors in Postmortem Prefrontal Cortex of Subjects with Major Depressive Disorder: Effect of Antidepressant Treatment. *Neuropharmacology* **2014**, *86*, 311–318.

115. Gray, J. A.; Roth, B. L. Paradoxical Trafficking and Regulation of 5-HT$_{2A}$ Receptors by Agonists and Antagonists. *Brain Res. Bull.* **2001**, *56*, 441–451.

116. Carhart-Harris, R.; Nutt, D. Serotonin and Brain Function: A Tale of Two Receptors. *J. Psychopharmacol.* **2017**, *31*, 1091–1120.

117. Vollenweider, F. X.; Vollenweider-Scherpenhuyzen, M. F. I.; Bäbler, A.; Vogel, H.; Hell, D. Psilocybin Induces Schizophrenia-like Psychosis in Humans via a Serotonin-2 Agonist Action. *NeuroReport* **1998**, *9*, 3897–3902.

118. Glennon, R. A.; Dukat, M. α-Ethyltryptamine: A Ratiocinatory Review of a Forgotten Antidepressant. *ACS Pharmacol. Transl. Sci.* **2023**, *6*, 1780–1789.

119. U.S. Bans Sales of Drug Monase. *New York Times*. March 21, 1962, pp 26–26.

120. Anthony, W. C. Antidepressant Compositions and Methods Using Alpha-Ethyltryptamine. US Patent. 3,531,573. August 4, 1964.

121. *Federal Registry Temporary Placement of Alpha-Ethyltryptamine into Schedule I. 58, 13533*; 1993.

122. Govier, Wm. M.; Howes, B. G.; Gibbons, A. J. The Oxidative Deamination of Serotonin and Other 3-(Beta-Aminoethyl)-Indoles by Monamine Oxidase and the Effect of These Compounds on the Deamination of Tyramine. *Science* **1953**, *118*, 596–597.

123. Greig, M. E.; Walk, R. A.; Gibbons, A. J. The Effect of Three Tryptamine Derivatives on Serotonin Metabolism in Vitro and in Vivo. *J. Pharmacol. Exp. Ther.* **1959**, *127*, 110–115.

124. Blough, B. E.; Landavazo, A.; Partilla, J. S.; Decker, A. M.; Page, K. M.; Baumann, M. H.; Rothman, R. B. Alpha-Ethyltryptamines as Dual Dopamine–Serotonin Releasers. *Bioorg. Med. Chem. Lett.* **2014**, *24*, 4754–4758.

125. Hester, J. B. Cyclodehydration Reactions of Tryptamine Derivatives with Acetone. *J. Org. Chem.* **1964**, *29*, 2864–2867.

126. Heinzelman, R. V.; Anthony, W. C.; Lyttle, D. A.; Szmuszkovicz, J. The Synthesis of α-Methyltryptophans and α-Alkyltryptamines. *J. Org. Chem.* **1960**, *25*, 1548–1558.

127. Dresp-Langley, B. From Reward to Anhedonia-Dopamine Function in the Global Mental Health Context. *Biomedicines* **2023**, *11*, 2469.

128. Rasheed, N.; Alghasham, A. Central Dopaminergic System and Its Implications in Stress-Mediated Neurological Disorders and Gastric Ulcers: Short Review. *Adv. Pharmacol. Sci.* **2012**, *2012*, 1–11.

129. Lewis, R. G.; Florio, E.; Punzo, D.; Borrelli, E. The Brain's Reward System in Health and Disease. In *Circadian Clock in Brain Health and Disease*; Engmann O., Brancaccio M., Eds.; Springer International Publishing: Cham, Switzerland, 2021; pp 57–69.

130. Wise, R. A. Dopamine and Reward: The Anhedonia Hypothesis 30 Years On. *Neurotox. Res.* **2008**, *14*, 169–183.

131. Volkow, N. D.; Koob, G. F.; McLellan, A. T. Neurobiologic Advances from the Brain Disease Model of Addiction. *N. Engl. J. Med.* **2016**, *374*, 363–371.

132. Robinson, T. The Neural Basis of Drug Craving: An Incentive-Sensitization Theory of Addiction. *Brain Res. Rev.* **1993**, *18*, 247–291.

133. Everitt, B. J.; Robbins, T. W. Neural Systems of Reinforcement for Drug Addiction: From Actions to Habits to Compulsion. *Nat. Neurosci.* **2005**, *8*, 1481–1489.

134. Frank, M. J.; Seeberger, L. C.; O'Reilly, R. C. By Carrot or by Stick: Cognitive Reinforcement Learning in Parkinsonism. *Science* **2004**, *306*, 1940–1943.

135. Hyman, S. E.; Malenka, R. C.; Nestler, E. J. Neural Mechanisms of Addiction: The Role of Reward-Related Learning and Memory. *Annu. Rev. Neurosci.* **2006**, *29*, 565–598.

136. Dalley, J. W.; Mar, A. C.; Economidou, D.; Robbins, T. W. Neurobehavioral Mechanisms of Impulsivity: Fronto-Striatal Systems and Functional Neurochemistry. *Pharmacol. Biochem. Behav.* **2008**, *90*, 250–260.

137. Volkow, N. D.; Wang, G. J.; Fowler, J. S.; Tomasi, D.; Baler, R. Food and Drug Reward: Overlapping Circuits in Human Obesity and Addiction. In *Brain Imaging in Behavioral Neuroscience. Current Topics is Behavioral Neurosciences*, Vol. 11; Carter, C., Dalley, J., Eds. Springer: Berlin, Heidelberg. 2011; pp 1–24.

138. Kalivas, P. W.; Volkow, N. D. The Neural Basis of Addiction: A Pathology of Motivation and Choice. *Am. J. Psychiatry* **2005**, *162*, 1403–1413.

139. Roberts, D. C. S.; Corcoran, M. E.; Fibiger, H. C. On the Role of Ascending Catecholaminergic Systems in Intravenous Self-Administration of Cocaine. *Pharmacol. Biochem. Behav.* **1977**, *6*, 615–620.

140. Volkow, N. D.; Morales, M. The Brain on Drugs: From Reward to Addiction. *Cell* **2015**, *162*, 712–725.

141. Kalivas, P. W.; O'Brien, C. Drug Addiction as a Pathology of Staged Neuroplasticity. *Neuropsychopharmacology* **2008**, *33*, 166–180.

142. Shaham, Y.; Erb, S.; Stewart, J. Stress-Induced Relapse to Heroin and Cocaine Seeking in Rats: A Review. *Brain Res. Rev.* **2000**, *33*, 13–33.

143. *National Institute on Drug Abuse, Drug Overdose Death Rates*; 2024.

144. Masand, P. S.; Tesar, G. E. Use of Stimulants in the Medically Ill. *Psychiatr. Clin. N. Am.* **1996**, *19*, 515–547.

145. Edeleano, L. Ueber Einige Derivate Der Phenylmethacrylsäure Und Der Phenylisobuttersäure. *Ber. Dtsch. Chem. Ges.* **1887**, *20*, 616–622.

146. Barger, G.; Dale, H. H. Chemical Structure and Sympathomimetic Action of Amines. *J. Physiol.* **1910**, *41*, 19–59.

147. Alles, G. A. The Comparative Physiological Action of Phenylethanolamine. *J. Pharmacol. Exp. Ther.* **1927**, *32*, 121.

148. Alles, G. A. The Comparative Physiological Actions of *dl-β*-Phenylisopropylamines I. Pressor Effect and Toxicity. *J. Pharmacol. Exp. Ther.* **1933**, *47*, 339.

149. Prinzmetal, M. The Use of Benzedrine for the Treatment of Narcolepsy. *J. Am. Med. Assoc.* **1935**, *105*, 2051.

150. Guttmann, E.; Sargant, W. Observations on Benzedrine. *BMJ* **1937**, *1*, 1013–1015.

151. Panenka, W. J.; Procyshyn, R. M.; Lecomte, T.; MacEwan, G. W.; Flynn, S. W.; Honer, W. G.; Barr, A. M. Methamphetamine Use: A Comprehensive Review of

Molecular, Preclinical and Clinical Findings. *Drug Alcohol Depend.* **2013**, *129*, 167–179.

152. Anglin, M. D.; Burke, C.; Perrochet, B.; Stamper, E.; Dawud-Noursi, S. History of the Methamphetamine Problem. *J. Psychoactive Drugs* **2000**, *32*, 137–141.

153. Wada, K. The History and Current State of Drug Abuse in Japan. *Ann. N. Y. Acad. Sci.* **2011**, *1216*, 62–72.

154. Roque Bravo, R.; Faria, A. C.; Brito-da-Costa, A. M.; Carmo, H.; Mladěnka, P.; Dias da Silva, D.; Remião, F. Cocaine: An Updated Overview on Chemistry, Detection, Biokinetics, and Pharmacotoxicological Aspects Including Abuse Pattern. *Toxins (Basel)* **2022**, *14*, 278.

155. Phillips, K.; Luk, A.; Soor, G. S.; Abraham, J. R.; Leong, S.; Butany, J. Cocaine Cardiotoxicity: A Review of the Pathophysiology, Pathology, and Treatment Options. *Am. J. Cardiovasc. Drugs* **2009**, *9*, 177–196.

156. Drake, L. R.; Scott, P. J. H. DARK Classics in Chemical Neuroscience: Cocaine. *ACS Chem. Neurosci.* **2018**, *9*, 2358–2372.

157. *UNODC. World Drug Report 2021*; Vienna Austria, 2021.

158. *EMCDDA. European Drug Report 2021: Trends and Development. European Monitoring Centre for Drugs and Drug Addiction;* Luxembourg, 2021.

159. Soares, J.; Costa, V. M.; Bastos, M. de L.; Carvalho, F.; Capela, J. P. An Updated Review on Synthetic Cathinones. *Arch. Toxicol.* **2021**, *95*, 2895–2940.

160. Boyce, G. R.; Gluck-Thaler, E.; Slot, J. C.; Stajich, J. E.; Davis, W. J.; James, T. Y.; Cooley, J. R.; Panaccione, D. G.; Eilenberg, J.; De Fine Licht, H. H.; Macias, A. M.; Berger, M. C.; Wickert, K. L.; Stauder, C. M.; Spahr, E. J.; Maust, M. D.; Metheny, A. M.; Simon, C.; Kritsky, G.; Hodge, K. T.; Humber, R. A.; Gullion, T.; Short, D. P. G.; Kijimoto, T.; Mozgai, D.; Arguedas, N.; Kasson, M. T. Psychoactive Plant- and Mushroom-Associated Alkaloids from Two Behavior Modifying Cicada Pathogens. *Fungal Ecol.* **2019**, *41*, 147–164.

161. Krikorian, A. D. Kat and Its Use: An Historical Perspective. *J. Ethnopharmacol.* **1984**, *12*, 115–178.

162. Patel, N. B. Khat (Catha Edulis Forsk) - And Now There Are Three. *Brain Res. Bull.* **2019**, *145*, 92–96.

163. Al-Hebshi, N. N.; Skaug, N. Khat (Catha Edulis)-An Updated Review. *Addict. Biol.* **2005**, *10*, 299–307.

164. Fluckiger, F. A.; Gerock, J. E. Contribution to the Knowledge of Catha Leaves. *Pharm. J. Transvaal.* **1887**, *18*, 221.

165. Wolfes, O. Über das Vorkommen von *d*-nor-iso-Ephedrin in Catha Edulis. *Arch. Pharm. (Weinheim)* **1930**, *268*, 81–83.

166. Document UN. *III Investigations on the Phenylalkylamine Fraction. Studies on the Chemical Composition of Khat.*; GE, 1975.

167. Glennon, R. A.; Schechter, M. D.; Rosecrans, J. A. Discriminative Stimulus Properties of *S*(−)- and *R*(+)-Cathinone, (+)-Cathine and Several Structural Modifications. *Pharmacol. Biochem. Behav.* **1984**, *21*, 1–3.

168. Hyde, J. F.; Browning, E.; Adams, R. Synthetic Homologs of *d,l*-Ephedrine. *J. Am. Chem. Soc.* **1928**, *50*, 2287–2292.

169. Glennon, R. A.; Yousif, M.; Naiman, N.; Kalix, P. Methcathinone: A New and Potent Amphetamine-like Agent. *Pharmacol. Biochem. Behav.* **1987**, *26*, 547–551.

170. Sanchez, S. Sur Un Homologue de l'ephedrine. *Bull. Soc. Chim. Fr.* **1929**, *45*, 284–286.

171. Seaton, D. A.; Duncan, L. J. P.; Rose, K.; Scott, A. M. Diethylpropion in the Treatment of "Refractory" Obesity. *BMJ* **1961**, *1*, 1009–1011.

172. *UNODC United Nations Convention on Psychotropic Substances. In: United Nations Conference for the Adoption of a Protocol on Psychotropic Substances*; Vienna, Austria, 1971.

173. *Diethylpropion and Phentermine; Temporary Placement in Schedule IV; Interim Regulations. Fed. Regist.*, *38*, *65371−65375*; 1973.

174. Clark, A.; Tate, B.; Urban, B.; Schroeder, R.; Gennuso, S.; Ahmadzadeh, S.; McGregor, D.; Girma, B.; Shekoohi, S.; Kaye, A. D. Bupropion Mediated Effects on Depression, Attention Deficit Hyperactivity Disorder, and Smoking Cessation. *Health Psychol. Res.* **2023**, *11*, 81043.

175. Glennon, R. A.; Dukat, M. Structure-Activity Relationships of Synthetic Cathinones. In *Neuropharmacology of New Psychoactive Substances (NPS). Current Topics in Behavioral Neurosciences*; Vol. 32; Baumann M., Glennon R. A., Wiley J., Eds.; Springer International Publishing: New York City, 2017; pp 19–47.

176. Glennon, R. A.; Dukat, M. Synthetic Cathinones: A Brief Overview of Overviews with Applications to the Forensic Sciences. *Ann. Forensic Res. Anal.* **2017**, *4*, 1040.

177. Yadav-Samudrala, B. J.; Eltit, J. M.; Glennon, R. A. Synthetic Cathinone Analogues Structurally Related to the Central Stimulant Methylphenidate as Dopamine Reuptake Inhibitors. *ACS Chem. Neurosci.* **2019**, *10*, 4043–4050.

178. Sury, E.; Hoffmann, K. Über Alkylenimin-Derivate. II Mitteilung. Piperidin-Derivate Mit Zentralerregender Wirkung I. *Helv. Chim. Acta.* **1954**, *37*, 2133–2145.

179. Kim, D. I.; Deutsch, H. M.; Ye, X.; Schweri, M. M. Synthesis and Pharmacology of Site-Specific Cocaine Abuse Treatment Agents: Restricted Rotation Analogues of Methylphenidate. *J. Med. Chem.* **2007**, *50*, 2718–2731.

180. Nadal-Gratacós, N.; Alberto-Silva, A. S.; Rodríguez-Soler, M.; Urquizu, E.; Espinosa-Velasco, M.; Jäntsch, K.; Holy, M.; Batllori, X.; Berzosa, X.; Pubill, D.; Camarasa, J.; Sitte, H. H.; Escubedo, E.; López-Arnau, R. Structure–Activity Relationship of Novel Second-Generation Synthetic Cathinones: Mechanism of Action, Locomotion, Reward, and Immediate-Early Genes. *Front. Pharmacol.* **2021**, *12*, 749429.

181. Simmler, L.; Buser, T.; Donzelli, M.; Schramm, Y.; Dieu, L.-H.; Huwyler, J.; Chaboz, S.; Hoener, M.; Liechti, M. Pharmacological Characterization of Designer Cathinones *in Vitro*. *Br. J. Pharmacol.* **2013**, *168*, 458–470.

182. Chen, Y.; Blough, B. E.; Murnane, K. S.; Canal, C. E. The Synthetic Cathinone Psychostimulant α-PPP Antagonizes Serotonin 5-HT$_{2A}$ Receptors: In Vitro and in Vivo Evidence. *Drug Test. Anal.* **2019**, *11*, 990–998.

183. Jones, C. B.; Eltit, J. M.; Dukat, M. Do 2-(Benzoyl)Piperidines Represent a Novel Class of hDAT Reuptake Inhibitors? *ACS Chem. Neurosci.* **2023**, *14*, 741–748.

184. Hansch, C.; Leo, A.; Unger, S. H.; Kim, K. H.; Nikaitani, D.; Lien, E. J. Aromatic Substituent Constants for Structure-Activity Correlations. *J. Med. Chem.* **1973**, *16*, 1207–1216.

185. Fujita, Toshio.; Iwasa, Junkichi.; Hansch, C. A New Substituent Constant, π, Derived from Partition Coefficients. *J. Am. Chem. Soc.* **1964**, *86*, 5175–5180.

186. Jaffé, H. H. A Reëxamination of the Hammett Equation. *Chem. Rev.* **1953**, *53*, 191–261.

187. Kolanos, R.; Partilla, J. S.; Baumann, M. H.; Hutsell, B. A.; Banks, M. L.; Negus, S. S.; Glennon, R. A. Stereoselective Actions of Methylenedioxypyrovalerone (MDPV) To Inhibit Dopamine and Norepinephrine Transporters and Facilitate Intracranial Self-Stimulation in Rats. *ACS Chem. Neurosci.* **2015**, *6*, 771–777.

188. Yamashita, A.; Singh, S. K.; Kawate, T.; Jin, Y.; Gouaux, E. Crystal Structure of a Bacterial Homologue of Na$^+$/Cl$^-$-Dependent Neurotransmitter Transporters. *Nature* **2005**, *437*, 215–223.

189. Coleman, J. A.; Green, E. M.; Gouaux, E. X-Ray Structures and Mechanism of the Human Serotonin Transporter. *Nature* **2016**, *532*, 334–339.

190. Penmatsa, A.; Wang, K. H.; Gouaux, E. X-Ray Structure of Dopamine Transporter Elucidates Antidepressant Mechanism. *Nature* **2013**, *503*, 85–90.

191. Huang, X.; Zhan, C.-G. How Dopamine Transporter Interacts with Dopamine: Insights from Molecular Modeling and Simulation. *Biophys. J.* **2007**, *93*, 3627–3639.

192. Yuan, Y.; Huang, X.; Midde, N. M.; Quizon, P. M.; Sun, W.-L.; Zhu, J.; Zhan, C.-G. Molecular Mechanism of HIV-1 Tat Interacting with Human Dopamine Transporter. *ACS Chem. Neurosci.* **2015**, *6*, 658–665.

193. Penmatsa, A.; Wang, K. H.; Gouaux, E. X-Ray Structures of Drosophila Dopamine Transporter in Complex with Nisoxetine and Reboxetine. *Nat. Struct. Mol. Biol.* **2015**, *22*, 506–508.

194. Wang, K. H.; Penmatsa, A.; Gouaux, E. Neurotransmitter and Psychostimulant Recognition by the Dopamine Transporter. *Nature* **2015**, *521*, 322–327.

195. Haddad, Y.; Heger, Z.; Adam, V. Guidelines for Homology Modeling of Dopamine, Norepinephrine, and Serotonin Transporters. *ACS Chem. Neurosci.* **2016**, *7*, 1607–1613.

196. Ortore, G.; Orlandini, E.; Betti, L.; Giannaccini, G.; Mazzoni, M. R.; Camodeca, C.; Nencetti, S. Focus on Human Monoamine Transporter Selectivity. New Human DAT and NET Models, Experimental Validation, and SERT Affinity Exploration. *ACS Chem. Neurosci.* **2020**, *11*, 3214–3232.

197. Coleman, J. A.; Navratna, V.; Antermite, D.; Yang, D.; Bull, J. A.; Gouaux, E. Chemical and Structural Investigation of the Paroxetine-Human Serotonin Transporter Complex. *Elife* **2020**, *9*, e56427.

198. Šali, A.; Blundell, T. L. Comparative Protein Modelling by Satisfaction of Spatial Restraints. *J. Mol. Biol.* **1993**, *234*, 779–815.

199. Melo, F.; Sali, A. Fold Assessment for Comparative Protein Structure Modeling. *Protein Sci.* **2007**, *16*, 2412–2426.

200. Reva, B. A.; Finkelstein, A. V; Skolnick, J. What Is the Probability of a Chance Prediction of a Protein Structure with an Rmsd of 6 Å? *Fold Des.* **1998**, *3*, 141–147.

201. Jones, C. B.; Dukat, M. Review of 3D Templates for in Silico Homology Models of MATs: Improved 3D Model of HDAT. *Med. Chem. Res.* **2022**, *31*, 643–651.

202. Kellogg, G. E.; Semus, S. F.; Abraham, D. J. HINT: A New Method of Empirical Hydrophobic Field Calculation for CoMFA. *J. Comput. Aided Mol. Des.* **1991**, *5*, 545–552.

203. Thai, D. L.; Sapko, M. T.; Reiter, C. T.; Bierer, D. E.; Perel, J. M. Asymmetric Synthesis and Pharmacology of Methylphenidate and Its Para-Substituted Derivatives. *J. Med. Chem.* **1998**, *41*, 591–601.

204. Barker, E. L.; Perlman, M. A.; Adkins, E. M.; Houlihan, W. J.; Pristupa, Z. B.; Niznik, H. B.; Blakely, R. D. High Affinity Recognition of Serotonin Transporter Antagonists Defined by Species-Scanning Mutagenesis. *J. Biol. Chem.* **1998**, *273*, 19459–19468.

205. Chen, J.-G.; Sachpatzidis, A.; Rudnick, G. The Third Transmembrane Domain of the Serotonin Transporter Contains Residues Associated with Substrate and Cocaine Binding. *J. Biol. Chem.* **1997**, *272*, 28321–28327.

206. Mager, S.; Min, C.; Henry, D. J.; Chavkintt, C.; Hoffman, B. J.; Davidson, N.; Lester, H. A. Conducting States of a Mammalian Serotonin Transporter. *Neuron* **1994**, *12*, 845–859.

207. Sonders, M. S.; Zhu, S.-J.; Zahniser, N. R.; Kavanaugh, M. P.; Amara, S. G. Multiple Ionic Conductances of the Human Dopamine Transporter: The Actions of Dopamine and Psychostimulants. *J. Neurosci.* **1997**, *17*, 960–974.

208. Ruchala, I.; Cabra, V.; Solis, E.; Glennon, R. A.; De Felice, L. J.; Eltit, J. M. Electrical Coupling between the Human Serotonin Transporter and Voltage-Gated Ca^{2+} Channels. *Cell Calcium* **2014**, *56*, 25–33.

209. Cameron, K. N.; Solis, E.; Ruchala, I.; De Felice, L. J.; Eltit, J. M. Amphetamine Activates Calcium Channels through Dopamine Transporter-Mediated Depolarization. *Cell Calcium* **2015**, *58*, 457–466.

210. Steele, T. W. E.; Eltit, J. M. Using Ca2+-Channel Biosensors to Profile Amphetamines and Cathinones at Monoamine Transporters: Electro-Engineering

Cells to Detect Potential New Psychoactive Substances. *Psychopharmacology* **2019**, *236*, 973–988.

211. Clark, T.; Hennemann, M.; Murray, J. S.; Politzer, P. Halogen Bonding: The σ-Hole. *J. Mol. Model.* **2007**, *13*, 291–296.

212. Clark, T. Σ-Holes. *Wiley Interdiscip. Rev.: Comput. Mol. Sci.* **2013**, *3*, 13–20.

213. Kolarič, A.; Germe, T.; Hrast, M.; Stevenson, C. E. M.; Lawson, D. M.; Burton, N. P.; Vörös, J.; Maxwell, A.; Minovski, N.; Anderluh, M. Potent DNA Gyrase Inhibitors Bind Asymmetrically to Their Target Using Symmetrical Bifurcated Halogen Bonds. *Nat. Commun.* **2021**, *12*, 150.

214. Metrangolo, P.; Murray, J. S.; Pilati, T.; Politzer, P.; Resnati, G.; Terraneo, G. Fluorine-Centered Halogen Bonding: A Factor in Recognition Phenomena and Reactivity. *Cryst. Growth Des.* **2011**, *11*, 4238–4246.

215. Schrödinger Release 2024-3: Maestro, Schrödinger, LLC, New York, NY, 2024.

216. Kim, K.; Che, T.; Panova, O.; DiBerto, J. F.; Lyu, J.; Krumm, B. E.; Wacker, D.; Robertson, M. J.; Seven, A. B.; Nichols, D. E.; Shoichet, B. K.; Skiniotis, G.; Roth, B. L. Structure of a Hallucinogen-Activated G_q-Coupled 5-HT$_{2A}$ Serotonin Receptor. *Cell* **2020**, *182*, 1574-1588.e19.

217. Kimura, K. T.; Asada, H.; Inoue, A.; Kadji, F. M. N.; Im, D.; Mori, C.; Arakawa, T.; Hirata, K.; Nomura, Y.; Nomura, N.; Aoki, J.; Iwata, S.; Shimamura, T. Structures of the 5-HT$_{2A}$ Receptor in Complex with the Antipsychotics Risperidone and Zotepine. *Nat. Struct. Mol. Biol.* **2019**, *26*, 121–128.

218. Heath-Brown, B.; Philpott, P. G. 1321. Studies in the Indole Series. Part I. Indolylalkylamines. *J. Chem. Soc. (Resumed)* **1965**, 7165.

219. Wolfard, J.; Xu, J.; Zhang, H.; Chung, C. K. Synthesis of Chiral Tryptamines via a Regioselective Indole Alkylation. *Org. Lett.* **2018**, *20*, 5431–5434.

220. Glennon, R. A.; Bartyzel, P.; Teitler, M. Binding of Benz[*e*]-and Benz[*g*]-Fused Tryptamine Derivatives at Serotonin Receptors: Evidence for a Region of Bulk Tolerance. *Med. Chem. Res*. **1991**, *1*, 201–206.

221. Wallach, J.; Cao, A. B.; Calkins, M. M.; Heim, A. J.; Lanham, J. K.; Bonniwell, E. M.; Hennessey, J. J.; Bock, H. A.; Anderson, E. I.; Sherwood, A. M.; Morris, H.; de Klein, R.; Klein, A. K.; Cuccurazzu, B.; Gamrat, J.; Fannana, T.; Zauhar, R.; Halberstadt, A. L.; McCorvy, J. D. Identification of 5-HT2A Receptor Signaling Pathways Associated with Psychedelic Potential. *Nat. Commun.* **2023**, *14*, 8221.

222. Snyder, B. H. R.; Katz, L. The Alkylation of Aliphatic Nitro Compounds with Gramine. A New Synthesis of Derivatives of Tryptamine. *J. Am. Chem. Soc.* **1947**, *69*, 3140–3142.

223. Upjohn Co. Cl-and 1-Alpha Ethyltryptamines . FR2097052, 1972.

224. Somei, M.; Kizu, K.; Kunimoto, M.; Yamada, F. The Chemistry of Indoles. XXIV. Syntheses of 3-Indoleacetic Acid and 3-Indoleacetonitrile Having a Halogeno Group and a Carbon Functional Group at the 4-Position. *Chem. Pharm. Bull. (Tokyo)* **1985**, *33*, 3696–3708.

225. Lajarín-Cuesta, R.; Nanclares, C.; Arranz-Tagarro, J.-A.; González-Lafuente, L.; Arribas, R. L.; Araujo de Brito, M.; Gandía, L.; de los Ríos, C. Gramine Derivatives Targeting Ca^{2+} Channels and Ser/Thr Phosphatases: A New Dual Strategy for the Treatment of Neurodegenerative Diseases. *J. Med. Chem.* **2016**, *59*, 6265–6280.

226. Cook, J. W.; Loudon, J. D.; McCloskey, P. 269. The Chemistry of the Mitragyna Genus. Part II. Synthesis of 7-Methoxy-2-methyl- and 7-Methoxy-1 : 2-dimethyl-β-carboline. *J. Chem. Soc.* **1951**, 1203–1207.

227. de la Fuente Revenga, M.; Shah, U. H.; Nassehi, N.; Jaster, A. M.; Hemanth, P.; Sierra, S.; Dukat, M.; González-Maeso, J. Psychedelic-like Properties of Quipazine and Its Structural Analogues in Mice. *ACS Chem. Neurosci.* **2021**, *12*, 831–844.

VIII. Vita

Charles Bernard Jones III was born to Charles and Nancy Jones on December 20, 1989 in Lynn Haven, Florida. He received his Bachelor of Science in Chemistry from University of Central Florida, Orlando, Florida in December 2014. After receiving his bachelor degree, he worked as a research scientist on high purity quartz at Unimin in Red Hill, North Carolina. In 2019 he enrolled in Virginia Commonwealth University's School of Pharmacy Medicinal Chemistry graduate program where he received his Master's degree in 2021.